Aus dem Max-Delbrück-Centrum für Molekulare Medizin

DISSERTATION

# Properties and functions of glial cells in the developing and injured brains

zur Erlangung des akademischen Grades
Doctor of Philosophy in Medical Neurosciences
(PhD in Medical Neurosciences)

vorgelegt der Medizinischen Fakultät
Charité – Universitätsmedizin Berlin

von

**Giselle Cheung**

aus Hong Kong, China

Gutachter: 1. Prof. Dr. H. Kettenmann
2. Prof. Dr. med. J. Priller
3. Prof. Dr. med. I. Bechmann

Datum der Promotion: 29.09.2008

## Acknowledgements

I sincerely thank my supervisor Prof. Dr. Helmut Kettenmann for giving me an opportunity to work in his laboratory and for supporting and believing in me each step of the way; Dr. Katrin Färber who led me into microglial research and provided assistance throughout my studies; and Dr. Liping Wang who made me an electrophysiologist and introduced me to interesting projects one of which concerning astrocytes and stroke is described in this thesis. I thank our collaborators Dr. Oliver Kann for extracellular potassium measurements; Prof. Dr. Matthias Endres, Prof. Dr. Gerd Kempermann, Dr. Golo Kronenberg, Shengbo Ji and Karen Gertz for stroke experiments; and Dr. Shinichi Kohsaka for providing Iba1-EGFP mice. Many thanks go to our skillful technicians Irene Haupt for generating primary microglia cultures; Christiane Gras for biocytin immunohistochemistry; Rainer Kröber for maintaining the setups and equipments in very good conditions; and Karin Heufelder for keeping the lab organized and well-supplied. I am grateful for financial and academic support from the *International PhD programme in Molecular Cell Biology* at Max-Delbrück-Center and *International Graduate Program of Medical Neurosciences* at Charité-Universitätsmedizin Berlin; helpful administrative assistance by Sylvia Sibilak, Lutz Steiner and especially our irreplaceable secretary Birgit Jarchow who always made everything a lot easier. To all former and present colleagues, I express my fullest appreciation for their kindness and support and for making my time in the laboratory and in Berlin an enjoyable experience. Particularly, I would like to thank my very special friends Joo-Hee Wälzlein who always knew exactly what I was thinking and proof read everything down to the smallest details; Hannes Kiesewetter whose warm welcome and help extended much beyond the laboratory; and Jochen Müller who provided endless laughter and support including the German translation of the summary text. I am thankful for my family for their unconditional love and encouragements; my friends for their support from different places of the world. Last but not least, I would not have done it without Simon who always saw something in me. I have been and will continue to be inspired by his strong motivation and belief in scientific research.

# Table of Contents

# List of Figures

# List of Tables

# List of Abbreviations

Acetoxymethyl (AM)
Adenosine triphosphate (ATP)
Ameboid microglia (AMG)
Aspartic acid (Asp)
Blood-brain barrier (BBB)
Bovine serum albumin (BSA)
Bromodeoxyuridine (BrdU)
Central nervous system (CNS)
Connexin (Cx)
Corpus callosum (CC)
Current/voltage (I/V)
6-Cyano-7-nitroquinoxaline-2,3-dione (CNQX)
Cytochalasin D (CytoD)
Delayed rectifying potassium ($K_{dr}$)
Diaminobenzidine (DAB)
Dulbecco's Modified Eagle Medium (DMEM)
Enhanced green fluorescent protein (EGFP)
Enzyme-Linked ImmunoSorbent Assay (ELISA)
Ethylene glycol tetraacetic acid (EGTA)
Excitatory to inhibitory (E-I)
Extracellular potassium concentration ($[K^+]_o$)
Fetal calf serum (FCS)
(relative) Fluorescent intensity ($F/F_0$)
Gamma-amino-butyric acid (GABA)
Glial fibrillary acidic protein (GFAP)
Growth regulated oncogene (GRO)
Hank's Balanced Salt Solution (HBBS)
Holding potential (HP)
Image Cells Easily (ICE)

Interleukin (IL)

Intracellular calcium concentration ($[Ca^{2+}]_i$)

Intracellular chloride concentration ($[Cl^-]_i$)

Inward rectifying potassium ($K_{ir}$)

Ionized calcium-binding adaptor molecule (Iba)

Kainic acid (KA)

Keratinocyte-derived chemokine (KC)

Lipopolysaccharide (LPS)

Macrophage inflammatory protein (MIP)

Membrane potential (MP)

Membrane resistance ($R_m$)

Middle cerebral artery occlusion (MCAo)

Monocyte chemoattractant protein (MCP)

Naval Medical Research Institute (NMRI)

Neuron-glia 2 (NG2)

Phosphate buffer (PB)

Phosphate buffer saline (PBS)

Pipette resistance ($R_p$)

Regulated upon Activation - Normal T cell Expressed and Secreted (RANTES)

Room temperature (RT)

Stromal cell-derived factor (SDF)

Tetraethylammonium (TEA)

Tetrodotoxin (TTX)

Tris-HCl buffer (TB)

Tumor necrosis factor (TNF)

# 1 Introduction

## *1.1 Microglia in the developing brain*

### 1.1.1 Microglial dynamics in development

Microglia, unlike neurons and macroglial cells, are of mesodermal lineage and infiltrate the central nervous system (CNS) early in development (Perry and Gordon, 1991; Cuadros and Navascues, 2001). Rio-Hortega (1932) identified regions of microglial invasion at the corpus callosum and other white matter areas and named them *fountains of microglia*. In rodents, the number of microglia transiently increases during the last days of embryonic and first two weeks of postnatal days (Milligan et al., 1991). Ling (1979) demonstrated that blood monocytes invade the early postnatal brain at the corpus callosum and become ameboid microglia (AMG). It appears that several routes of entry constitute subpopulations of microglia in the CNS at different stages of life (Provis et al., 1996). A large number of cells enter through the meninges by traversing the pial surface. They can also enter through the ventricular space by squeezing between the neuroepithelial cells. Other cells in the circulating blood may enter the brain parenchyma through the endothelial wall (Navascues et al., 2000). The fact that the blood-brain barrier (BBB) is not fully developed until the second week of birth in rodents allows an efficient early invasion of microglia required for later development (Xu et al., 1993). It is generally believed that the majority of microglial precursors come from the meninges and ventricular lumen during embryonic development, while entry through blood stream predominates in mature brains (Navascues et al., 2000).

Once in the CNS, these highly motile AMG perform active phagocytosis of cellular debris in response to naturally occurring cell death (Ferrer et al., 1990; Brockhaus et al., 1996). They could also promote brain tissue remodeling by directly influencing neuronal survival and growth of their processes (Thery et al., 1991; Chamak et al., 1994; Mallat and Chamak, 1994). Microglial migration has been well documented in retina, optic tectum and cerebellum (Navascues et al., 2000). It is believed that AMG in these and other CNS regions make use of their processes in dispersing themselves (Brockhaus et al., 1996; Cuadros et al., 1997). They migrate first tangentially parallel to the CNS surface along

axonal tracts and then radially perpendicular to the surface into different layers of the nervous parenchyma (Cuadros et al., 1994; 1997). This is in line with the observation that AMG are first seen in the white then grey matter (Perry et al., 1985). Naturally occurring cellular processes like axon growth and cell rearrangement modulate microglial behavior in the developing brain (Cuadros and Navascues, 1998). Similarly, cell death may also be an important cue for microglial migration (Pearson et al., 1993). Ameboid but not ramified microglia are strongly immunoreactive to thrombospondin, a prominent factor present during axonal growth suggesting that microglia alter their receptor expression patterns throughout development (Chamak et al., 1995).

Proliferation of microglia occurs in many regions of the developing CNS including the corpus callosum (Ling and Tan, 1974; Imamoto and Leblond, 1978; Kaur and Ling, 1991). Márin-Teva et al. (1999) have demonstrated that AMG in the developing quail retina undergo alternating stages of migration and mitosis. This process peaks between postnatal day 5 and 10 and progressively decreases as the brain matures (Perry and Gordon, 1991; Ling and Wong, 1993). Studies mostly carried out *in vitro* have identified factors like neurotrophin-3, interleukin-4 (IL-4), IL-5, pigment epithelium-derived factor, and adrenergic agonists in regulating microglial proliferation (Suzumura et al., 1994; Ringheim, 1995; Elkabes et al., 1996; Sugita et al., 1997; Fujita et al., 1998). Astrocytes and neurons may modulate microglial proliferation presumably by secreted factors (Elkabes et al., 1996; Dobbertin et al., 1997; Streit et al., 1999). Although many of these factors are found in the developing brain, direct evidence of their effects on the expansion of microglial population *in vivo* has not yet been resolved.

At their destinations, microglia differentiate into a ramified phenotype and show changes in immunophenotypical characteristics including expression of surface markers (Cuadros and Navascues, 1998). Such transformation occurs between the second and third postnatal weeks (Ling and Wong, 1993). In adult CNS, proliferation of resident microglia and recruitment of circulating monocytes across intact BBB account for a slow turnover of microglial population (Lawson et al., 1992). It is believed that microglia are less ramified in brain regions rich in plasma proteins which are normally excluded by complete BBB in other regions (Perry and Gordon, 1991). Astrocytes also promote ramification of microglia *in vitro* (Suzumura et al., 1994; Eder et al., 1997; Fujita et al., 1998; Tanaka et al., 1999).

While these cells have always been thought to be quiescent and resting, recent advances in *in-vivo* imaging clearly showed that they are constantly sensing the environment with their processes (Davalos et al., 2005; Nimmerjahn et al., 2005). Thus, it is believed that microglia carry out active tissue scanning and quickly respond to injury by transforming to their activated states (Hanisch and Kettenmann, 2007). Activated microglia then undergo microgliosis and efficiently increase in number (Streit et al., 1999). This is accompanied by the recruitment of bone marrow-derived cells into the neural parenchyma (Ladeby et al., 2005). Interestingly, many immunohistochemical features present in AMG but lost in ramified microglia reappeared after activation (Streit et al., 1988).

As various mechanisms account for entrance, colonization, proliferation and differentiation of microglial populations at different developmental and injury states, it is essential that invading microglia early in development should be considered as a unique population and studied only in relevant context. *Fig. 1* illustrates dynamics and expansion of microglial populations in the developing brain. While many microglial behaviors are influenced by the environment, details of how invading microglia incorporate themselves into the neural parenchyma *in vivo* are yet to be elucidated.

### 1.1.2 Microglial potassium channels

Like peripheral macrophages, microglia express a variety of ion channels conducting the movement of $K^+$, $Na^+$, $H^+$, $Ca^{2+}$ and $Cl^-$ ions across the plasma membrane (Eder, 1998, 2005; Farber and Kettenmann, 2005). They have important roles in regulating membrane potential (MP), cell volume and intracellular ion concentrations which in turn modulate microglial proliferation, migration, cytokine secretion, as well as shape changes (Eder, 1998, 2005). Among them, $K^+$ channels are particularly important for stabilizing microglial MP at around -70 mV. The inward rectifying $K^+$ ($K_{ir}$) channels detected in all microglia preparations are open upon membrane hyperpolarization and sensitive to extracellular $Ba^{2+}$, $Cs^+$, tetraethylammonium (TEA), and quinine (Norenberg et al., 1994). A single channel conductance of 30 pS typical for classical $K_{ir}$ channels was previously recorded in cultured microglia (Kettenmann et al., 1990). Time- and voltage-dependent inactivation of $K_{ir}$ currents occurs due to blockade by extracellular $Na^+$ (Standen and Stanfield, 1979).

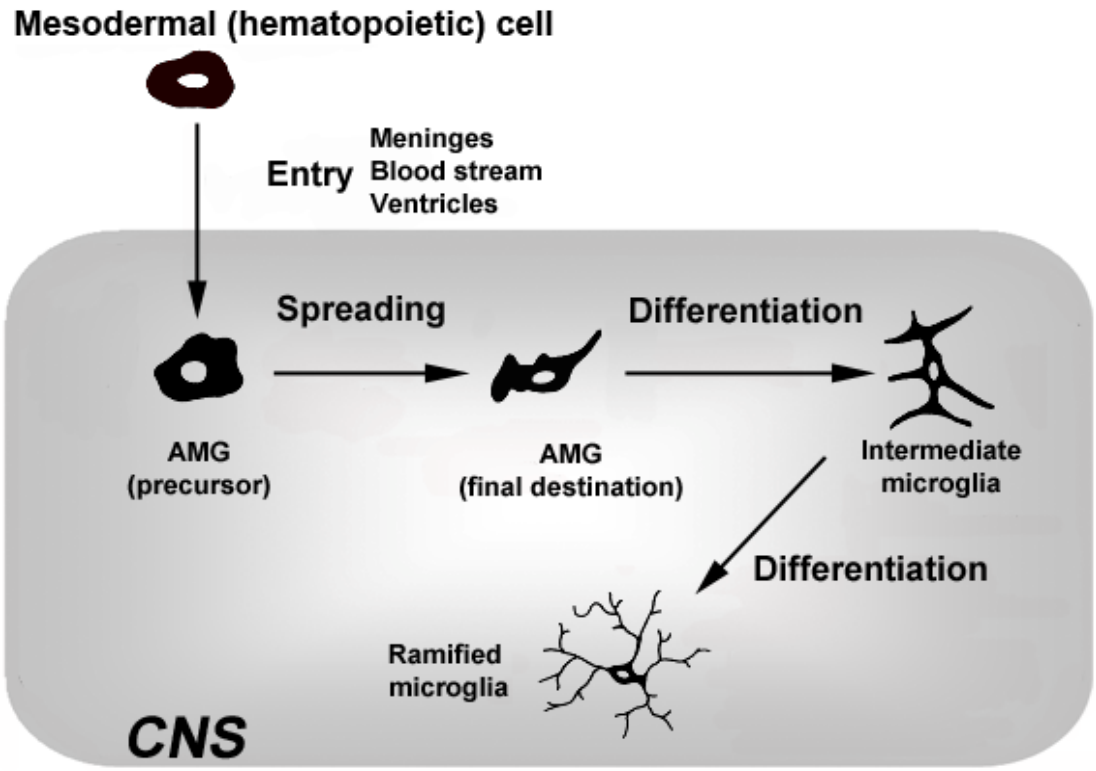


**Fig. 1. Developmental fate of microglia.** Most authors believe that microglial precursors are of mesodermal origin and enter the developing CNS through different routes. Upon entry, ameboid microglia (AMG) proliferate and migrate through the CNS ('spreading'). Once they reach their final locations, differentiation into ramified microglia occurs. *Adapted from (Cuadros and Navascues, 1998)*.

With elevated extracellular potassium concentration ($[K^+]_o$), the reversal potential of $K_{ir}$ current becomes more positive leading to an increase in chord conductance (Eder et al., 1995b). It is believed that Kir2.1 encodes for microglial $K_{ir}$ channels given its characteristic properties of macrophage Kir2.1 channels and the presence of Kir2.1 transcripts in microglia culture (Kubo et al., 1993; DeCoursey et al., 1996; Schilling et al., 2000). In many cases where $K_{ir}$ channels are closed, voltage-gated delayed rectifying $K^+$ ($K_{dr}$) channels take over in regulating $K^+$ homeostasis. For example, $K_{dr}$ channels are important in stabilizing activated microglia in which $K_{ir}$ channels are mostly closed (Norenberg et al., 1994). They are activated at -40 mV and increase in amplitude as the cell depolarizes and are blocked by substances like 4-aminopyridine, TEA, $Ba^{2+}$, $Cd^{2+}$, and $Zn^{2+}$ (Norenberg et al., 1994; Schilling et al., 2000). Apart from maintaining MP, $K^+$ channels may also modulate microglial cytokine release and proliferation. In particular, microglial nitric oxide

release and proliferation are regulated by Kv1.5 and/or Kv1.3 channel expression (Pannasch et al., 2006). Furthermore, it was demonstrated that $K^+$ efflux via $K_{dr}$ channels was required for the conversion of proinflammatory cytokine IL-1β into its mature and active form (Cheneval et al., 1998; Sanz and Di Virgilio, 2000). Prominent $K_{ir}$ current was detected in proliferating microglia implying its potential regulatory functions (Schlichter et al., 1996). Conversely, proliferation of activated microglia lacking $K_{ir}$ current relied on $K_{dr}$ channels (Kotecha and Schlichter, 1999).

Functional importance of microglial $K^+$ channels is reflected by changes in membrane currents throughout development and pathology (*Fig. 2*). Ramified microglia *in situ* express very little, if any, voltage-gated current and are considered “resting” (Boucsein et al., 2000). Postnatal (Brockhaus et al., 1993) and cultured microglia (Kettenmann et al., 1990), on the other hand, express large $K_{ir}$ currents. Upon stimulation with lipopolysaccharide (LPS), a membrane component of gram-negative bacteria, pronounced $K_{dr}$ current often accompanied by decreased $K_{ir}$ current is detected (Norenberg et al., 1992). In response to brain injury imposed by facial nerve axotomy, microglia *in situ* transiently acquire first inward then outward rectifying $K^+$ currents (Boucsein et al., 2000).

Apparently, microglial $K^+$ channel activities are tightly regulated to maintain ion homeostasis for many cellular processes. Further understanding of potential functions of these channels, especially during brain development, will be of great benefits.

### 1.1.3 Chemokines as neuromodulators

Cytokines are small proteins used to signal between cells and are important for many physiological and pathological cellular processes in the nervous systems. Those that are responsible for regulating cell migration are called chemotactic cytokines or chemokines. They are divided into four subclasses based on spacing of cysteine residues which are C, C-C (β), C-X-C (α), and C-$X_3$-C (Laing and Secombes, 2004). In general, α- and β-chemokines predominantly attract neutrophils and mononuclear phagocytes, respectively. While constitutive microglial release of chemokines is often low, rapid release occurs under stress or in the presence of pathogens (Hanisch, 2002). Thus, the majority of studies focus on their functions in inflammation, neuroprotection, as well as glial activation (Aloisi, 2001; Bajetto et al., 2002). Upon stimulation, microglia release chemokines like growth regulated

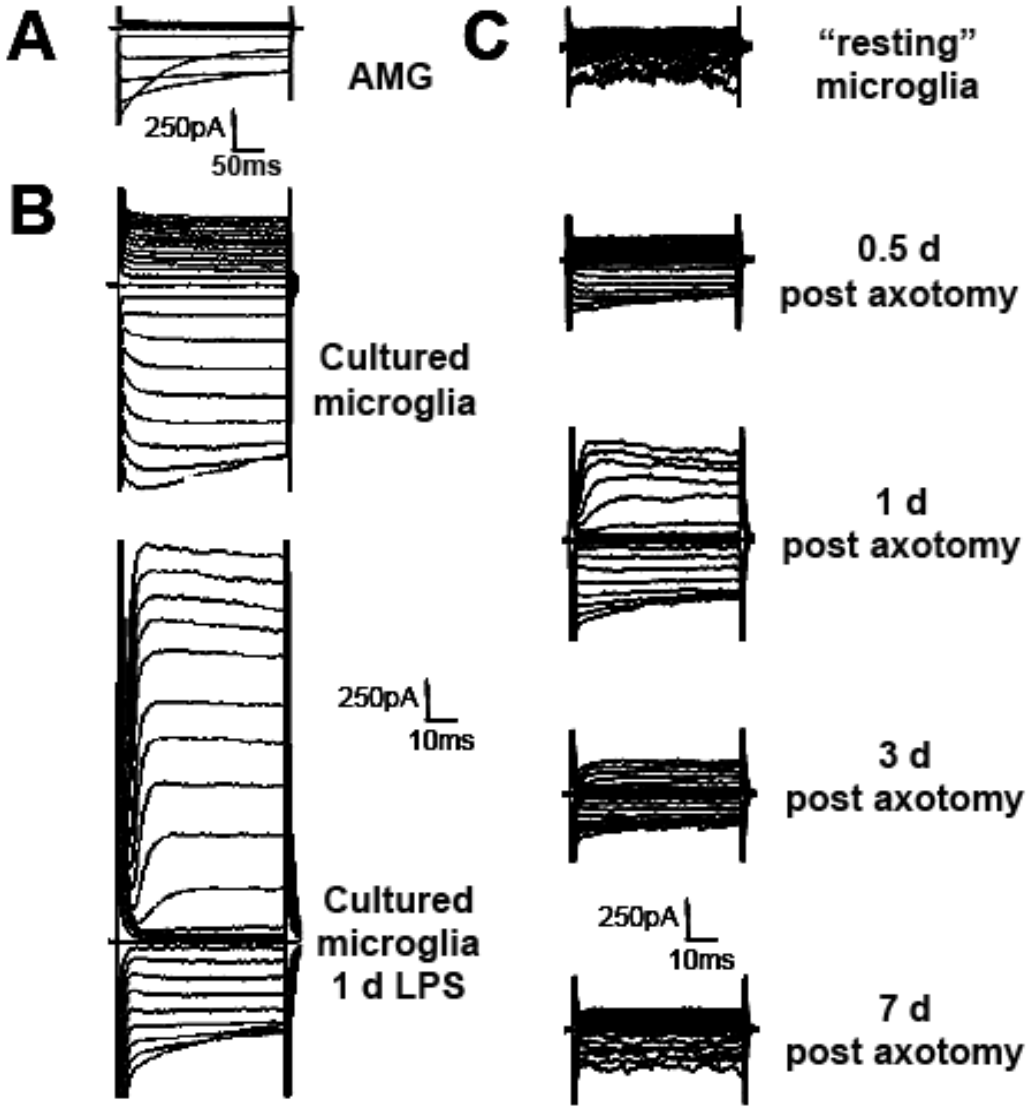


**Fig. 2. Dynamics of microglial $K^+$ currents.** Changes in $K^+$ currents are shown for **(A)** an ameboid microglia on postnatal corpus callosum brain slice; **(B)** cultured microglia before and after LPS stimulation; and **(C)** microglia on adult brain slice 0 ("resting"), 0.5, 1, 3 and 7 days after facial nerve axotomy. Each cell was voltage clamped at -70 mV. Membrane currents were activated by de- and hyperpolarizing voltage steps at 10-mV increments. *Adapted from (Haas et al., 1996; Boucsein et al., 2000; Farber and Kettenmann, 2005).*

oncogene α or keratinocyte-derived chemokine (GROα or KC), macrophage inflammatory protein 1 $\alpha$ (MIP-1α), MIP-1β, MIP-2, monocyte chemoattractant protein-1 (MCP-1), RANTES (for "regulated upon activation, normal T cell expressed and secreted"), interferon-inducible protein-10, and IL-8 to recruit leukocytes to the sites of injury (Hanisch, 2002; Ambrosini and Aloisi, 2004). As immune cells of the CNS, microglia also express

functional receptors allowing them to sense and to be modulated by chemokines (Hanisch, 2002; Farber and Kettenmann, 2005). Most of them are G-protein coupled receptors leading to mobilization of $Ca^{2+}$ from internal stores to the cytosol which in turn modulate microglial chemotaxis and downstream immune responses. Microglial receptors for β-chemokines MCP-1, RANTES, and MIP-1α have been detected *in vitro* (Boddeke et al., 1999). Furthermore, Albright et al. (1999) have observed functional CCR5 and CXCR4 receptors which bind MIP-1β and stromal cell-derived factor-1 (SDF-1), respectively. Activation of CXCR3 by CCL21 also promoted chemotaxis and triggered a long lasting $Cl^-$ conductance in cultured microglia (Biber et al., 2001; Rappert et al., 2002).

Recent findings have supported chemokines as neuromodulators which play important roles in development, neuronal survival, neurohormonal actions, and behavior (Rostene et al., 2007). In particular, the similarities between hematopoiesis and neuropoiesis have led to investigations of possible roles of chemokines in attracting neurons and glial cells in the CNS. Several known chemokine and receptor systems including SDF-1/CXCL12, RANTES/CCL5, MCP-1/CCL2, MIP-1α/CCL3, IL-8/CXCL8, GRO-α(or KC)/CXCL1, and fractalkine/CX3CL1 are constitutively expressed in the CNS and appear to be regulated by developmental processes (Ambrosini and Aloisi, 2004). It was demonstrated that SDF-1 could promote migration of embryonic neural progenitor cells *in vitro* (Lazarini et al., 2000; Tran et al., 2004) and regulate axonal patterning in developing hippocampal neurons (Pujol et al., 2005). The release of dopamine and vasopressin from neurons can also be modulated by SDF-1 (Callewaere et al., 2006; Skrzydelski et al., 2007). *In vivo* studies using mice deficient for SDF-1 and its receptor revealed the importance of this chemokine system in cell migration in normal brain development (Ma et al., 1998). Cultures of human fetal glial cells express receptors for chemokines and release MCP-1 upon stimulation, suggesting possible involvement of chemokines as regulatory factors during development (Rezaie et al., 2002a; Cartier et al., 2005). MIP-1α regulates proliferation of hematopoietic stem cells at different stages of development (Broxmeyer and Kim, 1999). MIP-1α and MCP-1 treatment could also promote astrocyte migration *in vitro* possibly via novel astrocytic receptors (Heesen et al., 1996). Moreover, subnanomolar concentration of MIP-1α could induce chemotactic response in astrocytes *in vitro* (Tanabe et al., 1997). Interestingly, roles of chemokines like IL-8 and GROα in synaptic activity in mouse

cerebellum have also been postulated (Giovannelli et al., 1998). In addition, synergy between GROα and platelet derived growth factor (PDGF) mediates oligodendrocyte precursor proliferation (Robinson et al., 1998). While roles of chemokines and their receptors in inflammatory response are well accepted, other functions including those related to expansion of glial and precursor cell population during development cannot be overlooked. In this respect, contribution of microglia, the major source of chemokines in the CNS, to these processes is to be further investigated.

### 1.1.4 Neurotransmitters and development

As active sensors of the environment, microglia express a large repertoire of functional neurotransmitter receptors, some of which are relevant for the developing brain (Farber and Kettenmann, 2005; Pocock and Kettenmann, 2007). Stimulation of these receptors is often coupled to changes in $K^+$ conductance and/or intracellular calcium concentration ($[Ca^{2+}]_i$) leading to downstream effects important for microglial functions. From a basal $[Ca^{2+}]_i$ of 50 – 150 nM, receptor-mediated transient $Ca^{2+}$ influx into microglia is an important mechanism present in many signal transduction pathways. Microglia including AMG express a variety of purinergic receptor subtypes whose activation by adenosine triphosphate (ATP) increases cationic and $K^+$ conductance as well as $[Ca^{2+}]_i$ (Haas et al., 1996; Farber and Kettenmann, 2006). As a result, microglial properties like motility and migration (Honda et al., 2001; Nimmerjahn et al., 2005; Haynes et al., 2006; Farber et al., 2008), cytokine release (Hide et al., 2000; Suzuki et al., 2004); reactive oxygen species release (Parvathenani et al., 2003), and phagocytosis (Koizumi et al., 2007) were modulated. It was observed that microglia *in situ* could sense astrocytic $Ca^{2+}$ waves via their purinergic receptors (Schipke et al., 2002). In addition, functional expressions of adrenaline and dopamine receptors have also been detected on cultured microglia and AMG (Farber et al., 2005). It is speculated that enhanced migration as a result could attract microglia towards regions of purinergic, adrenergic and dopaminergic transmission relevant for the developing brain (Farber et al., 2005). Although no synaptic connections between microglia and neurons has ever been observed, receptors for major neurotransmitters mostly associated to inflammatory responses are present on microglia. Glutamate receptors were detected on rat microglia *in vitro* whose activation were coupled to transient

increase in $[Ca^{2+}]_i$ and release of tumor necrosis factor-$\alpha$ (TNF-α) and Fas ligand which in turn regulated neuronal death and protection (Pin and Duvoisin, 1995; Noda et al., 2000; Taylor et al., 2003; Hagino et al., 2004; Taylor et al., 2005). Microglia *in vitro* and *in situ* can sense gamma-amino-butyric acid (GABA) via $GABA_B$ receptors resulting in an increase in $K^+$ conductance and $[Ca^{2+}]_i$ (Kuhn et al., 2004). The authors have demonstrated that cytokine release by activated microglia was attenuated by simultaneous $GABA_B$ receptor activation suggesting anti-inflammatory effect.

In the developing brain, GABA is released from growth cones of developing axons prior to synapse formation (Gao and van den Pol, 2000). It acts as a trophic factor regulating various important processes in development. Haydar et al (2000) showed that GABA and glutamate activities modulate proliferation of neural progenitor cells. Cortical migration of postmitotic cells was also regulated by differential $GABA_A$ receptor stimulation (Behar et al., 2000; Heck et al., 2007). It was also observed that $GABA_A$ receptor activation together with L-type $Ca^{2+}$ channels in differentiating neurons promote neurite outgrowth (Maric et al., 2001). Furthermore, Barbin et al. (1993) observed that $GABA_A$ receptors played a role in outgrowth of hippocampal neurons *in vitro*. The formation of neuronal circuits during brain development requires intricate mechanisms involving different cell types and signaling molecules. GABAergic precedes glutamatergic activities in a developing brain acting as a source for neuronal excitation (Balslev et al., 1996). This is enabled by the fact that $GABA_A$ receptors are expressed on neurons since embryonic stages and are excitatory in immature neurons (Cobas et al., 1991; Balslev et al., 1996). Although presynaptic $GABA_B$ receptors are present since birth, those mediating postsynaptic inhibition appears only later (Gaiarsa et al., 1995). Subsequently, glutamate receptors which are previously 'silent' become functional mediating glutamatergic synapses (Isaac et al., 1997). Kullmann et al. (1996) attributed this to glutamate spill-over preferentially promoting functional receptors (Patneau and Mayer, 1990). Thus, it is suggested that $GABA_A$ and glutamate receptors display activity dependent sequential participation to neuronal excitation (Ben-Ari et al., 1997).

$GABA_A$ receptors are ligand-gated ion channels permeable to $Cl^-$. The direction of ion flux is directly related to intracellular chloride concentration ($[Cl^-]_i$) (Kaila, 1994). In mature neurons, stimulation of $GABA_A$ receptor is hyperpolarizing thus inhibitory (*Fig. 3*). In

immature neurons, on the other hand, membrane depolarization occurs due to high $[Cl^-]_i$ giving rise to an excitatory response (Martina et al., 2001; Marandi et al., 2002; Gulledge and Stuart, 2003). As $[Cl^-]_i$ progressively decrease in development, the negative shift of the reversal potential of GABA during the second postnatal week parallels excitatory to inhibitory (E-I) switch of the action of GABA. (Kuner and Augustine, 2000; Marandi et al., 2002). Ganguly et al., (2001) observed that GABA itself promotes such switch in GABAergic responses. In particular, $GABA_A$ receptor-mediated $Ca^{2+}$ influx regulates the late expression of KCC2, a transporter responsible for extruding $Cl^-$ ions from the cells.

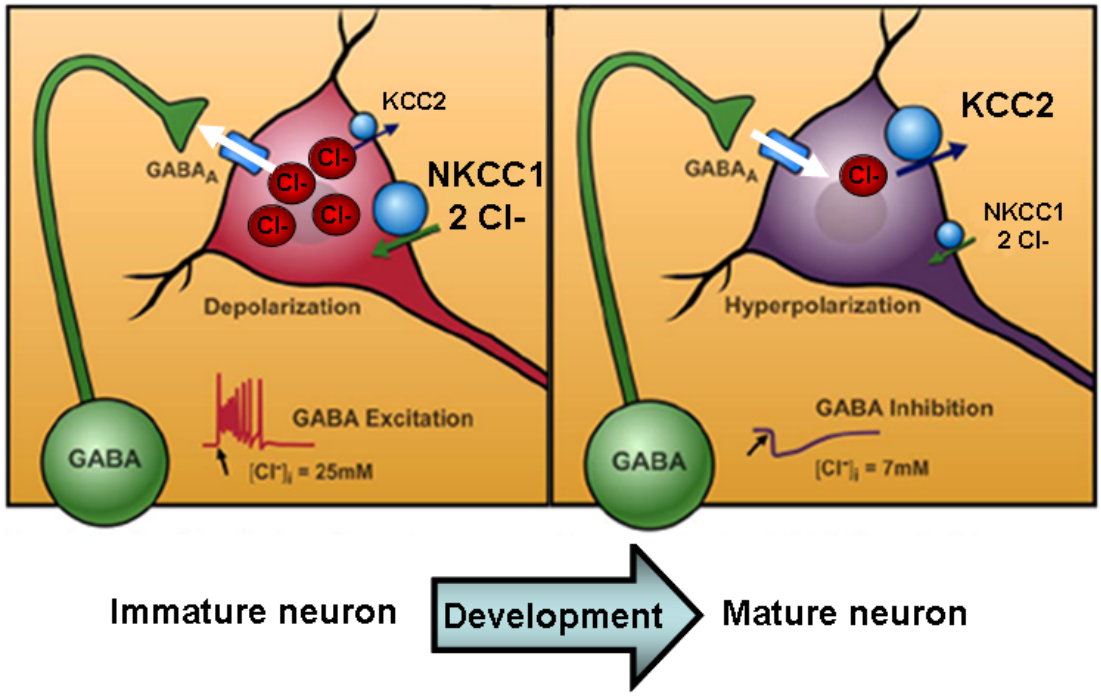


**Fig. 3. E-I switch of neuronal $GABA_A$ receptors.** High $[Cl^-]_i$ is maintained in immature neurons by NKCC1. As a result, $GABA_A$ receptor activation leads to efflux of $Cl^-$ and depolarization. $Cl^-$ extruder KCC2 is expressed late in development and contributes to low $[Cl^-]_i$ in mature neurons. Thus, hyperpolarization occurs due to $Cl^-$ influx upon $GABA_A$ receptor. *Adapted from (Ben-Ari et al., 2007)*.

Vertebrate macroglial cells also express glutamate and GABA receptors (Von Blankenfeld et al., 1991). Due to constantly high $[Cl^-]_i$, $GABA_A$ receptor stimulation by GABA or the specific agonist, muscimol, is always depolarizing as observed in cultured astrocytes and oligodendrocytes (Bowman and Kimelberg, 1984; Gilbert et al., 1984). This was also demonstrated in mouse postnatal corpus callosum (Berger et al., 1992) and hippocampal

slices (Steinhauser et al., 1994), as well as Bergmann glial cells (Muller et al., 1994) suggesting their extrasynaptic functions.

Apart from acting as a classical inhibitory neurotransmitter, GABA has other functional roles synergistic to glutamate in the developing brain. The potential involvement of glial $GABA_A$ receptors in developmental processes promotes further studies exploring interactions between glia and developing networks. At present, functional $GABA_A$ receptors have not been detected on any microglia preparations.

## *1.2 Astrocytes in the injured brain*

### 1.2.1 Functional heterogeneity of astrocytes

It has become evident that astrocytes express a large variety of ion channels and receptors through which communications with neurons take place (Verkhratsky and Steinhauser, 2000; Haydon, 2001). Electrophysiological properties of glial cells have been extensively investigated in the hippocampus using acute brain slices. Steinhauser et al. (1992; 1994) have differentiated two types of astroglial cells in the hippocampus and called them passive and complex cells based on their membrane properties. Later studies have shown that complex cells express functional glutamate receptors but lack transporters and vice versa in passive cells (Seifert and Steinhauser, 1995; Zhou and Kimelberg, 2001). Morphological distinctions among astrocytes were further revealed using transgenic mice in which enhanced green fluorescent protein (EGFP) is expressed under the control of the glial fibrillary acidic protein (GFAP) promoter (Matthias et al., 2003). In the hippocampus, brightly fluorescent cells have branching nets of processes and are mostly GFAP immunopositive; whereas the weakly fluorescent cells consistently lack GFAP protein expression and have short, thin processes (Matthias et al., 2003). Furthermore, the majority of brightly and weakly fluorescent cells have typical passive and complex membrane currents, respectively (Matthias et al., 2003). The expression of glutamate transporters by brightly fluorescent astrocytes allowed glutamate uptake and release which is important for regulating glutamatergic synaptic activities (Anderson and Swanson, 2000). The weakly fluorescent cells, on the other hand, also include glial cells positive for proteoglycan NG2 which stands for “neuron-glia 2” (Matthias et al., 2003). These NG2 cells were first considered precursor cells in the oligodendrocyte lineage and have been shown

to receive glutamatergic synaptic input (Bergles et al., 2000). Furthermore, synapses between neurons and NG2 positive cells undergo activity-dependent modifications analogous to long-term potentiation at excitatory synapses (Ge et al., 2006). Thus, astrocytes comprise of heterogeneous populations with distinctive membrane properties, GFAP promoter activity, morphology as well as response towards glutamate. These differences are essential for distinct functions in the brain.

### 1.2.2 Astrocytes in response to brain injury

Functional properties of astrocytes change during injury and disease (Verkhratsky and Steinhauser, 2000). In the process called astrogliosis, the brain responds to injury by an increase in the number of hypertrophic astrocytes with up-regulation of GFAP. As a result, these reactive astrocytes express voltage-gated currents depending on their proliferation state (MacFarlane and Sontheimer, 1997; Bordey et al., 2000; Hinterkeuser et al., 2000; Bordey et al., 2001). Up-regulation in outwardly rectifying $K^+$ currents in reactive astrocytes thought to be involved in controlling cell proliferation was observed *in situ* (Bordey and Sontheimer, 1998; Bordey et al., 2001) and *in vitro* (MacFarlane and Sontheimer, 1997; Perillan et al., 1999; 2000; Anderova et al., 2004). Furthermore, after focal cortical freeze-lesion, dividing cells showed an enhanced expression of $K_{dr}$ channels but did not express $K_{ir}$ channels (Bordey et al., 2000; 2001). Astrocytes also respond towards brain ischemia and associated neuronal death (Contreras et al., 2004; Rossi et al., 2007).

One way by which astrocytes communicate among themselves is through gap junctions. These are specialized transmembrane pores between two cells made up of two opposing hemichannels composed of connexins. As ions and small molecules < 1 kDa can pass freely between these cells, intracellular signaling molecules and electrical currents can propagate from one cell to the next (Giaume and McCarthy, 1996). In $K^+$ spatial buffering, astrocytes remove $K^+$ ions from the extracellular space at one location and transport them within a network of cells and eventually extrude the ions at other sites (Horio, 2001). The expression and permeability of gap junctions are tightly regulated under physiological and pathological conditions. In the hippocampus, astrocytes expressing glutamate transporters display extensive gap junction coupling which is completely absent in cells with glutamate receptor expression (Wallraff et al., 2004). It has been established that membrane

depolarization as a result of ischemia promotes gap junction opening while other signals like dephosphorylation, lowered *pH*, and elevated $Ca^{2+}$ level lead to closure (Contreras et al., 2004). Short-term middle cerebral artery occlusion (MCAo) followed by reperfusion has been used as a model for mild brain ischemia to study the impact of ischemia on astrocyte physiology. Thirty minutes MCAo/reperfusion confers delayed neuronal cell death and astrogliosis in the striatum sparing the cortex (Endres et al., 1998; Katchanov et al., 2001; 2003). Astrocytic coupling plays diverse and important roles during focal ischemia in that toxic substance from astrocytes in the core of lesion can diffuse to healthier cells in the penumbra. Conversely, health-promoting molecules can diffuse into dying cells in the reversed direction (Rossi et al., 2007). At present, both beneficial and detrimental effects of gap junction coupling have been supported (Blanc et al., 1998; Lin et al., 1998; Frantseva et al., 2002; Nakase et al., 2003a; Nakase et al., 2003b; Perez Velazquez et al., 2003).

Increased levels of extracellular glutamate and other neurotransmitters occur in response to ischemia (Phillis et al., 1996). Whereas vesicular release of glutamate from astrocytes occur in response to increased $[Ca^{2+}]_i$ (Montana et al., 2006), the major source of extracellular glutamate accumulation is through reversed glutamate uptake (Phillis et al., 2000; Rossi et al., 2000). Specifically, it appears that during early phases of ischemia, neurons release glutamate and astrocytes take it up as transporters on neurons are more likely to reverse (Ottersen et al., 1996; Silver et al., 1997). This process may serve as a mechanism of glutamate clearance thus conferring neuroprotection. However, as uptake of glutamate continues in prolonged ischemia, astrocytes may eventually reach a stage where they begin to release glutamate and thereby promote neurodegeneration (Mitani and Tanaka, 2003).

# 2 Objectives and Hypotheses

Increasing evidence revealed distinctive roles of glial cells in the brain under both physiological and pathological situations. Microglia can sense the environment via ion channels and neurotransmitter receptors (Farber and Kettenmann, 2005; Pocock and Kettenmann, 2007). While many studies focused on immunomodulatory properties of microglia, their functions in postnatal brain development are yet largely unknown. In particular, postnatal invading microglia as a unique subpopulation may have potential interactions with GABAergic innervations in the maturing brain (Ben-Ari et al., 2007). Similarly, astrocytes are heterogeneous in terms of morphology, protein expression, membrane currents and neurotransmitter receptor expression (Matthias et al., 2003). In contrast to microglia, one population of astrocytes in the hippocampus forms extensive gap junction networks propagating signals across the brain (Wallraff et al., 2004) whereas another glial subtype receives synaptic signals from neurons (Bergles et al., 2000). These properties are particularly important during brain ischemia where toxic substances like glutamate and $K^+$ accumulate in the extracellular space upon neuronal death (Rossi et al., 2007). As an experimental model, short mild brain ischemia affects the striatum where changes in glial properties have been explored (Katchanov et al., 2001; 2003; Kronenberg et al., 2005).

## *2.1 Objectives*

The aim of this study was to investigate properties of glial cells during development and disease in two independent projects.

**Project 1** was designed to establish the role of invading microglia in the developing mouse brain. In particular, their response towards GABAergic activities in acute brain slices was investigated. Specific aims were to:

1. detect and characterize functional $GABA_A$ receptors on microglia;
2. compare microglial response between postnatal and developed brain;
3. investigate functional outcome in microglial behaviors, namely motility, migration, proliferation, and cytokine release; and

4. develop convenient and reliable methods to study properties of invading microglia.

**Project 2** was designed to investigate physiological properties of astrocytes in response to mild brain ischemia. In particular, using whole cell patch-clamp recordings, GFAP-EGFP expressing astrocytes in the striatum were characterized before and after mild stroke induced by MCAo/reperfusion. Specific aims were to:

1. characterize subpopulations of astrocytes in terms of GFAP-EGFP expression, morphology, current patterns, glutamate receptor/transporters expression, and gap junction networks; and
2. compare characteristic properties before and at different time points after 30 min MCAo/reperfusion.

## *2.2 Hypotheses*

With **Project 1**, it was hypothesized that invading microglia can sense $GABA_A$ receptor activities in postnatal brain directly by expressing functional receptors and/or indirectly via signals from neighboring cell types. In turn, characteristic microglial properties relevant for development would be modulated. With these, it was intended that functional significance of invading microglia, particularly towards postnatal neurotransmitter innervations, could be revealed. With **Project 2**, it was predicted that, like in other brain regions, astrocytes could be characterized into subpopulations with distinctive physiological properties serving unique functions in the striatum. In response to ischemia, these properties would be altered further revealing their functions in physiology and pathology. These findings may add to the growing evidence of the role of astrocytes in neuroprotection. As a result, specific properties of glial cells in development and injury could be recognized by these studies.

# 3 Materials and Methods

## *3.1 Materials*

### 3.1.1 Drugs and chemicals

**Table 1. List of drugs and chemicals**

| Name | Company |
|---|---|
| Adenosine triphosphate (ATP) | Sigma-Aldrich, Munich, Germany |
| (D)-Aspartic acid (D-Asp) | Sigma-Aldrich, Munich, Germany |
| Baclofen | Sigma-Aldrich, Munich, Germany |
| Biocytin | Sigma-Aldrich, Munich, Germany |
| Bovine Serum Albumin (BSA) | Fluka Chemie, Buchs, Switzerland |
| 6-Cyano-7-nitroquinoxaline-2,3-dione (CNQX) | Sigma-Aldrich, Munich, Germany |
| Cytochalasin D (CytoD) | Sigma-Aldrich, Munich, Germany |
| Deoxyribonuclease | Worthington, Lakewood, NJ, USA |
| Diaminobenzidine (DAB) | Sigma-Aldrich, Munich, Germany |
| Diff-Quik® stain set | Medion Diagnostics, Düdingen, Switzerland |
| Dimethylsulfoxide | Sigma-Aldrich, Munich, Germany |
| Dulbecco's Modified Eagle Medium (DMEM) | Gibco, Eggenstein, Germany |
| Elite ABC kit | Vector Lab.,Burlingame, CA, USA |
| Ethylene glycol tetraacetic acid (EGTA) | Sigma-Aldrich, Munich, Germany |
| Fetal Calf Serum (FCS) | Gibco, Eggenstein, Germany |
| Gabazine | Tocris Cookson Inc., Bristol, UK |
| Glial fibrillary acidic protein (GFAP) antibody | DAKO, Hamburg, Germany |
| Glutamate | Fluka Chemie, Buchs, Switzerland |
| (L)-Glutamine | Biochrom AG, Berlin, Germany |
| Glutaraldehyde | Sigma-Aldrich, Munich, Germany |
| Glycerol | Sigma-Aldrich, Munich, Germany |
| Hank's Balanced Salt Solution (HBBS) | Biochrom AG, Berlin, Germany |
| HEPES | Carl Roth, Karlsruhe, Germany |
| Isolectin $B_4$ (*Griffonia simplicifolia)* | Sigma-Aldrich, Munich, Germany |
| Kainic acid (KA) | Tocris Cookson Inc., Bristol, UK |
| Lipopolysaccharide (LPS) | Sigma-Aldrich, Munich, Germany |
| Muscimol | Tocris Cookson Inc., Bristol, UK |

| | |
|---|---|
| Paraformaldehyde | Merck, Damstadt, Germany |
| Penicillin/Streptomycin | Biochrom AG, Berlin, Germany |
| Poly-L-lysine | Sigma-Aldrich, Munich, Germany |
| Potassium ionophore I cocktail A (Selectophore®) * | Fluka Chemie, Buchs, Switzerland |
| Streptavidin-HRP Conjugate | Biosource, Nivelles, Belgium |
| Sucrose | Merck, Damstadt, Germany |
| Tetramethylbenzidine | Moss Inc., Maryland, USA |
| Tetrodotoxin (TTX) | Tocris Cookson Inc., Bristol, UK |
| Trypsin | Gibco, Eggenstein, Germany |
| Tween 20 | Merck, Hohenbrunn, Germany |

** Institute for Neurophysiology, Charité-Universitätsmedizin Berlin, Germany*

**Table 2. List of fluorescent indicators**

| **Name** | **Company** |
|---|---|
| Tomato lectin-conjugated Alexa Fluor®594 (Linkage) | BioTez GmbH, Berlin, Germany |
| Alexa Fluor®594 | Invitrogen, Carlsbad, CA, USA |
| Tomato (*lycopersicon esculentum)* lectin | Vector Lab.,Burlingame, CA, USA |
| Fluo-4 AM | Invitrogen, Carlsbad, CA, USA |

### 3.1.2 Intra- and extracellular solutions

**Table 3. Solutions for acute brain slices and cell cultures**

| | **Standard Brain Slice Buffer** | **HEPES Buffer** | **Standard Internal Solution** |
|---|---|---|---|
| NaCl | 134 | 150 | - |
| KCl | 2.5 | 5.4 | 130 |
| $C_6H_{12}O_6$ | 10 | 10 | - |
| $MgCl_2 \cdot 6H_2O$ | 1.3 | 1 | 2 |
| $CaCl_2 \cdot 2H_2O$ | 2 | 2 | 0.5 |
| $K_2HPO_4 \cdot 3H_2O$ | 1.25 | - | - |
| $NaHCO_3$ | 26 | - | - |
| HEPES | - | 5 | 10 |
| EGTA | - | - | 5 |
| *pH* | 7.4 | 7.4 | 7.3 |
| Osmolarity (mmol/kg) | 349 | 335 | 283 |

### 3.1.3 Cytokine and proliferation assays

**Table 4. List of antibodies and standards for cytokine assays**

| Name | µg/ml | Company |
|---|---|---|
| ***Anti-mouse capture antibody*** | | |
| IL-12 p40/70 | 1.25 | BD Pharmingen, Heidelberg, Germany |
| IL-6 | 1 | R&D Systems, Wiesbaden, Germany |
| KC | 1 | R&D Systems, Wiesbaden, Germany |
| MIP-1α | 2 | R&D Systems, Wiesbaden, Germany |
| TNF-α* | 0.8 | R&D Systems, Wiesbaden, Germany |
| ***Biotinylated anti-mouse detection antibody*** | | |
| IL-12 p40/70 | 0.625 | BD Pharmingen, Heidelberg, Germany |
| IL-1 | 0.1 | R&D Systems, Wiesbaden, Germany |
| KC | 0.1 | R&D Systems, Wiesbaden, Germany |
| MIP-1α | 0.05 | R&D Systems, Wiesbaden, Germany |
| TNF-α* | 0.3 | R&D Systems, Wiesbaden, Germany |
| ***Recombinant mouse cytokines*** | | |
| IL-12 p40/70 | 0 - 0.002 | R&D Systems, Wiesbaden, Germany |
| IL-6 | 0 - 0.002 | R&D Systems, Wiesbaden, Germany |
| KC | 0 - 0.002 | R&D Systems, Wiesbaden, Germany |
| MIP-1α | 0 - 0.004 | R&D Systems, Wiesbaden, Germany |
| TNF-α* | 0 - 0.002 | R&D Systems, Wiesbaden, Germany |

** Mouse TNF-α/TNFSF1A Duoset Kit (R&D Systems, Wiesbaden, Germany)*

**Table 5. Solutions for cytokine assays**

| Solution | Assay | Content | pH |
|---|---|---|---|
| PBS | TNF-α | 137 mM NaCl + 2.7 mM KCl +8.1 mM $Na_2HPO_4$ + 1.5 mM $KH_2PO_4$ | 7.4 |
| | Others | 20mM $NaH_2PO_4/Na_2HPO_4$ + 140mM NaCl | 7.4 |
| Capture PBS | All | PBS | 7.5 |
| Washing Buffer | All | PBS + 0.05% Tween20 | 7.4 |
| Blocking Buffer | IL-12 | PBS + 1% BSA | 7.4 |
| | Others | PBS + 1% BSA + 5% Sucrose | 7.4 |
| Dilution Buffer | IL-12, TNF-α | PBS + 1% BSA | 7.4 |
| | Others | 20mM Tris base+ 150mM NaCl + 0.1% BSA + 0.05% Tween 20 | 7.3 |
| HRP-Diluent | All | PBS + 0.1% BSA + 0.05% Tween20 | 7.4 |

**Table 6. Solutions for proliferation assays**

| Solution | Content |
|---|---|
| BrdU | 1:90 BrdU* in DMEM (10% FCS) |
| Fixative | 70% EtOH + 0.5 M HCl |
| Washing Buffer | PBS* + 10% FCS |
| Nuclease stock | Nuclease* + 50% glycerol |
| Nuclease Solution | 1:100 nuclease stock in incubation buffer* |
| Anti-BrdU Solution | 1:100 Anti-BrdU-POD* in washing buffer + 10 mg/ml BSA |
| ABTS-substrate buffer | ABTS-substrate* in substrate buffer* |
| Peroxidase Solution | 1 mg/ml substrate enhancer* in ABTS-substrate buffer |

** BrdU labeling and detection kit III (Roche, Mannheim, Germany)*

**Table 7. Solutions for immunohistochemistry**

| Solution | Content | pH |
|---|---|---|
| Phosphate buffer (PB) - 0.1 M | 100 mM $Na_2HPO_4$ + 100 mM $NaH_2PO_4$ | 7.4 |
| Tris-buffered saline - 0.05 M | 100 mM Tris-HCl + 100 mM NaCl | 7.4 |
| Tris-HCl buffer (TB) - 0.1 M | 100 mM Tris-HCl | 7.6 |

### 3.1.4 Equipments, apparatus, and computer software

**Table 8. List of equipments and apparatus**

| Name | Company |
|---|---|
| Amplifier (EPC-9) | HEKA Electronics, Lambrecht, Germany |
| Capillaries (borosilicate) | Hilgenberg, Malsfeld, Germany |
| Capillaries (theta glass – double barrel) * | Science Products, Hofheim, Germany |
| CCD Camera (Quanticam) | Phase, Lübeck, Germany |
| Culture flasks and plates | Nunc, Wiesbaden, Germany |
| Digital camera (AxioCam) | Zeiss, Jena, Germany |
| ELISA plates (IMMUNO™plates, MaxiSorp™) | Nunc, Wiesbaden, Germany |
| Filter set for EGFP and Fluo-4<br>Dichroic mirror = 502 nm<br>Emission filter = 535 nm | Omega Optical, Austin, TX, USA |
| Filter sets for Alexa Fluor®594<br>Dichroic mirror = 595 nm<br>Emission filter = 645 nm | Omega Optical, Austin, TX, USA |

| | |
|---|---|
| Filter tips for internal solution (0.22 µm) | Millipore, Carrigtwohill, Ireland |
| Laser Doppler flow meter[+] | Perimed, Jarfälla, Sweden |
| Micro Chemotaxis Chamber (48-well) | Neuroprobe, Gaithersburg, MD, USA |
| Micromanipulator (Patchman) | Eppendorf, Hamburg, Germany |
| Microplate reader (Victor™ 1420) | Perkin Wallac, Freiburg, Germany |
| Microscope (Axioplan) | Zeiss, Jena, Germany |
| Microscope (Axioskop) | Zeiss, Jena, Germany |
| Microscope (Axioskop)* | Zeiss, Jena, Germany |
| Microscope (Axiovert25) | Zeiss, Jena, Germany |
| Monochromator (Polychrom IV) | Till Photonics, Martinsried, Germany |
| Nylon monofilament (8.0) coated with silicone resin /hardener mixture (Xantopren and Elastomer activator)[+] | Bayer Dental, Osaka, Japan |
| Objective 20X – numerical aperture 0.5w | Olympus, Hamburg, Germany |
| Objective 20X – numerical aperture 0.5w* | Zeiss, Jena, Germany |
| Objective 40X – numerical aperture 0.8w | Zeiss, Jena, Germany |
| Objective 4X – numerical aperture 0.1 | Olympus, Hamburg, Germany |
| Objective 40X – numerical aperture 0.5 | Zeiss, Jena, Germany |
| Pipette Puller (P-2000 Laser Based) | Sutter Instrument, Novato, CA, USA |
| Polycarbonate filter (5 µm) | Poretics Corp., Livermore, USA |
| Vaporizer (Fluotec 3)[+] | Colonial Medical, Amherst, NH, USA |
| Vibratome (HM 650V) | Microm, Walldorf, Germany |
| Vibratome (VT 1000 S) | Leica, Heidelberg, Germany |

** Institute for Neurophysiology, Charité-Universitätsmedizin Berlin, Germany*

*[+]Department of Experimental Neurology, Charité-Universitätsmedizin Berlin, Germany*

**Table 9. List of computer software**

| Name | Company |
|---|---|
| Adobe® Photoshop® CS 8.0 | Adobe Systems Inc., San Jose, CA, USA |
| FeliX™ | Photon Technology Int., Wedel, Germany |
| Image Pro® 5.0 | Media Cybernetics, Bethesda, MD, USA |
| Imaging Cells Easily (ICE) 3.5.99 | Max-Delbrück Center, Berlin, Germany |
| Microsoft® Office 2003 | Microsoft, Redmond, WA, USA |
| Origin® 7.0 | OriginLab, Northampton, MA, USA |
| TIDA Version 5.0 | HEKA Electronics, Lambrecht, Germany |
| Wallac 1420 Version 2.01 | Perkin Wallac, Freiburg, Germany |

## *3.2 Animals*

Wildtype Naval Medical Research Institute (NMRI) mice were provided by Charles River Laboratories (Sulzfeld, Germany). Transgenic mice expressing EGFP under the control of the ionized calcium-binding adaptor molecule 1 (Iba1) promoter on a C57/BL6 background were generated by Hirasawa et al. (2005) and obtained from Dr. Kohsaka (Tokyo, Japan). Another transgenic mouse line with GFAP promoter driven EGFP expression on a FVB/N background were generated by Nolte et al. (2001). All animals were bred and maintained in the institutional animal facilities of Max-Delbrück Center (Berlin, Germany) and Charité-Universitätsmedizin Berlin (Berlin, Germany). Animal experiments were approved by official committees and adhere to institutional guidelines.

## *3.3 Induction of mild brain ischemia*

Induction of cerebral ischemia in mice was performed by Shengbo Ji and Karen Gertz in the laboratory of Prof. Dr. Endres at the Department of Experimental Neurology, Charité-Universitätsmedizin Berlin. Mice were first anesthetized with 1.5% isoflurane and maintained in 1.0% isoflurane, 69% $N_2O$ and 30% $O_2$ using a Fluotec 3 vaporizer. Left MCAo was induced according to previously described protocols (Endres et al., 1998). An 8.0 nylon monofilament coated with a silicone resin/hardener mixture was inserted into the left internal carotid artery up to the anterior cerebral artery thereby occludes the middle cerebral artery and anterior choroidal arteries. After 30 min, the filament was withdrawn and reperfusion resumed. To ensure equivalent levels of ischemia, regional cerebral blood flow was measured using laser Doppler flowmetry. Core temperature of the mice was maintained at 36.5 ± 0.5$^{o}$C. Sham-operated animals had filaments inserted into the carotid artery without further advancement.

## *3.4 Acute brain slice preparation*

Postnatal brain slices were prepared from mice between 6 and 8 days old; adult slices from 35 - 40 days old mice. For ischemia experiments, animals were sacrificed on specific days after MCAo/reperfusion. In brief, mice were decapitated and forebrains were carefully removed and washed in freshly prepared standard brain slice buffer continuously gassed to

maintain 5% $CO_2$ and *pH* 7.4. 150 µm thick coronal slices were made at 4°C using a vibratome. They were then gently transferred and maintained in the brain slice buffer and allowed to rest at room temperature (RT; 21 to 25°C) for at least 1 hr before use. Acute slices were used within 6 hr after preparation.

## *3.5 Primary microglia cultures*

Primary microglia cultures were prepared from cerebral cortex of newborn NMRI mice as described previously (Prinz et al., 1999). In brief, cortical tissue was freed of blood vessels and meninges in Hank's Balanced Salt Solution (HBBS) and trypsinized in 1% trypsin and 0.05% deoxyribonuclease for 5 min at RT. It was then dissociated with a fire-polished pipette, and washed twice in HBBS. Dissociated cells were plated on glass coverslips coated with poly-L-lysine and cultured in Dulbecco's Modified Eagle Medium (DMEM) supplemented with 10% fetal calf serum (FCS), 2 mM L-glutamine, and antibiotics (100 units/ml penicillin and 100 µg/ml streptomycin). After 9 – 12 days with medium change every three days, microglia were separated from the underlying astrocytic layer by gentle shaking and collected at 800 rpm for 10 min at 4°C. The cells were then seeded on glass coverslips or 96-well plates at a density of $5 \times 10^4$ cells/coverslip or $2 \times 10^5$ cells/well, respectively. Cultures usually contained >95% microglia detected by isolectin $B_4$ (*Griffonia simplicifolia)* and were used for experiments within 1 to 3 days after plating.

## *3.6 Visualization of cell populations*

### 3.6.1 Setup and equipments

Acute brain slices or culture coverslips were placed in a holding chamber mounted on the stage of an upright light microscope. In order to secure the position of brain slices without disturbing areas of interest, they were kept between a glass coverslip and a U-shaped platinum grid lined with thin threads of nylon. To maintain constant condition during experiments, the chamber was continuously perfused (at 4 ml/min) with standard brain slice or HEPES buffer for brain slices or cultures, respectively. Specimens were viewed at different magnifications using 4X or 40X water immersion objectives. For fluorescence detection, excitation beams consisting of specified single wavelengths were generated by a monochromator controlled by TIDA software via an EPC-9 amplifier. The emitted light was

detected by appropriate sets of filters specific for the fluorophores used. Images were captured by a CCD camera and saved using Imaging Cells Easily (ICE) software.

### 3.6.2 Microglia

After at least 1 hr of rest, large numbers of AMG could be identified on the surface of postnatal brain slices at the corpus callosum region near the lateral ventricles as previously described (Brockhaus et al., 1993). Their distinctive round morphology and large size of over 10 µm in diameter allowed easy identification under light microscopy (*Fig. 4*).

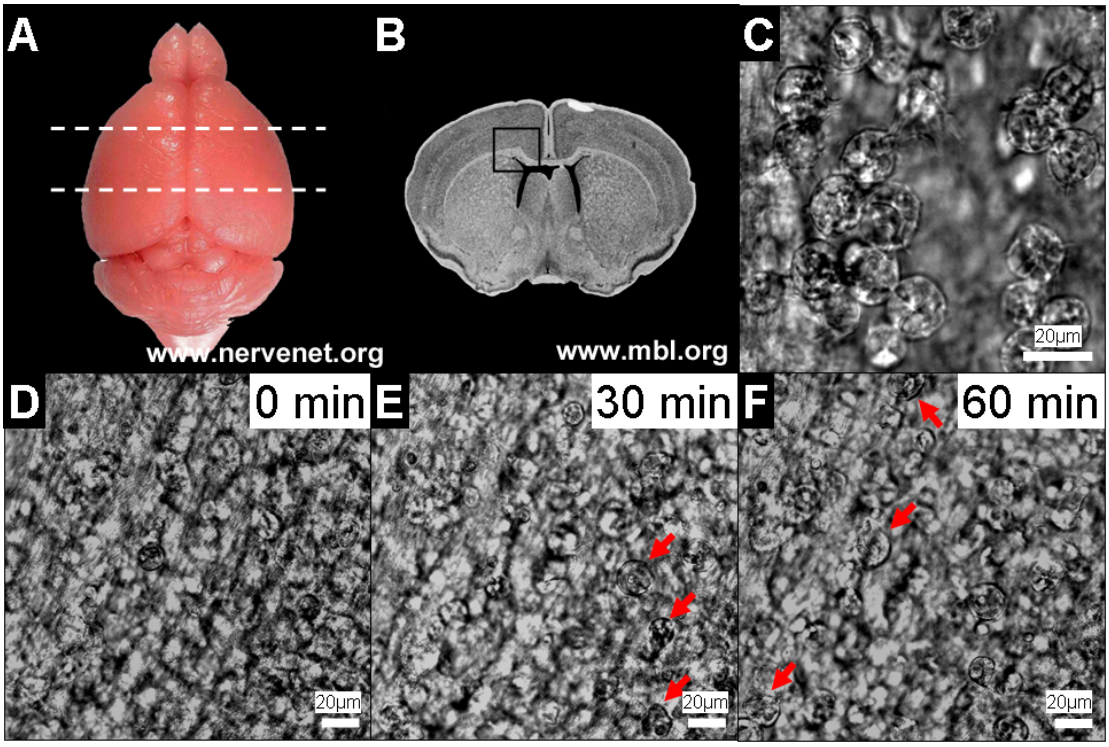


**Fig. 4. Acute brain slice preparation of AMG.** Images of **(A)** a mouse brain with dotted lines marking corpus callosum section, **(B)** coronal slice, and **(C)** large number of AMG on the surface of corpus callosum boxed in B. **(D-F)** Image sequence showing migration of AMG to the surface of slice at 0, 30 and 60 min after preparation. Red arrows denote newly emerged AMG from within brain slice.

In some experiments, AMG *in situ* were selectively labeled by staining brain slices for 30 min at RT in 60 µg/ml tomato lectin-conjugated Alexa Fluor®594. Tomato lectin is a marker for rodent blood vessels and microglia. The linked fluorophore can be excited at 591 nm and visualized by emitted light at 618 ± 4 nm. In brain slices obtained from Iba1-EGFP

mice, EGFP positive microglia were visualized using excitation and emission wavelengths at 488 and 530 ± 10 nm, respectively.

### 3.6.3 Astrocytes

Acute brain slices obtained from GFAP-EGFP mice were used to selectively observe astrocyte populations. Similar to Iba1-EGFP cells described above, EGFP fluorescence was excited at 488 nm and visualized at 530 ± 10 nm.

## *3.7 Electrophysiology*

### 3.7.1 Setup and equipments

Electrophysiological studies were carried out using setup described in *Section 3.6.1*. Patch pipettes were pulled from borosilicate capillaries (inner, outer, ∅ = 0.87, 1.5; with 0.15 mm filament) using a pipette puller and filled with standard internal (pipette) solution. In some cases, Alexa Fluor®594 (10 µg/ml) was added to the pipette solution to confirm intracellular access. For gap junction coupling experiments, 0.5 - 0.6% biocytin was also included in the pipette solution. Prior to use, this solution was passed through a filter tip (0.22 µm) in order to avoid blockage of pipette tips. For each patch-clamp experiment, filled pipette was first secured on a $Cl^-$-coated silver electrode and carefully guided towards the cell of interest using a micromanipulator. Mild positive pressure was always applied through a U-tube into the pipette while approaching the cell to avoid contamination at the tip. When cells below brain slice surface were targeted, positive pressure also aided in navigation through the cell layers. Electrical potential and current between the patch electrode and ground electrode inserted into the perfusion were measured by EPC-9 amplifier and monitored on screen using TIDA software. Pipette resistance ($R_p$) ranged from 5 to 8 MΩ. All experiments were performed at RT.

### 3.7.2 Whole cell voltage-clamp configuration and biocytin dye-filling

Conventional whole cell voltage-clamp studies of cells both *in vitro* and *in situ* were performed according to previously described protocols (Hamill et al., 1981). With patch pipette placed close to the membrane of a cell of interest, positive pressure was removed and steady continuous suction was applied at the pipette tip through the U-tube. This

normally led to giga-seal formation within 30 s which represented tight contact between pipette tip and cell membrane creating resistance of >1 GΩ. The patch of membrane was then broken by suction and current injection through the electrode (also called ‘zap'). Capacitative transients and series resistance were compensated by the software. MP and membrane resistance ($R_m$) were measured on screen. Only cells with stable membrane potential throughout measurements were used. To determine membrane properties, membrane current profile of each cell was obtained by measuring current associated with applied de- and hyperpolarizing 50-ms voltage steps from a holding potential (HP).

In experiments where biocytin was included in the pipette solution, cells were quickly approached and sealed to avoid leakage of biocytin. Subsequently, cells were filled for 20 min with continuous perfusion to wash out residue biocytin in the extracellular space. To avoid confusion, only a single cell was filled in a given brain slice. After carefully removing patch pipettes, slices were fixed in 4% paraformaldehyde and 0.1% glutaraldehyde in 0.1 M phosphate buffer (PB), *pH* 7.4 for 12 hr at 4$^{o}$C and subsequently washed with 0.1 M PB and stored at 4$^{o}$C before biocytin immunohistochemistry.

### 3.7.3 Voltage-clamp recordings

After establishing whole cell configuration and under voltage-clamp, membrane current traces were recorded over time with series of de- and hyperpolarizing voltage jumps from HP repeated every 5 s. Step protocols used are detailed in *Results* section. Test substances were applied via bath perfusion into the chamber for various time periods. To minimize indirect neuronal effects induced by neurotransmitter applications on glial cells, 0.5 µM TTX and 0.1 mM $CdCl_2$ were added to the bath solution to block voltage-gated $Na^+$ and $Ca^{2+}$ channels, respectively. 50 µM 6-Cyano-7-nitroquinoxaline-2,3-dione (CNQX) was also included while measuring glutamate transporter response to minimize interference by AMPA/kainate (KA) glutamate receptor activity.

In some experiments, single AMG were isolated from the brain slice surface to minimize influence from other cells. This was possible since they were normally sitting loosely on the surface. After establishing tight seal, they were gently moved away from the surface by moving the patch pipettes but maintained within the perfusion (*Fig. 5A*). Once the desired distance was reached, the cell was allowed to rest for at least 5 min before the patch was

opened. Most AMG remained stable and responsive even at a distance of 300 µm away from the slice surface. The patch was normally tight enough to sustain the weight of the cell and the movement. Similar procedures were previously carried out to detect the response of AMG towards ATP stimulation (Haas et al., 1996). Based on this, current response of cells towards 0.5 - 1 mM ATP at the end of each recording was used to confirm cell viability and patch quality.

In other cases, postnatal brain hemisphere slices were made by carefully cutting the coronal brain slices in halves with a blade (*Fig. 5B*). These hemisphere slices were placed above coverslips of microglia cultures which were transferred together to the recording chamber for path-clamp experiments. With this, cultured microglia located close to the corpus callosum region of the slices were studied. Contrary to the isolated AMG method, this allowed studies of cultured microglia in the presence of brain slice.

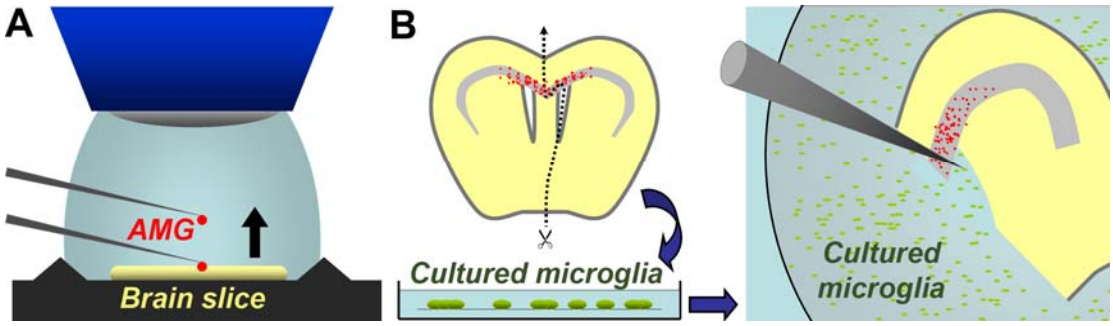


**Fig. 5. Modified settings for electrophysiological recordings.** Conventional patch-clamp settings were modified for studies of isolated AMG. **(A)** Single AMG was first voltage-clamped on the surface of the brain slice and then carefully lifted up. Membrane current recordings were made at desired distance after at least 5 min of rest. **(B)** In separate experiments, measurements from cultured microglia under the influence of acute slices were carried out. Half of an acute brain slice was placed on a coverslip of cultured microglia (left panel). Patch-clamp studies on a cultured microglia located near the corpus callosum of the brain slice followed (right panel). Red dots represent AMG from acute slices and green dots are cultured microglia.

## *3.8 Imaging experiments*

### 3.8.1 Setup and equipments

Imaging experiments were carried out using the same setup and equipments described in *Section 3.6.1 and 3.7.1*. Imaging protocols were generated and executed by TIDA and ICE software, which controlled the monochromator and CCD camera via EPC-9 amplifier. In cases of fluorescence imaging, series of excitation beams were generated from a monochromator and the emitted light was collected with appropriate sets of filters.

Resulting image sequences were captured with the CCD camera and stored. Test substances were applied via bath perfusion. All experiments were performed at RT.

### 3.8.2 Bright phase imaging of microglial motility

To quantify the movement of AMG on brain slices, series of bright field images were captured at 40X magnification at 1 image every 2 s. AMG motility in terms of displacement and arm movement were measured.

Displacement of AMG was assessed at a sampling rate of 1 image every 40 s. It is a measure of the total distance travelled by the cell in two dimensions. The center of each cell was manually tracked in each frame using the *Track Object* function on Image Pro® 5.0 and recorded as x and y-coordinates $(x_{(n)}, y_{(n)})$ for frame n. To account for minor drift of brain slice during recording, changes in cell position between frames were corrected by the displacement of a reference point on the brain slice. The corrected displacement ($D_n$) between 2 frames (from n-1 to n) was calculated using the following equation:

$$D_n^{\,2} = \left[\left(x_{C(n)} - x_{C(n-1)}\right) - \left(x_{R(n)} - x_{R(n-1)}\right)\right]^2 + \left[\left(y_{C(n)} - y_{C(n-1)}\right) - \left(y_{R(n)} - y_{R(n-1)}\right)\right]^2$$

where $C$ and $R$ stand for coordinates for the cell of interest and reference point, respectively. Coordinates were measured in pixels whereas 3.7 pixels = 1 µm. Total displacement was the sum of $D_n$ measured in all frames over time and was normalized to 100% baseline activity of corresponding cell.

Besides moving away from its original position, motility of AMG in terms of movement of their processes (or arms) was also quantified and compared (*Fig. 6*). At a sampling rate of 1 image every 2 s, differences between consecutive images were isolated using Image Pro® 5.0 so that only moving components were visible. A filter was then applied to enhance edges. With the *Line Profile* function, intensity along the perimeter of a given cell relative to a reference blank area was measured on a two dimensional plane. Thus, each distinct peak represented a moving arm. As a result, the sum of peaks detected in all frames was taken as a measure of arm movement of that cell. To account for variable cell size and

basal activity, relative arm movement during treatment period normalized to baseline activity of each cell was determined.

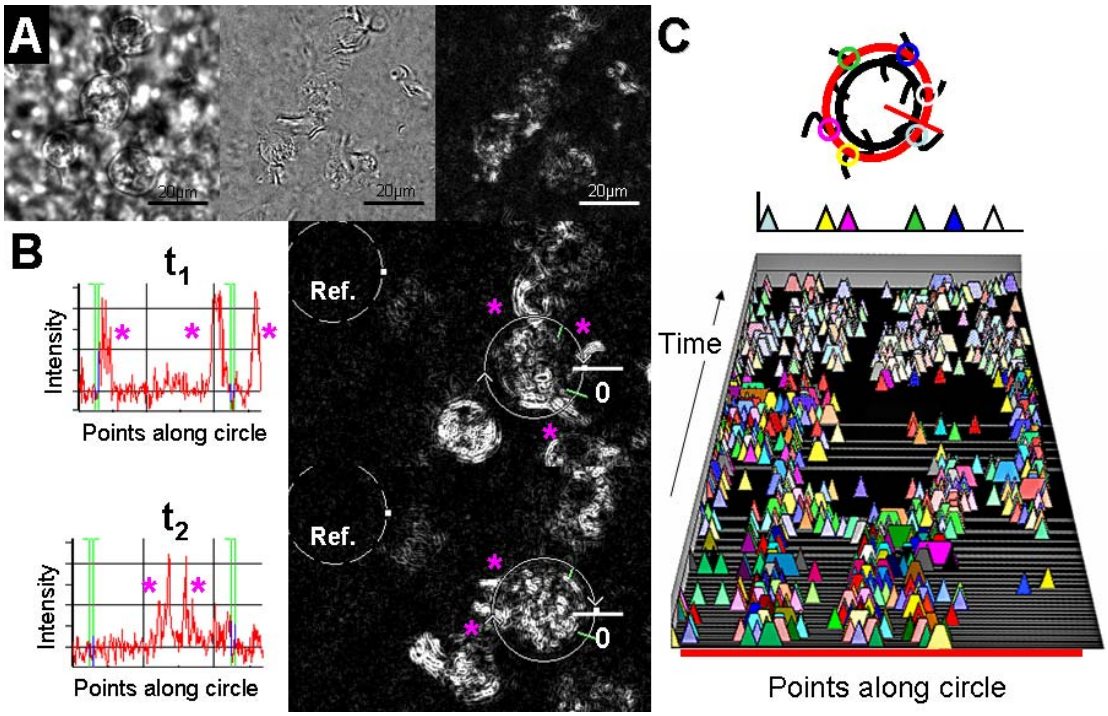


**Fig. 6. Determination of arm movement of AMG. (A)** Image sequences were processed and sample images are shown. Each bright field image (left panel) was compared to the previous one to obtain a difference image (middle panel). By doing so, background was removed and movement emphasized. This was then filtered to enhance edges (right panel) to allow detection of arms. **(B)** Intensity profiles around an AMG are shown for two time points ($t_1$ and $t_2$). This was corrected to a reference blank area (Ref.). Distinct peaks on the plots represent moving arms indicated by ✶. **(C)** Schematic diagrams illustrate the quantification of moving arms. Arm movement is quantified by the sum of peaks over time.

### 3.8.3 Intracellular calcium imaging of microglia

Intracellular $Ca^{2+}$ imaging experiments were designed using previously described protocols (Schipke et al., 2002; Kuhn et al., 2004). To label intracellular free $Ca^{2+}$, postnatal brain slices were loaded with a $Ca^{2+}$- sensitive dye Fluo-4 AM (10 µM) in standard brain slice buffer for 40 min at RT. Similarly, cultured microglia on coverslips were loaded with 5 µM Fluo-4 AM in HEPES buffer for 30 min at 37°C. In both cases, equilibration was achieved after washing samples in perfusion chamber for 5 min at RT. Fluo-4 AM is a cell-permeable acetoxymethyl (AM) ester. Once inside the cell, AM groups are cleaved by esterases thus entrapping the dye within the cytosol. Cleaved Fluo-4 binds to free $Ca^{2+}$ and leads to an increase in fluorescence intensity which can be detected by excitation and emission

wavelengths at 488 and 530 ± 10 nm, respectively. The measure of relative fluorescence intensity ($F/F_0$) for each cell over time was taken as a measure of $[Ca^{2+}]_i$.

As it was reported that Fluo-4 preferentially loads astrocytes over microglia in acute brain slices (Schipke et al., 2002), much stronger $Ca^{2+}$ signals were often observed in non-AMG neighboring cells. This interfered with the measurement of $[Ca^{2+}]_i$ in the AMG. To overcome this, single AMG from brain slices loaded with Fluo-4 were giga-sealed with patch pipettes and lifted up from the surface as described in *Section 3.7.3*. Here, the glass pipettes were filled with standard brain slice buffer and the membrane patches were not broken in order to maintain intracellular content. At a distance of 300 µm above brain slice surface, response in neighboring cells was no longer detectable. Secondary signals from these cells were also minimized. Similar to patch-clamp studies, cell viability and patch quality were tested by 0.5 - 1 mM ATP.

## *3.9 Extracellular potassium measurement*

Recordings of $[K^+]_0$ in acute brain slices were performed at the Institute of Neurophysiology, Charité-Universitätsmedizin Berlin, in the laboratory of Dr. Oliver Kann adapting previously described protocols (Heinemann, 1992; Kann et al., 2003). Acute brain slices from postnatal and adult NMRI mice were prepared and allowed to rest for at least 1 hr. They were then placed in a recording chamber mounted on a microscope with constant perfusion of standard brain slice buffer (at 4 ml/min). DC-coupled recordings of local field potentials and changes in $[K^+]_o$ were performed with double-barrel reference and $K^+$-sensitive microelectrodes. In brief, electrodes were pulled from double barrel theta glass. The reference barrel was filled with 154 mM NaCl; the ion-sensitive barrel with $K^+$ ionophore I cocktail A and 100 mM KCl. $K^+$-sensitive microelectrodes with a sensitivity of 59 ± 2 mV to a tenfold increase in $K^+$ concentration were used for experiments. The amplifier was equipped with negative capacitance feedback control, which permitted recordings of changes in $[K^+]_o$ with time constants of 50 to 200 ms. Changes in voltage were digitized at 10 Hz using FeliX$^{TM}$ software. Electrodes were placed on the surface or in the depth of about 30 µm of brain slices at the corpus callosum or other regions under 20X water immersion objective. To translate the recorded potential values in mV to $[K^+]_o$, a modified Nernst equation was used (Heinemann, 1992; Kann et al., 2003):

$$\log[Ion]_1 = E_M \times (s \times v)^{-1} + \log[Ion]_o$$

where $E_M$, recorded potential; $s$, electrode slope obtained at calibration; $v$, valence of the specific ion; $[Ion]_0$, ion concentration at rest; and $[Ion]_1$, ion concentration during activation. Throughout recordings, test substances were applied and washed out through the perfusion system at a rate of 4 ml/min.

## *3.10 Microglial migration assay*

Cell migration assays were performed in 48-well microchemotaxis chambers as described previously (Nolte et al., 1996). 29 µl of serum-free DMEM containing test substance at desired concentrations were added the lower wells. DMEM alone and DMEM containing 300 µM ATP were used as negative and positive controls, respectively. Upper and lower wells were separated by polycarbonate filter with 5 µm pore size. 50 µl DMEM containing 4 x $10^5$ microglia was added to the upper wells, and the chamber was incubated at 37°C and 5% $CO_2$ for 2 hr. Afterwards, the filter was removed and fixed with Diff-Quik®-Fix solution for 5 min. It was then stained in Diff-Quik®-I (red) for nuclei and Diff-Quik®-II (blue) for membrane for 5 min each. After washing in water for another 5 min, the filter was left air-dried. Top side of the filter (i.e. facing cells) was then washed out with water. The number of cells at each well on the filter was counted using a microscope with a 40X objective and averaged from 4 random fields per well. This was taken as the rate of microglial migration towards the test substance which was then normalized to control conditions.

## *3.11 Microglial proliferation assay*

Cultured microglia plated in 96-well plates were stimulated for 24 or 48 hr with test substance in DMEM/10% FCS with or without LPS (100 ng/ml). The negative control for basal and induced proliferation was treated with DMEM only or DMEM with LPS, respectively. To quantify cell proliferation, 10 µM Bromodeoxyuridine (BrdU) labeling solution was also added to the medium. Proliferation was assessed using BrdU labeling and detection kit according to manufacturer's instructions. The amount of BrdU

incorporated by the cells was taken as a measure of proliferation. In brief, cells were first fixed at -20°C for 30 min followed by partial digestion of cellular DNA with nuclease solution for another 30 min at 37°C. Digested samples were further incubated with anti-BrdU-POD solution for 30 min at 37°C under 5% $CO_2$. Finally, peroxidase solution with enhancer was added for 30 min at RT. Cleavage of ABTS produced a colored reaction product which was then quantified at 405 nm against 490 nm using a microplate reader and Wallac software. Basal and LPS-induced BrdU incorporation (i.e. proliferation) was normalized to respective controls.

## *3.12 Cytokine release quantification*

### 3.12.1 Cytokine release *in vitro*

To quantify cytokine release by cultured microglia, cells plated in 96-well plates were treated with test substances in DMEM/10% FCS. Negative controls were treated with DMEM only. After 24 hr, culture medium was collected and the amounts of cytokines released into the medium were measured using Enzyme-Linked ImmunoSorbent Assay (ELISA). In particular, the release of IL-6, IL-12, KC, TNF-α, and MIP-1α were investigated. ELISA plates were first coated with specific anti-mouse capture antibodies in phosphate buffer saline (PBS) overnight at RT. After incubation with blocking buffer for 1 hr at RT (or 2 hr at 37°C for IL-12 assay), prediluted samples and standards in DMEM/10% FCS were added for 2 hr at RT. After washing, captured cytokines were detected by specific biotinylated anti-mouse detection antibodies in dilution buffer for 2 hr at RT (or 1 hr at RT for IL-12 assay). Streptavidin-HRP conjugate (1:200,000 in HRP-diluent) was then added for 30 min for linkage to the bound detection antibodies. Subsequent binding of tetramethylbenzidine onto HRP generated a distinctive blue color within 5 to 7 min at which point color change was stopped by 1N $H_2SO_4$. The resulting yellow color was measured at 450 nm against 540 nm using a microplate reader and Wallac software. This was taken as the amount of cytokine release and was normalized to respective controls.

### 3.12.2 Cytokine release *in situ*

To determine cytokines released *in situ*, 150-µm thick postnatal acute slices were used. Here, half hemispheres of coronal slices containing corpus callosum were stored in 96-well

plates in standard brain slice buffer while maintaining 5% $CO_2$ and *pH* 7.4. After at least 1 hr of resting period, buffer was changed to 150 µl fresh buffer containing test substances and incubated for 1.5 or 3 hr. To study the effect of short stimulation on long-term cytokine release, some experiments were carried out by 15 min stimulation followed by fresh buffer for a total of 1.5 hr. Pure brain slice buffer was used as controls. Buffer containing secreted cytokines was collected for ELISA as described in *Section 3.12.1* with modifications. In order to optimize detection, 100 µl of sample buffer was used without dilution and standards were made with standard brain slice buffer instead of DMEM/10% FCS.

## *3.13 Immunohistochemistry for biocytin*

Biocytin-filled cells were identified according to a previously described protocol (D'Ambrosio et al., 1998). Briefly, sections were first rinsed in 0.1 M PB and then 0.1 M Tris-HCl buffer (TB), *pH* 7.4. Endogenous peroxidases were suppressed with 1% $H_2O_2$ for 2 hr. To reduce nonspecific background staining and to permeabilize membranes, samples were then incubated with 2% bovine serum albumin (BSA) and 0.25% dimethylsulfoxide in 0.05 M Tris-buffered saline, *pH* 7.4 for 1 hr. Samples were then treated using Elite ABC kit for 48 hr at 4$^{o}$C according to manufacturer's instructions. After preincubation with 0.025% diaminobenzidine (DAB) and 0.005% NiCl for 15 min to increase staining density, fresh DAB and NiCl containing 0.002% $H_2O_2$ were added for 60 min. Finally, 0.1 M TB was added to stop the reaction and sections were mounted, dried and coverslipped on gelatin-coated slides. Sections were examined under a light microscope and biocytin positive single cells through different brain slice were counted while adjusting focus.

## *3.14 Analyses and statistics*

Electrophysiological data were filtered at 2.9 kHz and analyzed by TIDA Version 5.0. Fluorescent images obtained from ICE 3.5.99 were merged in Adobe® Photoshop® CS 8.0 using gradient maps and merge options. Image sequences were processed and analyzed by ICE 3.5.99 and Image Pro® 5.0. Data for motility was analyzed using Microsoft® Excel 2003. Recordings of $[K^+]_0$ measurements were calibrated to basal $[K^+]_0$ and exported from FeliX™ and analyzed in Microsoft® Excel 2003. Absorbance readings were exported from

Wallac 1420 Version 2.01. All statistical analyses were carried out and plotted in Origin® 7.0 and Microsoft® Excel 2003. All values are expressed as mean ± standard error of the mean (SEM). Differences between groups were evaluated by unpaired two-sample Student's t-test on Microsoft® Excel 2003. Differences of single group from mean were evaluated by one-sample t-test on Origin® 7.0. P-values <0.05 were considered statistically significant with *, $p<0.05$; **, $p<0.01$.

# 4 Results

## *4.1 $GABA_A$ receptor stimulation and microglial current response*

### 4.1.1 Muscimol-induced current response in microglia

Accumulation of AMG was observed on the surface of the corpus callosum of acute slices prepared from 6 – 8 days old mouse brain (*Fig. 7A*). They could be identified by their distinctive round morphology and were approached with glass pipettes with $R_p$ ranging from 6 – 8 MΩ. At a HP of -70 mV, characteristic microglial membrane current profile was recorded as shown in *Fig. 7B*. Hyperpolarizing voltage steps evoked inward rectifying current while no voltage-gated current was detected upon depolarization. Current/voltage (I/V) plot in *Fig. 7C* further revealed time-dependent inactivation of inward current at hyperpolarizing voltage steps below -130 mV. Mean MP and $R_m$ of AMG were -64 ± 1 mV and 399 ± 23 MΩ, respectively (n = 145).

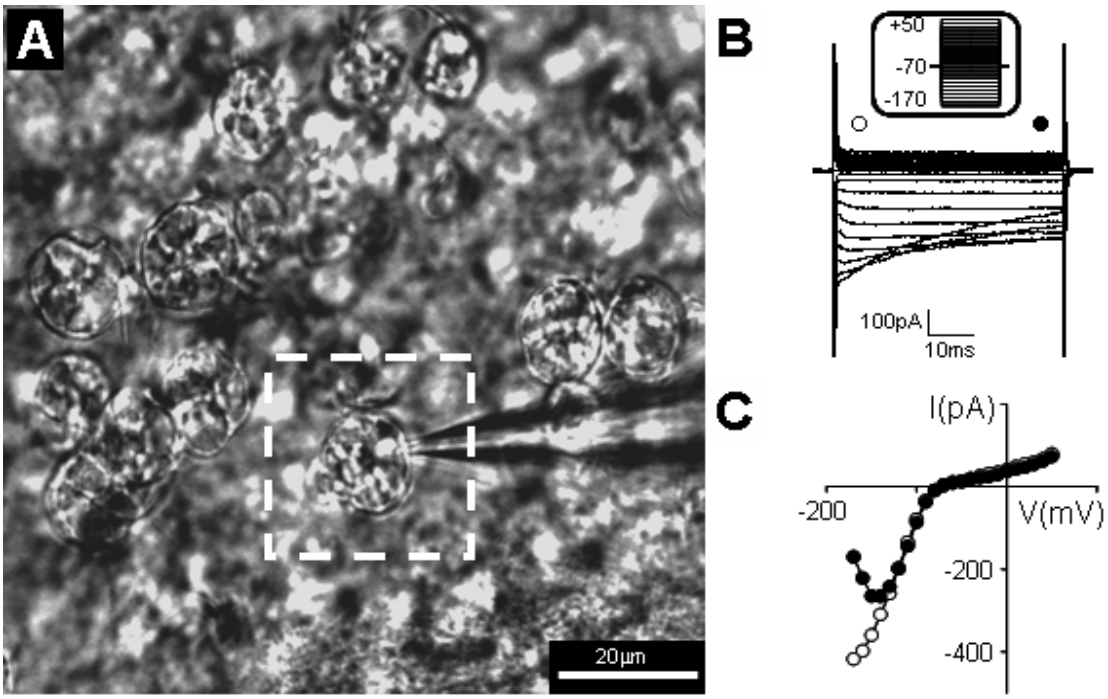


**Fig. 7. Membrane properties of AMG. (A)** AMG at the surface of the corpus callosum of acute brain slices obtained from 6 - 8 days old mouse were approached with a glass pipette and voltage-clamped as shown by dotted square. **(B)** Membrane current profile was obtained by applying de- and hyperpolarizing voltage steps ranging from -170 to +50 mV at 10-mV increments from a HP of -70 mV (see inset). **(C)** I/V plot was generated from transient (○) and steady (●) states of the current profile.

To study membrane current changes of AMG upon $GABA_A$ receptor stimulation, 100 μM muscimol, a specific $GABA_A$ receptor agonist was used. Membrane current was monitored using voltage-steps protocol repeated every 5 s. Muscimol application for 30 s elicited increase in inward current in all cells tested (n = 32; *Fig. 8A-B*).

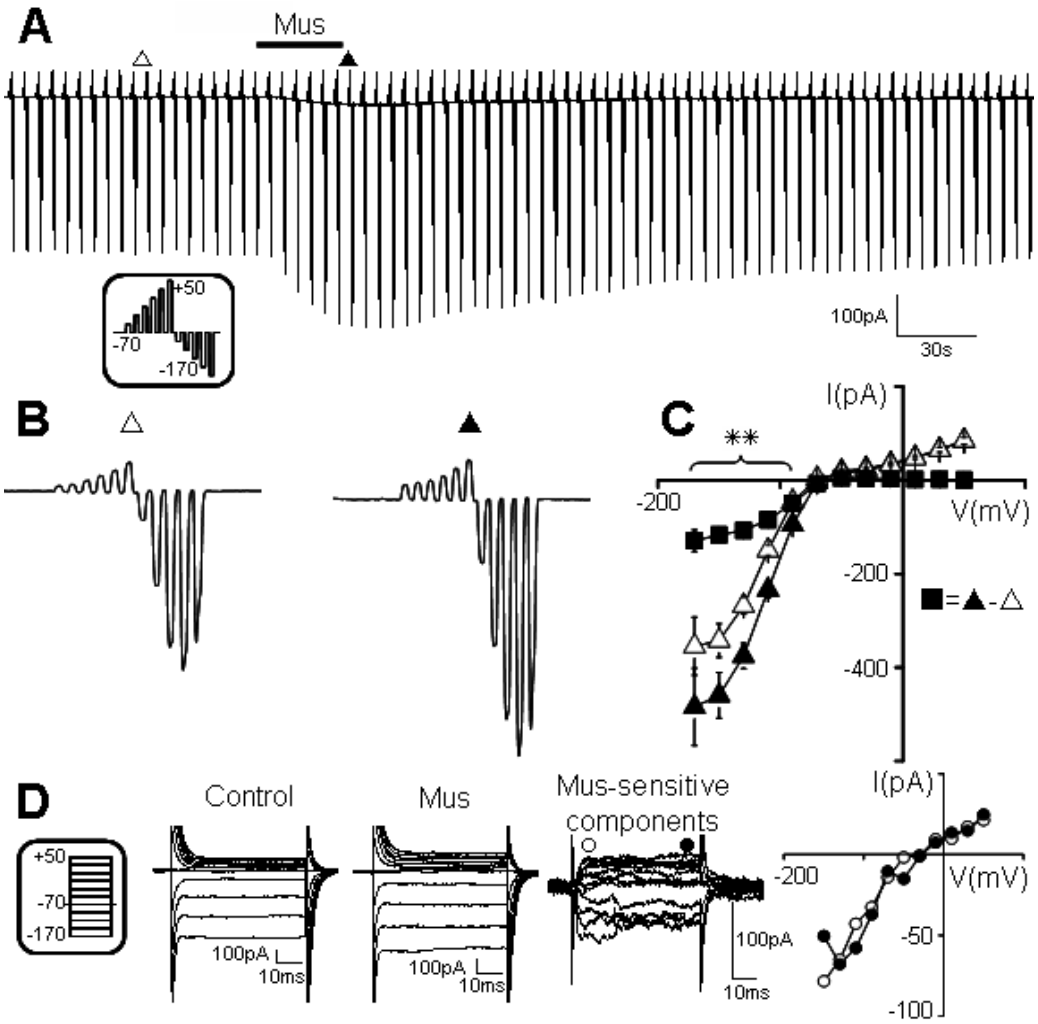


**Fig. 8. Muscimol-induced current response in AMG. (A)** Membrane current of AMG was monitored by applying series of de- and hyperpolarizing voltage steps ranging from -170 to +50 mV at 20-mV increments from a HP of -70 mV (see inset). Bath application of muscimol (Mus; 100 μM for 30 s) induced current changes as shown. **(B)** Sections before (△) and during (▲) muscimol-induced response are magnified. **(C)** I/V plot shows mean ± SEM current at △, ▲ and for muscimol-induced component (■=▲-△). **(D)** Membrane current profiles recorded before (Control) and during (Mus) muscimol stimulation by de- and hyperpolarizing voltage steps ranging from -170 to +50 mV at 20-mV increments (see inset) are shown. Mus-sensitive components were obtained by subtracting Control from Mus. I/V plot was made from transient (○) and steady (●) states. **, $p<0.01$ between △ and ▲.

This current increase reached 130 ± 23 pA at -170 mV ($p$ = 0.0001; *Fig. 8C*). The peak response occurred after 21 ± 2 s and membrane current returned to baseline after 149 ± 2 s. To further characterize the muscimol-induced current response, membrane current profile was recorded every 10 s (*Fig. 8D*). Muscimol-sensitive components were obtained by subtracting control current from the peak of the response during muscimol application and showed a time-dependent inactivation typical for the opening of $K_{ir}$ channels.

Repeated stimulation revealed that muscimol-induced current response in AMG could only be elicited once. A second muscimol application even after a 10 min washout did not trigger any response (n = 8; *Fig. 9A*) although they remained responsive to ATP (1 mM). Thus, the effects of blockers could only be tested on the first response.

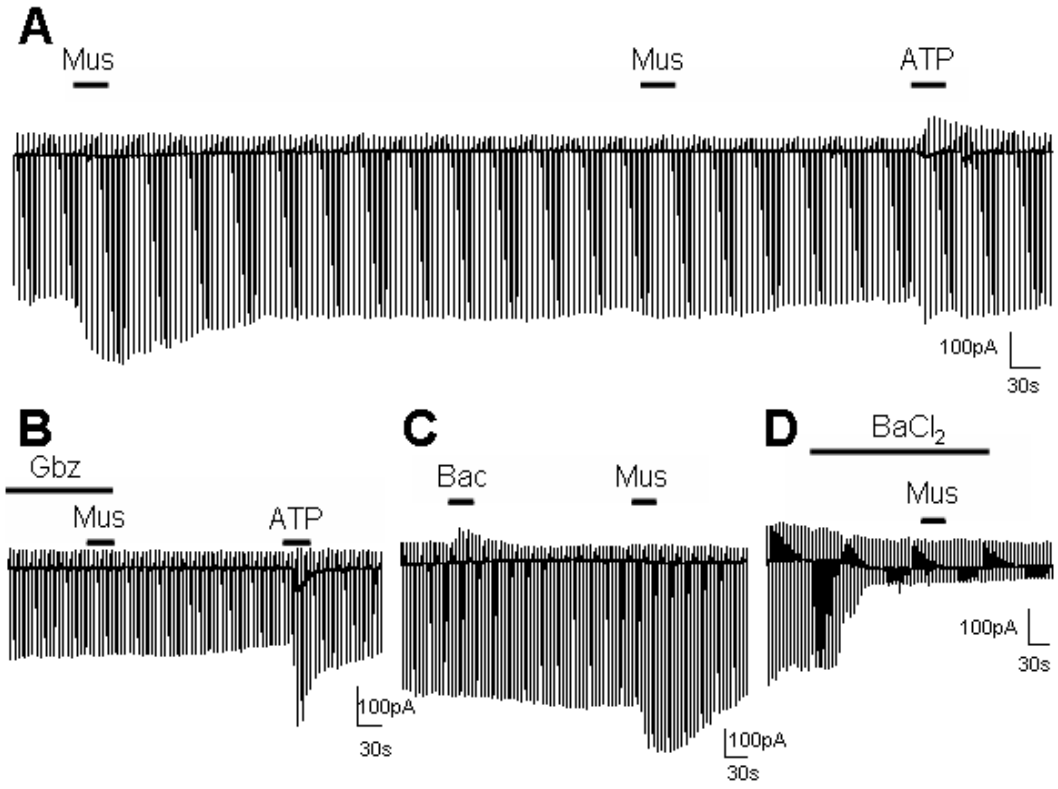


**Fig. 9. Sensitivity of muscimol-induced current response in AMG.** Membrane current of AMG was recorded using protocol as shown in inset of *Fig. 8A* and representative traces are shown. **(A)** Muscimol (Mus; 100 µM for 30 s) was applied twice with 10 min apart. Only the first application elicited current response. **(B)** Muscimol response was abolished by 90-s preincubation with gabazine (Gbz; 10 µM). **(C)** Baclofen (Bac; 500 µM for 30 s) application did not affect subsequent muscimol response. **(D)** Muscimol response was blocked by 2-min preincubation with $BaCl_2$ (100 µM). ATP (1 mM for 30 s) was used as a positive control in **A** and **B**.

In the presence of 10 µM gabazine, a selective, potent $GABA_A$ receptor antagonist, only 20% of cells responded towards muscimol (n = 10; *Fig. 9B*). Such response was only 47 ± 5 pA at -170 mV voltage step, significantly smaller than muscimol response without blocker ($p$ = 0.003). Since microglia express $GABA_B$ receptors (Kuhn et al., 2004), experiments were carried out to rule out possible interference by activities of this subtype. Cells were first treated with 500 µM baclofen, a specific $GABA_B$ receptor agonist. In 2 out of 10 cells showing current response towards baclofen, subsequent muscimol-induced inward current was unaffected (*Fig. 9C*). Furthermore, the involvement of $K^+$ channels was tested by a $K^+$ channel blocker $BaCl_2$. In 89% of cells (n = 9), muscimol response was blocked by preincubation with 100 µM $BaCl_2$ (*Fig. 9D*). Note that almost all of the intrinsic inward rectifying current was blocked by $Ba^{2+}$ at this concentration.

### 4.1.2 Influence of postnatal brain slice on muscimol-induced current response

#### *4.1.2.1 Isolated AMG*

To test whether muscimol directly stimulated AMG or indirectly via a secondary substance released from the acute brain slice, single AMG isolated from brain slices were studied. After establishing a tight seal with the recording pipette at the surface of the brain slice, the patched AMG were carefully lifted up to various distances and maintained for at least 5 min (*Fig. 10*). Whereas 100% of cells showed muscimol-induced response at the surface (see above), only 83% (n = 5 out of 6) and 20% (n = 3 out of 15) of cells responded at 150 and 300 µm above surface, respectively. The amplitudes of these responses were also significantly smaller than that measured at the surface. In cells which showed muscimol-induced response at 150 and 300 µm, the inward currents recorded with -170 mV voltage jump were only 30% (39 ± 13 pA) and 16% (20 ± 7 pA), respectively, of the average response at the surface. Current response towards 0.5 – 1 mM ATP at the end of the all recordings did not significantly change in relation to distance above surface. This confirmed that the isolated cells were viable, stable and equally responsive towards the positive control. The progressive loss of frequency and amplitude of muscimol response in AMG was a clear indication that AMG do not express functional $GABA_A$ receptors but showed prominent indirect response.

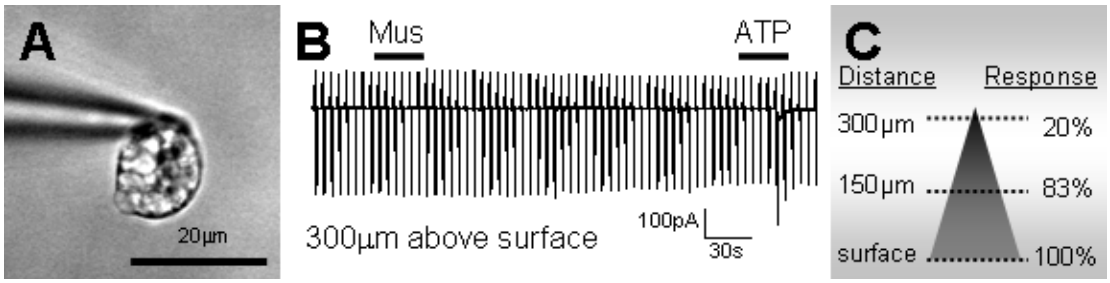


**Fig. 10. Current response in isolated AMG upon muscimol stimulation. (A)** At the surface of corpus callosum acute brain slices, the membrane of an AMG was tightly sealed with a patch pipette filled with pipette solution. It was then carefully lifted up by manipulating the patch pipette within bath perfusion. After 5-min rest period, the membrane was broken and the cell was voltage clamped. An image of an AMG at 300 µm above surface is shown. Note the absence of surrounding cells. **(B)** Using recording protocol shown in inset of *Fig. 8A*, muscimol (Mus; 100 µM for 30 s) was applied via bath perfusion. ATP (500 µM for 30 s) was used as positive control for cell viability. **(C)** Diagram illustrates decreasing percentage of AMG responsive to muscimol with increasing distance above surface of brain slices.

*4.1.2.2 Microglia cultures*

In order to further establish that muscimol response in microglia was indirect, primary cultures of mouse microglia plated on coverslips were used. They were voltage-clamped and recorded in the same manner described for AMG. Similar to AMG, inward rectifying currents could also be elicited in cultured microglia by hyperpolarizing voltage steps from a HP of -70 mV (*Fig. 11A*). Mean MP and $R_m$ were -63 ± 1 mV and 416 ± 32 MΩ, respectively (n = 86). Here, in the absence of an acute brain slice environment, no change in membrane current could be detected upon 100 µM muscimol application for 30 s (n = 43; *Fig. 11B*). To confirm that the lack of response was due to the absence of brain slice but not culturing procedures, brain slice environment was introduced to cultured microglia by carefully placing half hemisphere of postnatal slices on coverslips of cultured cells (*Fig. 11C*). As shown in the image, cultured microglia close to the corpus callosum region of the brain slices were subsequently approached with patch pipettes. Under these conditions, 89% of cultured microglia in close vicinity to the slice showed inward current response towards muscimol application. I/V relationship of muscimol current was similar to that observed in AMG (n = 18; *Fig. 11D-E*). Likewise, the peak of this response was observed 22 ± 3 s after muscimol application. Thus, cultured microglia, similar as the AMG, also lacked functional expression of $GABA_A$ receptors but readily responded towards muscimol in close vicinity of acute brain slices.

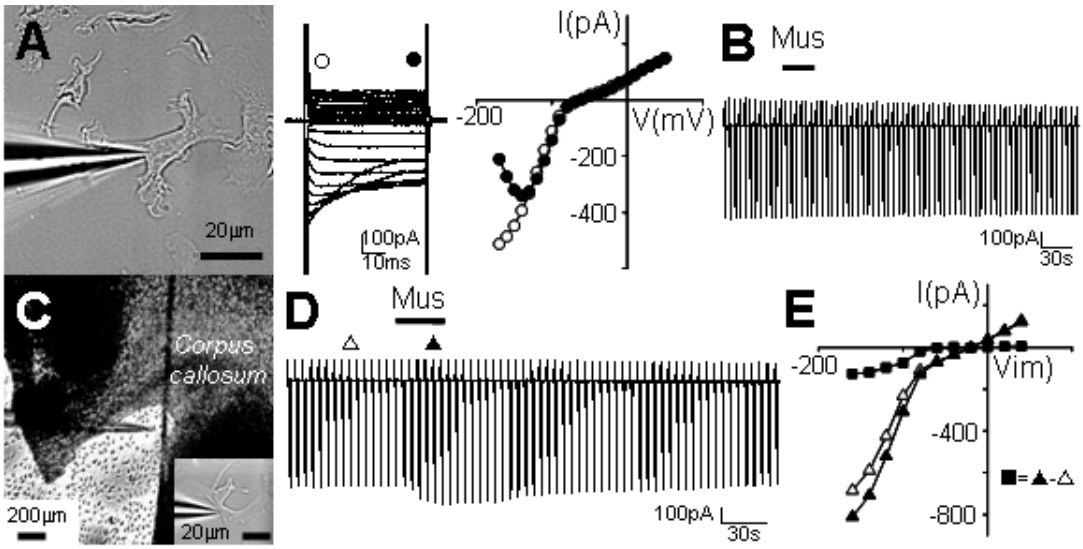


**Fig. 11. Current response in cultured microglia upon muscimol stimulation. (A)** Membrane current profile of a cultured microglia was recorded using protocol shown in inset of *Fig. 7B*. I/V plot was generated from the transient (○) and steady (●) states. **(B)** Using protocol as shown in inset of *Fig. 8A*, membrane current was monitored upon bath application of muscimol (Mus; 100 µM for 30 s). **(C)** In a separate experiment, half hemisphere of postnatal brain slice was placed over a coverslip with cultured microglia and a cultured cell near the corpus callosum region was voltage-clamped (enlarged image of the selected cell is shown in inset). **(D)** Similar as in **B**, membrane current was recorded upon muscimol stimulation. **(E)** I/V plot was generated from △ and ▲ and muscimol-induced current (■).

*4.1.2.3 Adult ramified microglia*

Microglia from adult brain slices were used to test whether the $GABA_A$ receptor mediated effect was specific for early postnatal brain. With 35 – 40 days old transgenic mice expressing EGFP under the control of the Iba1 promoter (Hirasawa et al., 2005), microglia could be identified in 150-µm thick brain slices. Most microglia had a ramified morphology as described previously (Boucsein et al., 2000). Unlike postnatal brain slices, no AMG accumulation could be observed at the corpus callosum region of these adult slices. In fact, EGFP positive cells were hardly observed in this area but were predominantly found in the neighboring cortical regions. These microglia with ramified morphology located in the cortical regions close to the corpus callosum were then voltage-clamped using similar protocols described for AMG. Alexa Fluor®594 (10 µg/ml) included in the patch pipettes revealed small soma and ramification (*Fig. 12A)*. Membrane current profiles showed only much smaller inward currents compared to AMG and cultured microglia. Bath application of 100 µM muscimol for 30 s did not trigger current changes in any cell tested while

subsequent ATP (1 mM) response confirmed cell viability and responsiveness (n = 8; *Fig. 12B*).

These observations demonstrated that $GABA_A$ receptor activities could be indirectly sensed by microglia in the postnatal corpus callosum but not by ramified ones in neighboring cortical regions of the adult brains.

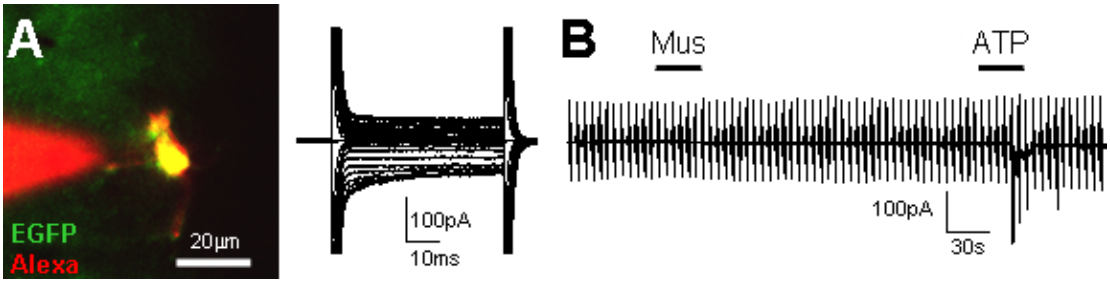


**Fig. 12. Current response in adult ramified microglia upon muscimol stimulation. (A)** Iba1-EGFP positive ramified microglia in cortical region near the corpus callosum of 35 - 40 days old mice were voltage-clamped. An image of such cell filled with Alexa Fluor®594 (10 µg/ml) included in the pipette solution is shown. Using protocol described in inset of *Fig. 7B*, membrane current profile revealed small inward currents. **(B)** Membrane current was also monitored by recording protocol described in inset of *Fig. 8A* upon bath application of muscimol (Mus; 100 µM for 30s). Subsequent ATP (1 mM for 30 s) application was used as a positive control for cell viability.

## *4.2 $GABA_A$ receptor stimulation and macroglial and neuronal current response*

To identify the source of indirect signal from the acute brain slice which triggered current response in AMG, macroglial cells and neurons within or near the postnatal corpus callosum were tested for the presence of functional $GABA_A$ receptors. Astrocytes were identified on brain slices obtained from GFAP-EGFP transgenic mice (*Fig. 13A-B*). Alexa Fluor®594 (10 µg/ml) was included in the pipette solution to further reveal cell morphology after achieving intracellular access. GFAP-EGFP positive astrocytes with fine processes located at the corpus callosum of postnatal brain slices were voltage-clamped and recorded using methods described for microglia. They were characterized by passive membrane currents sometimes with a small voltage-gated component elicited by depolarizing voltage jump from a HP of -70 mV. In all tested cells, bath application of muscimol (100 µM for 30 s) triggered an inward current response (n = 9; *Fig. 13A-B*). As shown by I/V plot generated from 1–3, it was consistently observed that the resting

conductance at depolarizing voltage steps permanently decreased after application of muscimol. To accurately determine the reversal potential of muscimol-induced current response, membrane conductance after washout was subtracted from that obtained at the peak of the response. I/V plots for 2–3 revealed that the resulting reversal potential of this response was close to 0 mV as expected for a $Cl^-$ conductance. In addition to astrocytes, two other macroglial populations within the corpus callosum were identified by their morphology in postnatal brain slices obtained from wildtype NMRI mice. Their identities were further confirmed by characteristic membrane current profiles and Alexa Fluor®594 dye filling. First, oligodendrocyte progenitor cells with fine processes parallel to the axonal tracts had passive membrane current and characteristic tail currents. Similar as reported previously in the same brain region (Berger et al., 1992), muscimol induced current changes in these cells which reversed at 0 mV (n = 3; *Fig. 13C*). Another cell type characteristic for glial precursor cells with prominent voltage-gated outward current but no inward current was also studied (n = 4; *Fig. 13D*). In these cells, a long-lasting decrease of resting conductance was also observed after muscimol application. Similar to the astrocytes, a reversal potential of muscimol-induced current changes was also close to 0 mV. Recordings in glial cells were performed in the presence of 0.5 µM TTX in order to minimize effects from neurons. Apart from glial cells found in the corpus callosum, neuronal $GABA_A$ receptors in neighboring cortical regions were also tested. Besides voltage-gated outward currents, these cells also had large $Na^+$ currents measurable at depolarizing voltage steps which was characteristic for neurons (n = 6; *Fig. 13E*). Bath application of 100 µM muscimol for 30 s triggered inward current much larger than that detected in glial cells. Muscimol-induced current could be isolated as in the astrocytes and glial precursor cells by subtracting conductance after the response from that during that peak of the response. As a result, a reversal potential close to 0 mV was observed. In these neighboring glial cells and neurons, peak response was reached after 12 ± 1 s of application which was significantly faster than that observed in AMG ($p$ = 0.0005).

It appeared that, upon muscimol stimulation, current changes involving the opening of $Cl^-$ channels could be first detected in macroglial cells and neurons. After a significant delay, AMG responded indirectly. Thus, the source of indirect signals sensed by the AMG was likely to be the neighboring cells in postnatal brain slices.

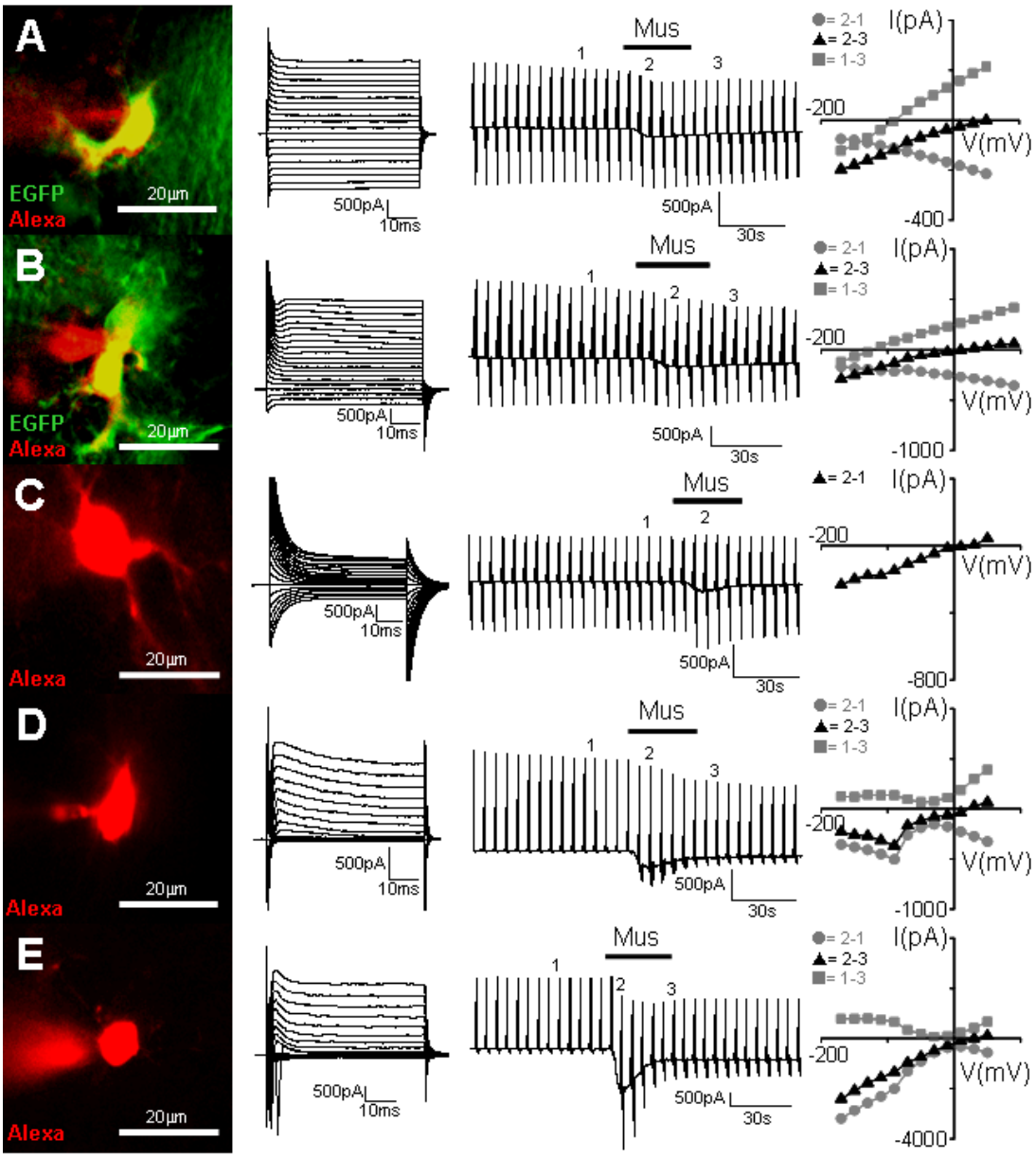


**Fig. 13. Current response in macroglia and neurons upon muscimol stimulation.** Images are shown for astrocytes with **(A)** no or **(B)** small voltage-gated components; **(C)** an oligodendrocyte progenitor cell; **(D)** a glial precursor cell with voltage-gated outward current; and **(E)** a cortical neuron. **A-B** were identified at the corpus callosum of postnatal brain slices obtained from GFAP-EGFP transgenic mice; **C-D** in the same area in wildtype mouse; and **E** in cortical region near corpus callosum of wildtype mouse. Alexa Fluor®594 (10 µg/ml) in pipette solution revealed morphology. Characteristic membrane currents were recorded and monitored using protocols as shown in inset of *Fig. 7B* and *8A*. To each cell type, muscimol (Mus; 100 µM) was applied for 30 s via bath perfusion. Membrane currents before (1), during (2) and after (3) muscimol-induced current response are marked. I/V plots were generated from respective isolated currents indicated by numbers and symbols. To minimize indirect effects on macroglial cells by neuronal activity, recordings in **A-D** were carried out in the presence of 0.5 µM TTX.

## *4.3 $GABA_A$ receptor stimulation and extracellular potassium*

### 4.3.1 Extracellular potassium level

$K^+$ sensitive microelectrodes were used to measure changes in $[K^+]_0$ in brain slices upon bath application of muscimol. By placing the electrodes on the surface of the corpus callosum of postnatal brain slices close to the AMG, it was measured that a first application of muscimol (100 µM for 30 s) increased $[K^+]_0$ transiently from 5 to 7.5 ± 0.2 mM (n = 6; *Fig. 14A, E*). The peak of the increase was reached after 54 ± 7 s of application and $[K^+]_0$ returned to baseline after 342 ± 18 s. Subsequent applications separated by 15-min washout induced significantly smaller increase only to 5.7 mM. In the presence of gabazine (10 µM), muscimol did not elicit an increase in $[K^+]_0$ (n = 4; *Fig. 14B, E*). With the $K^+$ sensitive electrodes inserted about 30 µm into the corpus callosum slice, a $[K^+]_0$ increase reaching 9.6 ± 0.8 mM was detected upon first application of muscimol (100 µM for 30 s); significantly greater than that observed at the surface (n = 4; *Fig. 14C, F*). Similar to the surface, changes elicited by second and third applications within slices were also much smaller than the first response. Furthermore, potential difference in $[K^+]_0$ elevation between postnatal corpus callosum and cortical regions (n = 6) was also assessed. However, $[K^+]_0$ elevation upon muscimol application was not different between two regions either on the surface or within slices indicating that $K^+$ released to the extracellular space was similar in neighboring brain regions (*Fig. 14F*). To study age-dependent $K^+$ release upon $GABA_A$ receptor stimulation, $[K^+]_0$ was measured in adult brain slices obtained from 35 - 40 days old mice. Significantly smaller $[K^+]_0$ increase was observed both at the surface (to 5.6 ± 0.1 mM; n = 5) and within adult slices (to 6.5 ± 0.2 mM; n = 3) compared to postnatal ones at the corpus callosum (*Fig. 14D, F*). In order to further understand the kinetics of $K^+$ release, rates of $K^+$ accumulation and removal were calculated from the slope of corresponding responses. In general, rates of muscimol-induced $K^+$ accumulation were 6 times greater than removal. Both accumulation and removal of $K^+$ in first muscimol stimulation were significantly faster than subsequent ones (*Fig. 14G*). Such processes were also faster within than on the surface of brain slices; in postnatal than in adult slices (*Fig. 14H*).

These experiments indicated that $[K^+]_0$ increase in the extracellular space upon $GABA_A$ receptor stimulation was more pronounced in postnatal reaching nearly 10 mM than adult brain.

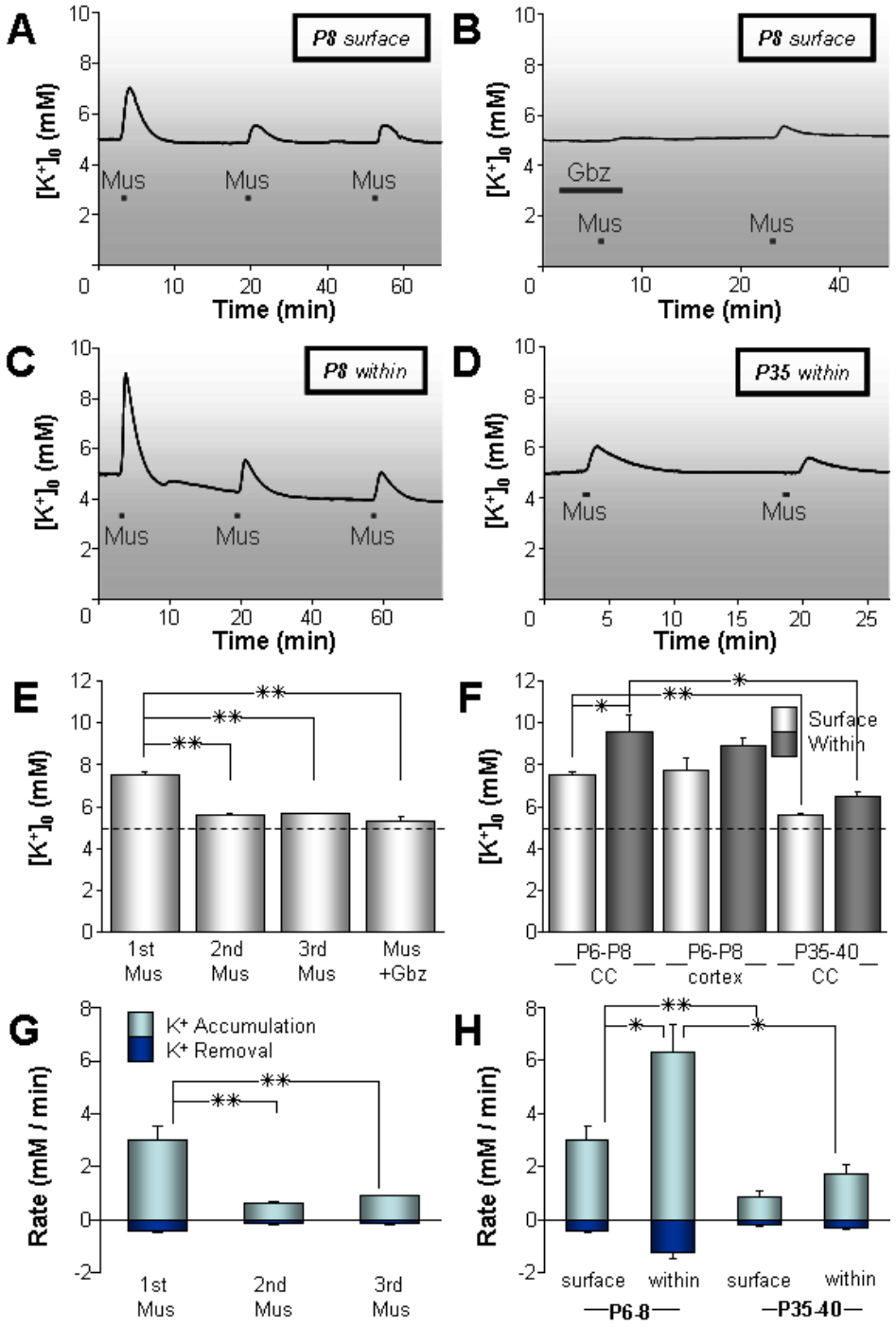


**Fig. 14. Muscimol-induced changes in $[K^+]_0$.** $K^+$ sensitive microelectrodes were used to monitor $[K^+]_0$ in brain slices over time. Representative traces are shown for **(A)** repeated muscimol applications (Mus; 100 µM for 30 s) 15 min apart; **(B)** muscimol stimulation in the presence of gabazine (Gbz; 10 µM for 3 min preincubation) followed by a recovery response on the surface of postnatal (P6 – P8) corpus callosum (CC); **(C)** repeated muscimol applications 15 min apart about 30 µm below surface of postnatal CC; **(D)** repeated muscimol stimulation 15 min apart about 30 µm below surface of adult (P35 – P40) CC. **(E – H)** Bar charts showing mean ± SEM values of peak amplitudes or rates of $K^+$ accumulation and removal. *, $p<0.05$; **, $p<0.01$. Significance level in **G** and **H** applies to both accumulation and removal.

### 4.3.2 Microglial response towards elevated extracellular potassium level

It was reported previously that conductance of microglial $K_{ir}$ channels increases with elevated $[K^+]_0$ (Kettenmann et al., 1990). However, the impact of changes in $[K^+]_0$ within physiological range has not been investigated. Microglia were tested for their response towards moderate elevation of $[K^+]_0$ by addition of KCl. 30-s bath application of 2.5, 5, and 7.5 mM KCl transiently increased $[K^+]_0$ from the basal level of 5 mM to 7.5, 10, and 12.5 mM, respectively. In response to these, dose-dependent increase of inward rectifying current in AMG (n = 16; *Fig. 15A*) and in cultured microglia (n = 19; *Fig. 15B*) was observed. Membrane conductance increased in AMG by 0.4, 0.8 and 1.2 pS; and in cultured microglia by 1.7, 3.3, and 5.0 pS with 2.5, 5 and 7.5 mM KCl, respectively. Conductance increase was determined by dividing the induced current by voltage between the -110 and -130 mV voltage steps from a HP of -70 mV.

To test whether an increase in $[K^+]_0$ could mimic muscimol-induced current response, membrane current in the same AMG was recorded during applications of muscimol (100 µM for 30 s) followed by KCl. In contrast to the lack of multiple muscimol-induced responses in AMG, KCl applications could always induce subsequent current changes after a muscimol application. In particular, after washout of a typical muscimol-induced current response, bath perfusion of 5 mM KCl for 30 s which increased $[K^+]_0$ from 5 to 10 mM triggered inward rectifying current response similar in amplitude to that induced by muscimol as shown in I/V plots (n =5; *Fig. 15C*). In addition, the average muscimol-induced conductance of 0.8 pS (n = 32) was similar to the increase triggered by 5 mM $[K^+]_0$ elevation. Furthermore, membrane current profiles obtained before and during the peak of response towards 5 mM KCl (n = 4; *Fig. 15D*) revealed typical current changes observed with muscimol. These findings suggest that the elevation of $[K^+]_0$ within physiological range could be the source of muscimol-induced current response in AMG on postnatal acute brain slices and cultured microglia placed close by.

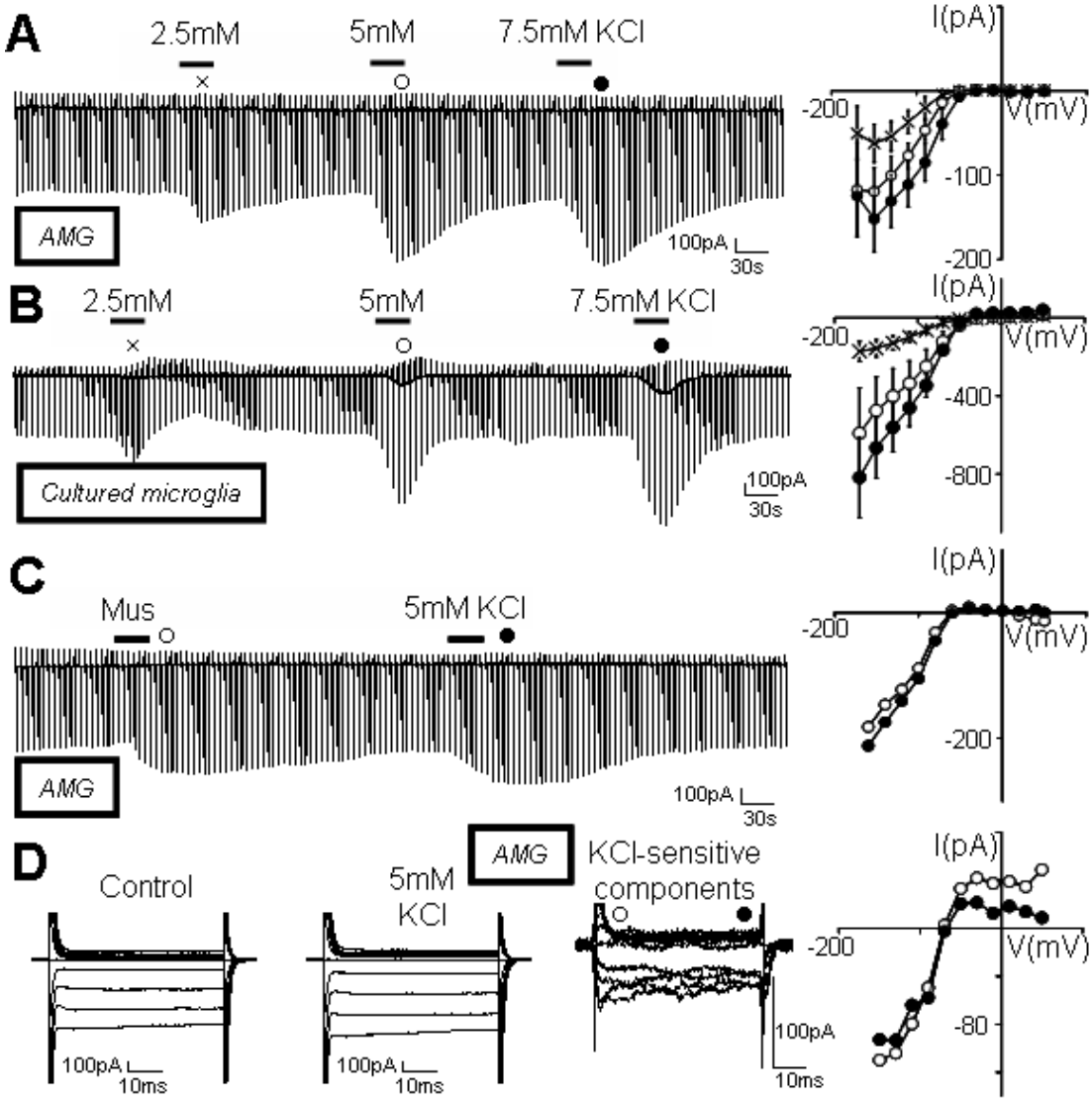


**Fig. 15. Current response in microglia towards $[K^+]_0$ elevation.** Using protocol as shown in inset of *Fig. 8A*, membrane currents were recorded from microglia upon repeated 30-s bath applications of increasing concentrations of KCl. Representative traces for **(A)** an AMG and **(B)** a cultured microglia are shown. 2.5, 5, and 7.5 mM KCl applications transiently increased basal $[K^+]_0$ from 5 to 7.5, 10, and 12.5 mM, respectively. For each application, induced current changes were determined by subtracting conductance of baseline from that measured at the peak of the current response. I/V plots reveal mean ± SEM amplitudes of induced currents indicated by corresponding symbols. **(C)** In an AMG, induced current responses were compared between 30-s application of muscimol (Mus; 100 μM) and 5 mM KCl (total $[K^+]_0$ = 10 mM). **(D)** KCl-induced current was further analyzed by recording membrane current profiles using protocols described in inset of *Fig. 8D*. KCl-sensitive currents were isolated by subtracted membrane profiles recorded during control from that recorded during peak of response. I/V plot was made from transient (○) and steady (●) states.

## *4.4 $GABA_A$ receptor stimulation and functional properties of microglia*

### 4.4.1 Intracellular calcium changes

Both AMG and cultured microglia were tested for muscimol-induced changes in $[Ca^{2+}]_i$. Cultured microglia were loaded with 5 µM Fluo-4 AM, a $Ca^{2+}$ sensitive dye (*Fig. 16A)*. 100 µM muscimol stimulation for 30 s did not trigger $Ca^{2+}$ response in any cell tested (n = 74; *Fig. 16B*). ATP (500 µM for 30 s) was always used as a control for cell responsiveness and only cells showing ATP response were counted.

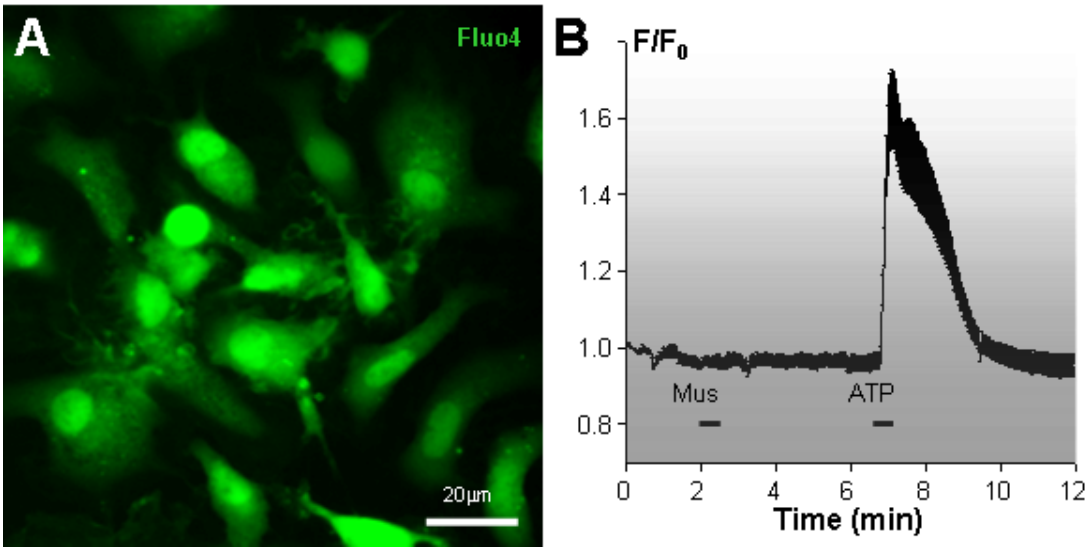


**Fig. 16. $Ca^{2+}$ response in cultured microglia upon muscimol stimulation. (A)** Image of cultured microglia loaded with a $Ca^{2+}$ sensitive dye Fluo-4 AM (5 µM) is shown. **(B)** Changes in $[Ca^{2+}]_i$ in terms of relative fluorescent intensity ($F/F_0$) was monitored upon stimulation with muscimol (Mus; 100 µM for 30 s). Representative plot of mean ± SEM values from a single experiment containing 150 cells is shown. ATP (500 µM for 30 s) was used as a control for cell responsiveness.

To observe changes in $[Ca^{2+}]_i$ in AMG, postnatal acute brain slices were loaded with 10 µM Fluo-4 AM and a microglia marker, tomato lectin coupled to Alexa Fluor®594 (60 µg/ml). At the surface of the acute brain slices, 97% of AMG located at the corpus callosum showed transient $Ca^{2+}$ response towards 100 µM muscimol application for 30 s via bath perfusion (n = 160; *Fig. 17A-B*). In the presence of gabazine (10 µM), muscimol-induced $Ca^{2+}$ response was only observed in 35% of cells (n = 65; *Fig. 17C*). To test whether such effect was associated with increase in $[K^+]_0$, 10 mM KCl was applied for 30 s (total $[K^+]_0$ = 15

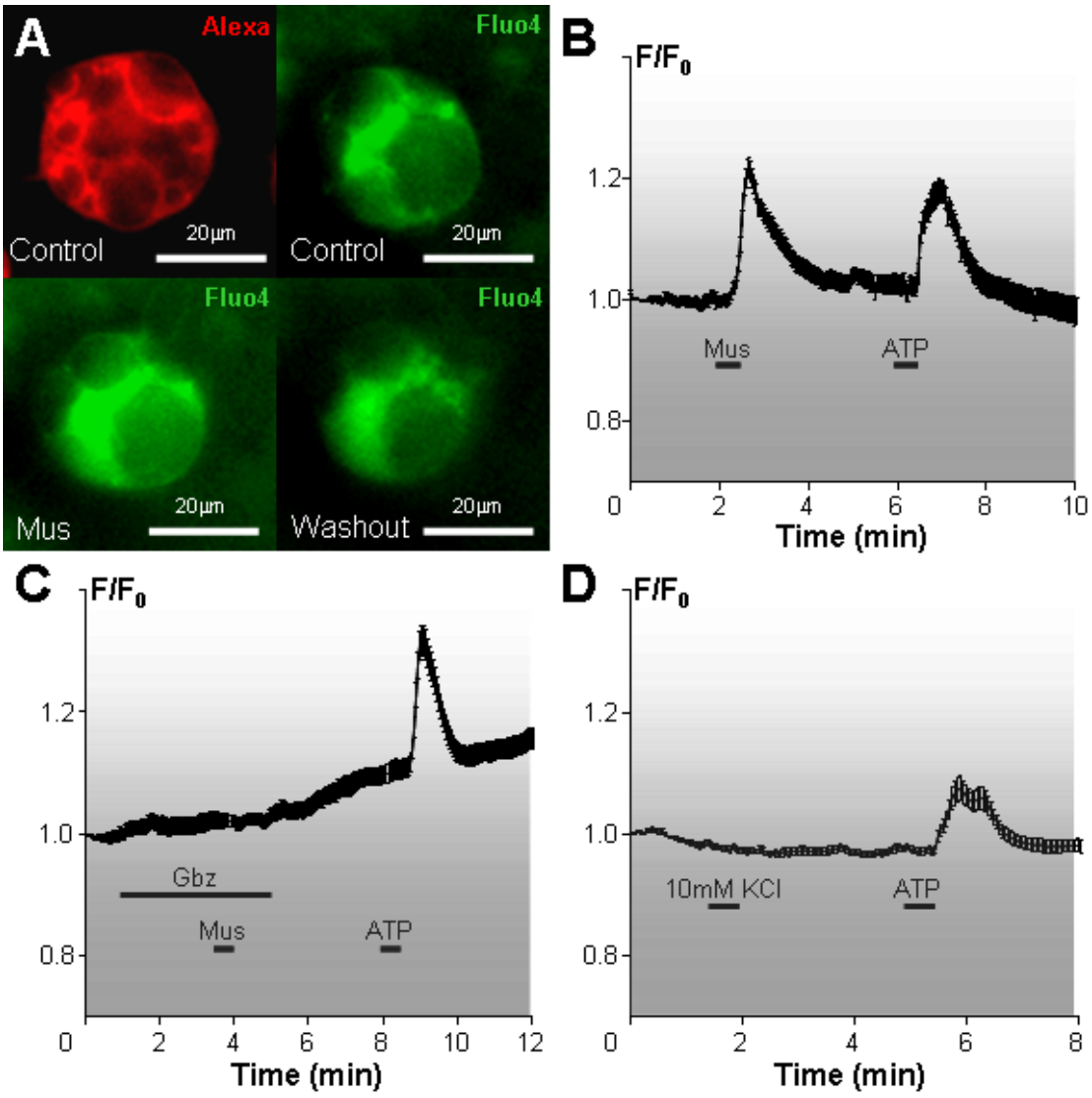


**Fig. 17. $Ca^{2+}$ response in AMG upon muscimol stimulation. (A)** Postnatal acute brain slices were loaded with a $Ca^{2+}$ sensitive dye Fluo-4 AM (10 µM) and a microglia marker, tomato lectin coupled to Alexa Fluor®594 (60 µg/ml). Images of an AMG on found on the surface of the corpus callosum are shown before (Control), during (Mus) and after (Washout) of 30-s bath application of muscimol (Mus; 100 µM). Representative plots of relative fluorescent intensity ($F/F_0$) over time are shown for application of **(B)** muscimol; **(C)** muscimol in the presence of gabazine (Gbz; 10 µM for 2-min preincubation) and **(D)** 10 mM KCl (total $[K^+]_0$ = 15 mM). ATP (1 mM for 30 s) was used to confirm cell responsiveness. Mean ± SEM values are shown from individual experiments containing 10 – 15 cells.

mM). However, no change in $[Ca^{2+}]_i$ could be detected (n = 96; *Fig. 17D*). As in the cultured microglia, only cells which responded towards ATP (1 mM for 30 s) were counted. As shown in *Fig. 18A*, a population of non-microglial cells in the corpus callosum region could be identified based on the absence of tomato lectin staining. Bath application of muscimol (100 µM for 30 s) also triggered transient $Ca^{2+}$ response in these cells which was stronger

and occurred quicker than that observed in AMG (*Fig. 18B*). To determine their identity, these cells were subsequently voltage-clamped. As a result, passive membrane profiles typical for astrocytes were measured from these cells (n = 10).

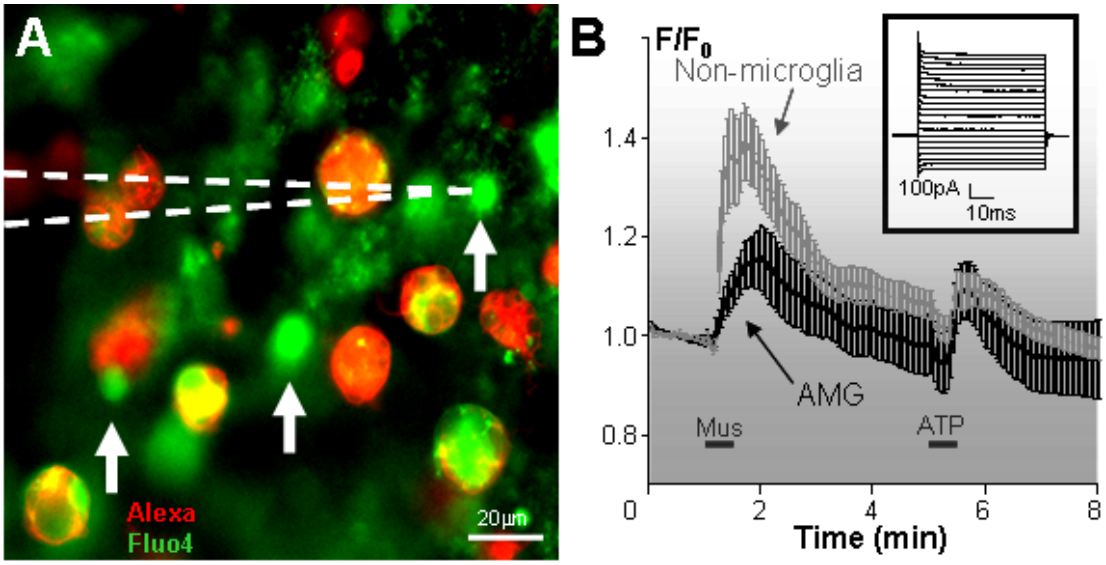


**Fig. 18. $Ca^{2+}$ response in neighboring cells upon muscimol stimulation. (A)** Image of the corpus callosum of a postnatal brain slice loaded with a $Ca^{2+}$ sensitive dye Fluo-4 AM (10 µM) is shown. Microglia were selectively labeled with tomato lectin coupled to Alexa Fluor®594 (60 µg/ml). **(B)** $Ca^{2+}$ response was recorded in AMG and a non-microglial population (indicated by arrows in **A**) upon 30-s bath application of muscimol (Mus; 100 µM). Mean ± SEM values of relative fluorescent intensity ($F/F_0$) over time from a single experiment containing 10 cells is shown. ATP (1 mM for 30 s) was used as control for cell responsiveness. To identify the non-microglial population, these cells were subsequently approached with patch pipettes (dotted lines in **A**). Using protocol described in inset of *Fig. 7B*, typical membrane current for astrocytes were measured from these cells (inset of **B**).

To study $Ca^{2+}$ response in isolated AMG, similar approach was carried out as in patch-clamp studies. Patch pipette filled with external solution were used to form a tight seal with the membrane of AMG loaded with Fluo-4. They were then lifted up above surface by manipulating the patch pipettes. In this case, membrane patch was not broken in order to keep intracellular content including $Ca^{2+}$ dye undisturbed. After 5 min of rest at 300 µm above brain slice surface, background $Ca^{2+}$ signal was no longer visible and $Ca^{2+}$ signal of the lifted-up AMG returned to stable baseline. 100 µM muscimol application for 30 s triggered $Ca^{2+}$ response only in 38% of cells tested (n = 8 out of 21; *Fig. 19*). ATP at 1 mM was applied at the end of the recording to confirm cell viability and responsiveness. It is apparent that cultured microglia, which did not show any current response to muscimol, also did not respond to it with mobilization of intracellular $Ca^{2+}$. On the other hand, AMG

which indirectly reacted to muscimol with current response also showed $Ca^{2+}$ response which was, however, unrelated to elevated $[K^+]_0$ and decreased with distance from the brain slice but still detectable at 300 µm above.

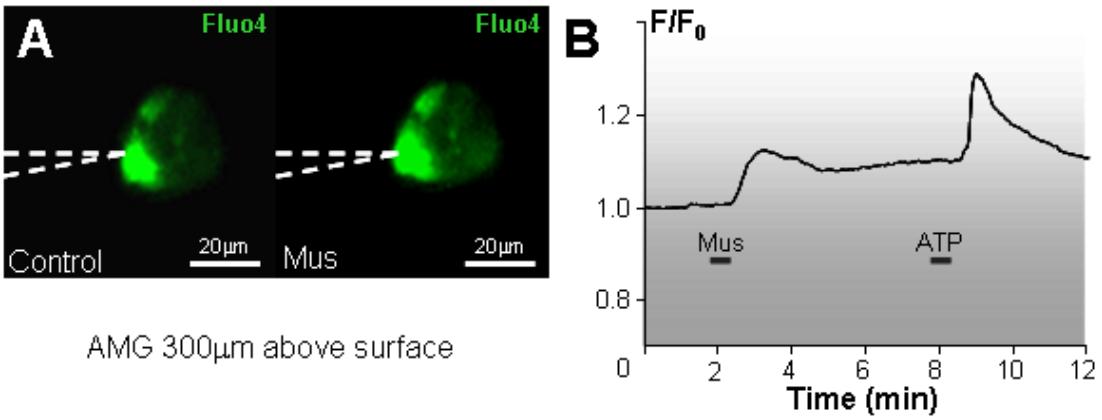


**Fig. 19. $Ca^{2+}$ response in isolated AMG upon muscimol stimulation. (A)** A single AMG from brain slice loaded with Fluo-4 AM was lifted 300 µm above surface of postnatal corpus callosum by manipulating the patch pipette (dotted lines). Membrane patch at the pipette tip was not broken to maintain intracellular content. Images before (Control) and during (Mus) muscimol stimulation (100 µM for 30 s) are shown. **(B)** Associated plot showing relative fluorescent intensity ($F/F_0$) over time. ATP (1 mM for 30 s) was used as control for cell responsiveness.

### 4.4.2 Chemotaxis and proliferation

The ability of cultured microglia to migrate towards ATP in the presence of different concentrations of $[K^+]_0$ was assessed using a microchemotaxis chamber. Over 2 hr, 300 µM ATP alone significantly increased microglial migration rate to 226 ± 27% of control. $[K^+]_0$ was elevated from 5 mM in control to 7.5, 10, 15 or 25 mM by addition of 2.5, 5, 10 or 20 mM KCl, respectively. From 5 independent experiments, no effect of increased $[K^+]_0$ on neither basal nor ATP-stimulated microglial migration was observed (*Fig. 20*). In other experiments, the effect of increased $[K^+]_0$ on microglial proliferation was assessed. Cultured microglia plated on 96-well pates were treated with different concentrations of KCl with or without LPS (100 ng/ml) for 24 and 48 hr. Proliferation was measured by the amount of BrdU incorporation during incubation periods relative to control. LPS significantly decreased proliferation by 81 ± 7 and 54 ± 7% after 24 and 48 hr, respectively. However, in 6 independent experiments, increase of $[K^+]_0$ by 2.5, 5, 10 or 20 mM did not affect basal nor LPS-attenuated proliferation at both time points (*Fig. 21*). Thus, both microglial chemotaxis and proliferation were not affected or modulated by elevated $[K^+]_0$.

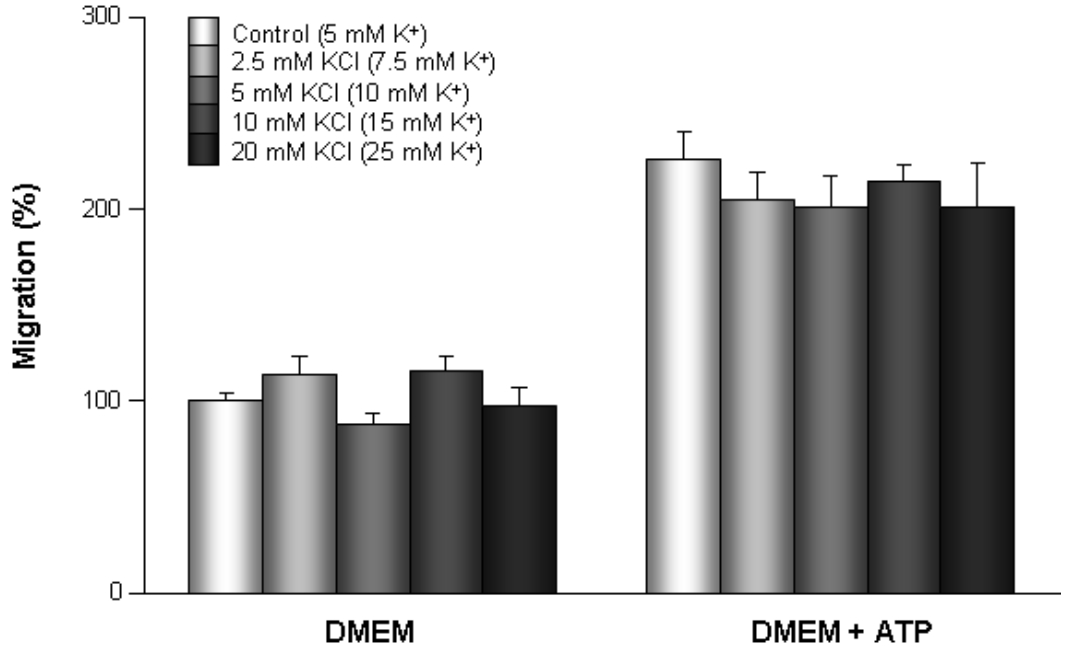


**Fig. 20. Effect of $[K^+]_0$ elevation on microglial chemotaxis.** Migration of cultured microglia towards different $[K^+]_0$ in DMEM with or without ATP (300 μM) was quantified by microchemotaxis assay. Migration rate over 2 hr was normalized to DMEM control. Results are expressed as mean ± SEM values.

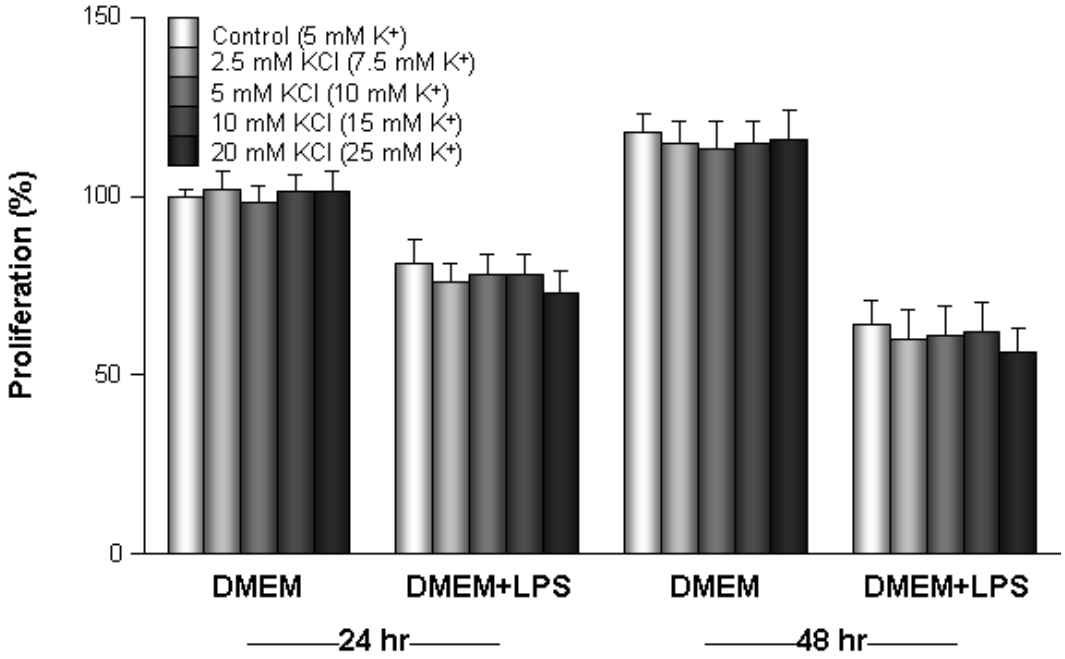


**Fig. 21. Effect of $[K^+]_0$ elevation on microglial proliferation.** Cultured microglia on 96-well plates were treated with different $[K^+]_0$ in DMEM with or without LPS (100 ng/ml) for 24 or 48 hr in the presence of 10 μM BrdU. Proliferation was quantified by BrdU incorporation assay and normalized to DMEM control after 24 hr. Results are expressed as mean ± SEM values.

### 4.4.3 Cytokine release

Cytokine release from microglia culture was studied upon stimulation with muscimol and elevated $[K^+]_0$. Cultured microglia plated on 96-well plates were treated with muscimol (100 or 200 µM) or KCl (2.5, 5, 10, 20 mM) for 24 hr. Culture medium was collected and tested for release of various cytokines by ELISA. Whereas muscimol had no effect, KCl from 5 – 20 mM dose-dependently enhanced microglial release of MIP-1α. In particular, 5 mM KCl significantly induced release to 145 ± 10% of control in 4 independent experiments (*Fig. 22*). Basal release of other cytokines, namely IL-6, IL-12, KC, and TNF-α was not affected by neither muscimol nor KCl.

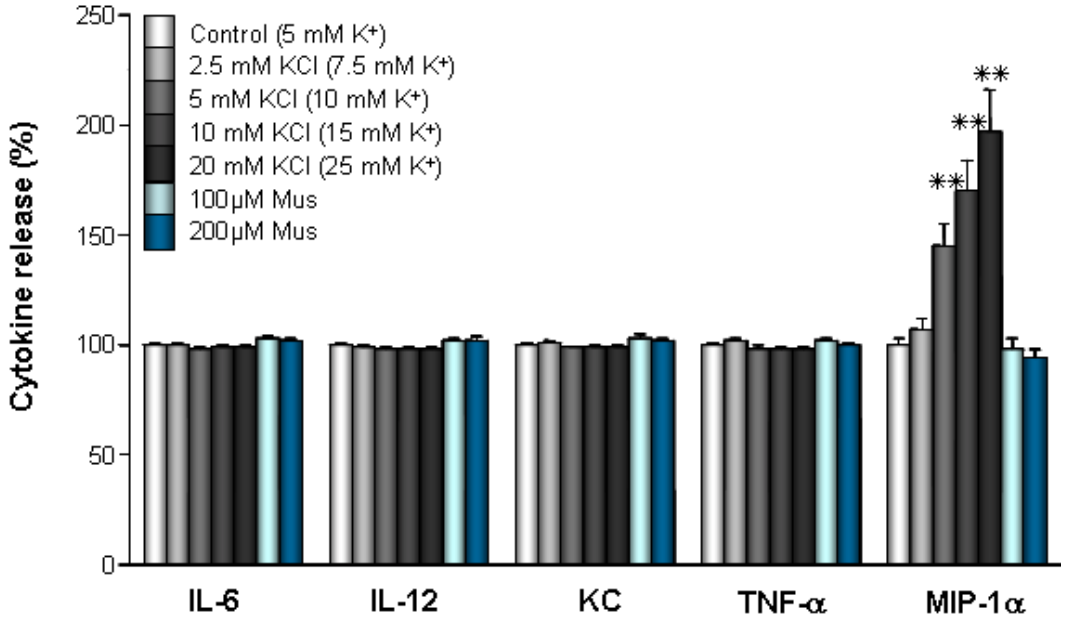


**Fig. 22. Effect of muscimol and $[K^+]_0$ elevation on cytokine release *in vitro*.** Cultured microglia on 96-well plates were treated with muscimol (100 or 200 µM) and different $[K^+]_0$ in DMEM for 24 hr. The amount of IL-6, IL-12, KC, TNF-α, and MIP-1α released into culture medium was quantified by ELISA and normalized to control for each cytokine. Results are expressed as mean ± SEM values. **, $p<0.01$ compared with MIP-1α control.

To better relate to the developing brain environment *in situ*, release of MIP-1α from postnatal brain slices was also tested. Slices containing the corpus callosum region were incubated with test substance for various time periods. MIP-1α released into buffer was quantified by ELISA as described for cultured microglia. After 1.5 hr, muscimol (100 µM) and KCl (5 mM) significantly induced MIP-1α production to 117 ± 5 (n = 15) and 115 ± 6 % (n = 16) of control, respectively (*Fig. 23A–B*). The muscimol-induced MIP-1α production

was blocked by gabazine (10 μM) and the effect of muscimol and KCl was not observed in the presence of $BaCl_2$ (100 μM). The KCl effect was not mimicked by equimolar NaCl indicating that increased osmolarity did not play a role in the induced release. Furthermore, as shown in *Fig. 23C*, 10 mM KCl resulted in a higher increase in MIP-1α production than 5

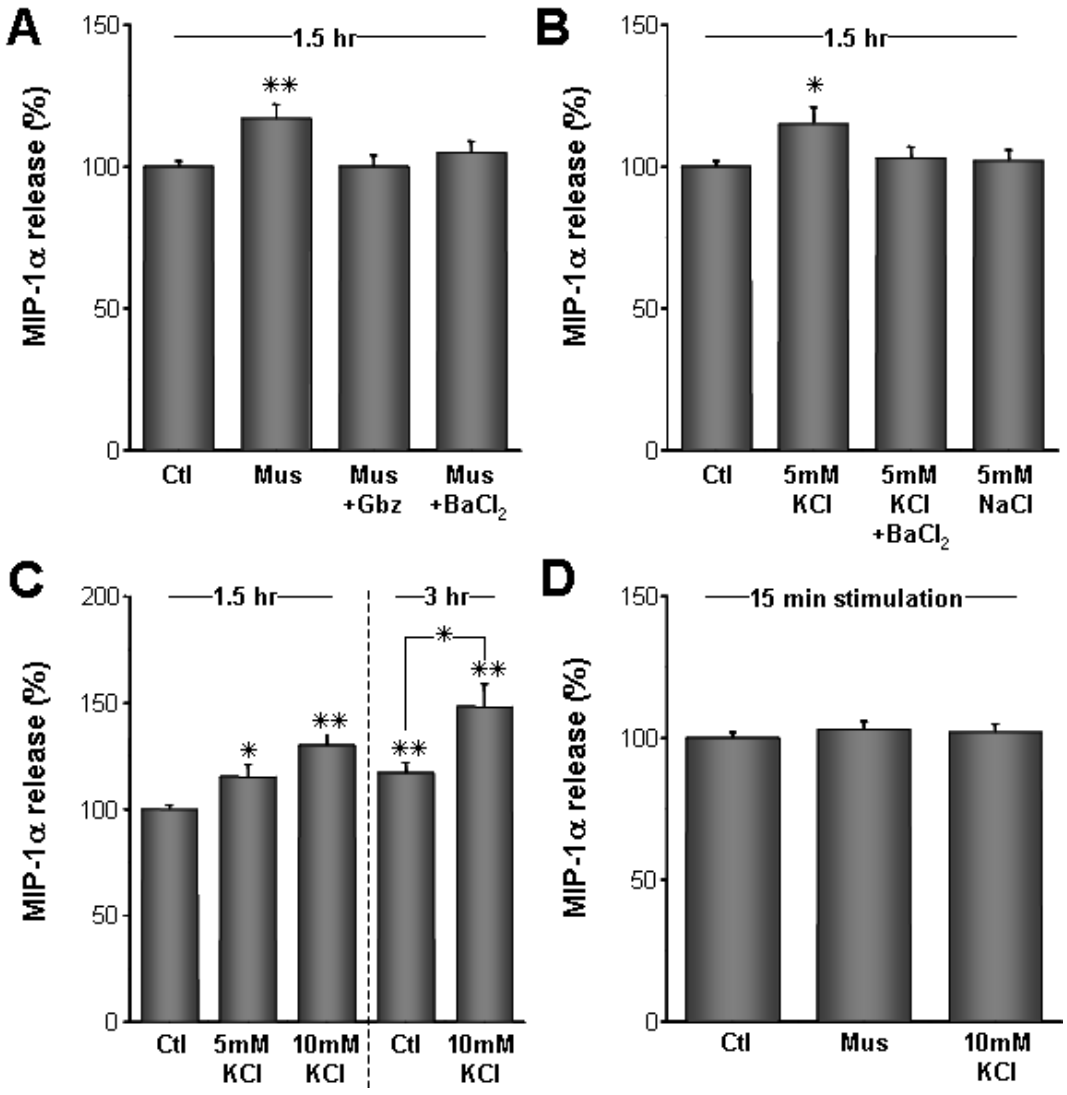


**Fig. 23. Effect of muscimol and $[K^+]_0$ elevation on cytokine release *in situ*.** Postnatal brain slices containing corpus callosum were incubated with various substances. The amount of MIP-1α released into the buffer was quantified by ELISA and normalized to corresponding controls. MIP-1α release was tested after 1.5 hr incubation of **(A)** muscimol (Mus; 100 μM) alone, in the presence of gabazine (Gbz; 10 μM) or $BaCl_2$ (100 μM); **(B)** 5 mM KCl (total $[K^+]_0$ = 10 mM) alone or in the presence of $BaCl_2$. 5 mM NaCl was added as a control for the effect of osmotic changes. **(C)** Brain slices treated with 10 mM KCl (total $[K^+]_0$ = 15 mM) for 1.5 and 3 hr were also tested. **(D)** To study the effect of short stimulation, Mus or KCl was added for only 15 min. Total release after 1.5 hr was measured and normalized to control where short 15-min stimulation was with buffer only. Results are expressed as mean ± SEM values. *, $p<0.05$; **, $p<0.01$ compared with corresponding controls unless stated otherwise.

mM (130 ± 7% of control; n = 11). The relative increase in MIP-1α release induced by 10 mM KCl after 3 hr was 127 ± 9% (n = 13), similar to that after 1.5 hr. In addition, the effect of short stimulation on long-term MIP-1α production was tested. Brain slices were treated with muscimol or 10 mM KCl for only 15 min. Total MIP-1α released after 1.5 hr was not different from control indicating that prolonged stimulation beyond 15 min was required (n = 8; *Fig. 23D*). Thus, both muscimol and elevated $[K^+]_0$ enhanced MIP-1α release *in situ*.

### 4.4.4 Motility

To observe and quantify cell movement, AMG located on postnatal corpus callosum brain slices were imaged at 2-s interval. After 15 min of baseline measurement, test substance was applied via bath perfusion. Images were subsequently analyzed for motility in terms of displacement and arm movement. Whereas displacement is a measure of the total distance travelled by a cell in two-dimension over 15 min, arm movement is quantified by activities around the cell in a single focal plane during the first 5 min of measurement. In general, baseline displacement and arm movement were 1.0 μm (n = 178) and 144 ± 0.5 (n = 92) arm movements per min, respectively. To correct for variability in basal activities among cells, relative motility during treatment normalized to basal activity of each cell was used. While the presence of 100 μM muscimol did not change basal displacement significantly (n = 22; *Fig. 24A*), relative arm movement increased to 160 ± 8% of baseline (n = 14; *Fig. 24B*). This increase was completely blocked by 10 μM gabazine (n = 8) and partially decreased by 100 μM $BaCl_2$ (n = 10). 5 mM KCl (total $[K^+]_0$ = 10 mM; n = 44) had no effect on displacement (n = 44) and mildly enhanced arm movement to 107 ± 1% of control (n = 17). It was sensitive to 100 μM $BaCl_2$ (n = 12) and not mimicked by equimolar NaCl (n = 12). As a positive control, ATP (500 μM), which increased microglial chemotaxis, significantly increased displacement to 156 ± 8% of control (n = 25). Analysis for associated arm movement was however unreliable due to considerable displacement. Thus, 15-min preincubation of brain slices with 5 μM cytochalasin D (CytoD), an inhibitor of actin filaments, was used as a negative control. As a result, AMG retracted most of their arms towards cell body which led to a significant reduction of arm movement (12 ± 2% of control; n = 12) accompanied by a decrease of displacement to 73 ± 12% of control (n = 13). Thus, arm movement of AMG was enhanced in the presence of muscimol.

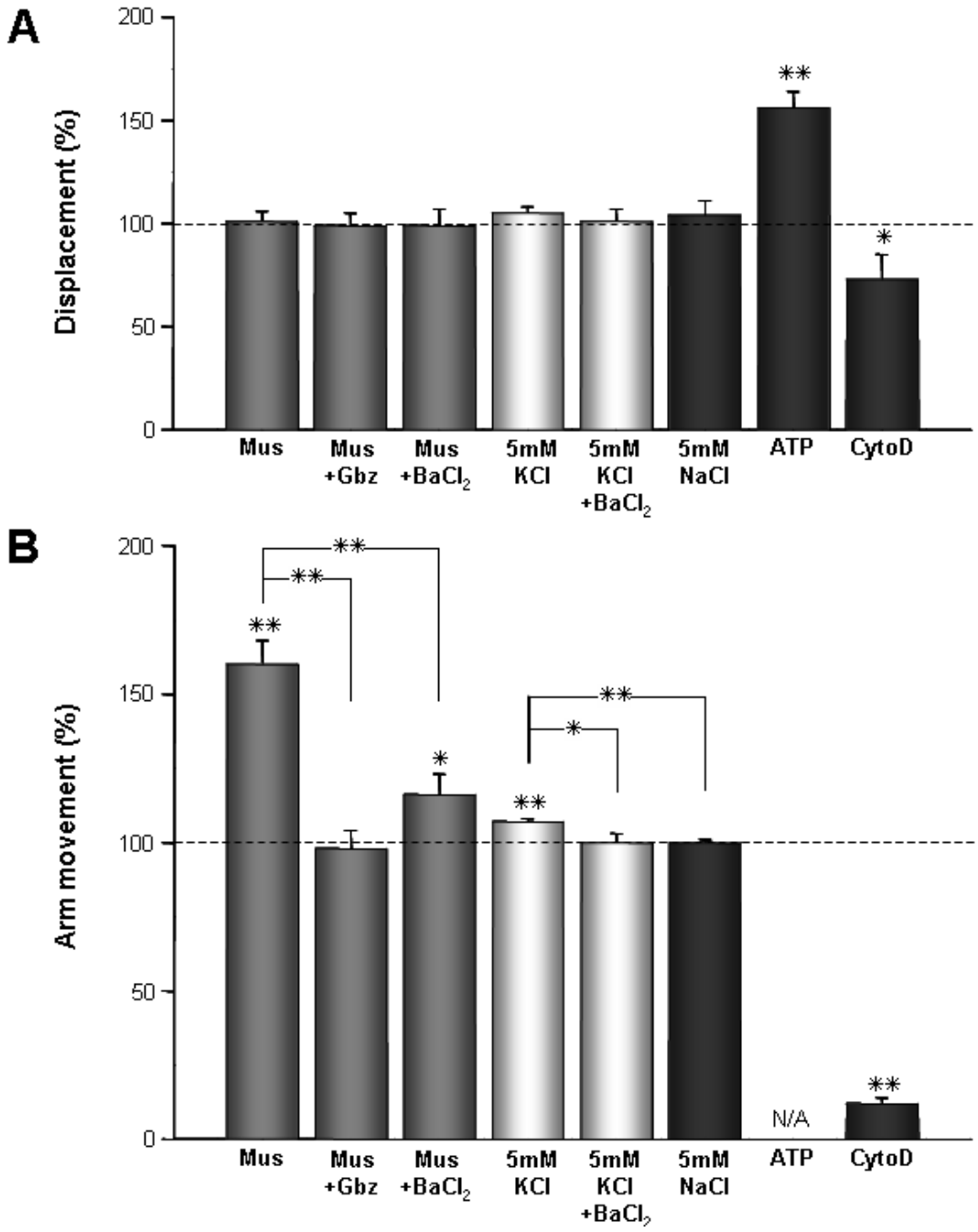


**Fig. 24. Effect of muscimol and $[K^+]_0$ elevation on AMG motility. (A)** Displacement of AMG on postnatal corpus callosum brain slices was measured from the total distance traveled in two dimension over time of stimulation (15 min). **(B)** Arm movement was estimated from activities along the perimeter of AMG over time of stimulation (5 min). To account for variable basal activities among cells, relative displacement and arm movement of each cell during bath perfusion of test substance was normalized to respective baseline activities (100%; dotted lines). Mean ± SEM values are plotted for displacement and arm movement under treatment with muscimol (Mus; 100 μM) in the presence or absence of gabazine (Gbz; 10 μM) or $BaCl_2$ (100 μM); and 5 mM KCl (total $[K^+]_0$ = 10 mM) in the presence or absence of $BaCl_2$. 5 mM NaCl was used to test for effect of changes in osmolarity. As positive and negative controls, ATP (500 μM) and cytochalasin D (CytoD; 5 μM for 15-min preincubation) were used. *, $p<0.05$; **, $p<0.01$ compared with corresponding baseline unless stated otherwise.

## *4.5 Properties of striatal astrocytes in response to stroke*

### 4.5.1 GFAP-EGFP fluorescence and morphology

Using 150-µm thick acute brain slices obtained from GFAP-EGFP transgenic mice, two astrocytic populations were identified in the striatum based on distinct fluorescent intensity and morphology. Brightly fluorescent cells displayed highly ramified processes, whereas weakly fluorescent cells had round soma and few processes with little, if any branching (*Fig. 25A-C*). By observing random visual fields, 40% of 476 GFAP positive cells were brightly and 60% weakly fluorescent. Only cells which clearly belonged to one of the groups were included. The morphological features of individual cells were even better visualized after cells were dialyzed with fluorescent dye Alexa Fluor®594 via the patch pipette (*Fig. 26*). This further revealed that some cells with low fluorescence intensity extended few thin processes emanating from the soma.

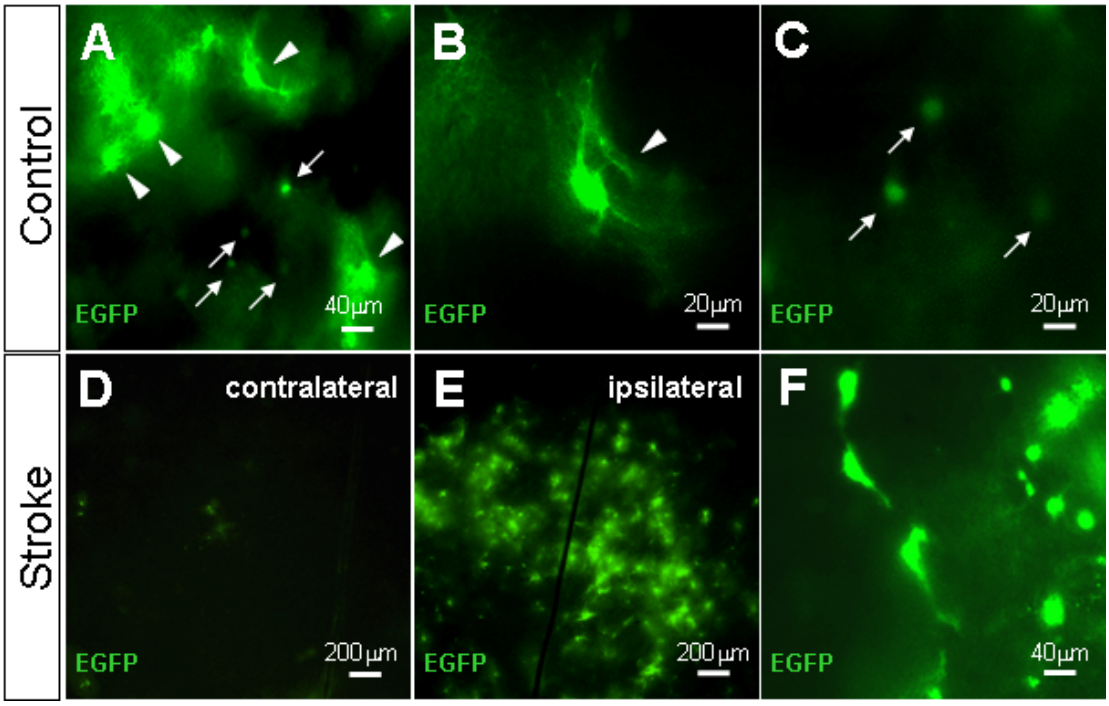


**Fig. 25. Effect of stroke on morphology of striatal astrocytes. (A)** EGFP fluorescence of the striatum in an acute brain slice from a control adult GFAP-EGFP transgenic mouse. Arrows and arrow heads denote weakly and brightly fluorescent cells, respectively. **(B-C)** Sections from A shown at higher magnification. **(D-E)** EGFP fluorescence of the contra- and ipsilateral striata 7 d after 30-min MCAo/reperfusion. **(F)** EGFP fluorescence from astrocytes in core of stroke lesion of the same time point after stroke.

Upon mild brain ischemia induced by 30 min MCAo/reperfusion, the majority of astrocytes in the core or border of the lesion area showed uniform up-regulated fluorescence. Representative images of an ipsilateral and contralateral striatum 7 days after stroke are shown (*Fig. 25D-E*). Note that using the same exposure time in capturing both images, hardly any fluorescent signals could be detected on the unaffected hemisphere. Although brightly fluorescent, the morphology of these cells resembled that of the weakly fluorescent cells in normal striatum (*Fig. 25F*). The number of processes appeared to have increased. Some astrocytes even had thickened, enlarged and long processes that terminated on blood vessels. From 12 animals (31 slices), less than 5% of EGFP positive cells (39 out of 818) could be classified, based on morphology and fluorescence level, as typical brightly or weakly fluorescent astrocytes found in control animals.

### 4.5.2 Membrane current

GFAP positive cells in the striatum were visually selected based on their fluorescence intensity and morphology and approached with patch pipettes. Membrane profiles were recorded with a series of 50-ms voltage jumps at 10-mV increments ranging from -200 to +80 mV from a HP of –70 mV. All brightly fluorescent cells were found to have passive membrane currents with no apparent time and voltage-dependence (n = 43; *Fig. 26A*). The MP and $R_m$ were -67.4 ± 1.4 mV and 49.4 ± 4.4 MΩ, respectively (n = 43). On the other hand, the majority of the weakly fluorescent cells (92%) expressed voltage-gated currents (n = 48; *Fig. 26B*). Outward currents triggered by depolarization exhibited delayed activation and subsequent inactivation. Inwardly rectifying currents were also recorded at hyperpolarizing voltages. MP and $R_m$ of these weakly fluorescent cells was -72.3 ± 0.8 mV and 57.1 ± 3.1 MΩ, respectively (n = 44). Only cells with stable MPs (between -50 and -85 mV) were analyzed.

To determine the impact of mild ischemia, membrane profiles of GFAP positive cells on 1, 4, 7, 14, 28, and 70 day(s) after MCAo/reperfusion were recorded. In the core or border of the stroke lesion, 85% of cells were found to express voltage-gated currents (n = 74; *Fig. 26C*). Depolarization triggered a delayed, inactivating outward current accompanied by inwardly rectifying currents recorded with hyperpolarization. The MP and $R_m$ of these cells were -72.5 ± 0.8 mV and 73.2 ± 6.6 MΩ, respectively (n = 62). These values were similar to

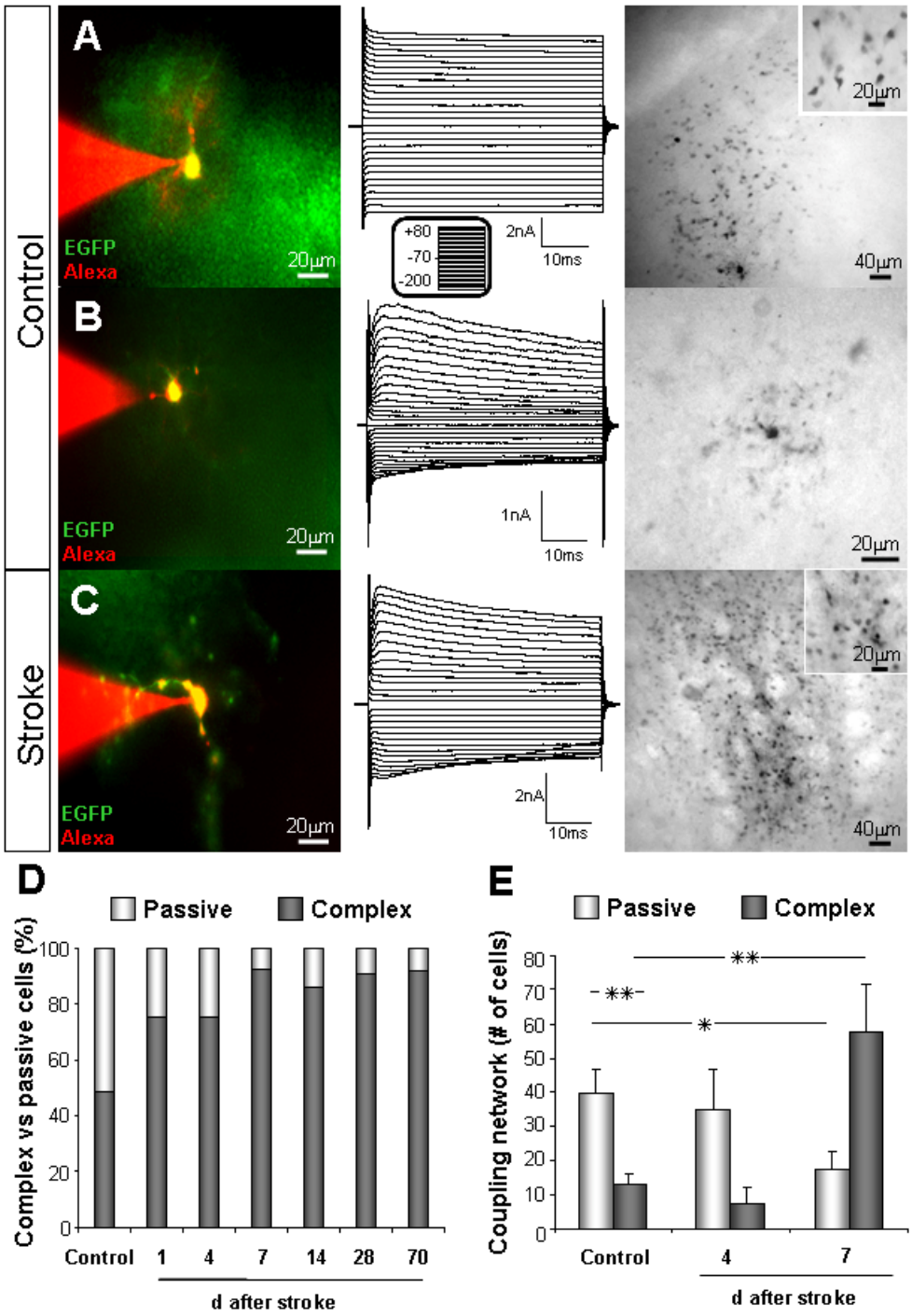


**Fig. 26. Effect of stroke on physiology and networks of striatal astrocytes. (A)** Left: A brightly fluorescent GFAP-EGFP cell from control striatum was filled with 10 µg/ml Alexa Fluor®594 and 0.5 - 0.6% biocytin. Middle: Membrane profile in response to de- and hyperpolarizing voltage steps as shown in inset. Right: Biocytin immunostaining revealed extent of gap junction coupling. Center of image is enlarged for clarity. **(B-C)** Similar approach as in **A** for a weakly fluorescent cell in control striatum and a complex cell in lesion site 7 d after stroke. **(D)** Bar chart indicating percentages of cells with complex versus passive membrane profile in control striatum as well as in the lesion sites 1, 4, 7, 14, 28, 70 d after stroke. **(E)** Mean ± SEM numbers of cells coupled to passive and complex cells are compared in control and lesion sites 4 and 7 d after stroke. *, $p<0.05$; **, $p<0.01$.

those of control complex cells but significantly different from control passive cells ($p < 0.01$). The remainder 15% of cells after stroke expressed passive currents. The relation between complex and passive cells is illustrated in *Fig. 26D*. In sham-operated animals 4 and 7 days after operation, two populations of astrocytes could be distinguished as in untreated control animals. In particular, all brightly fluorescent (n = 5) and weakly (n = 6) fluorescent cells were passive and complex, respectively. This indicated that physiological and morphological changes in astrocytes were not affected by factors associated with the intervention for example anesthesia, skin incision or stress related to the operation.

### 4.5.3 Gap junction network

To study the extent of gap junction coupling of subpopulations of astrocytes, patched cells were filled with 0.5 - 0.6% biocytin during whole-cell recording. Only cells with stable resting potential during the recording period were evaluated. Subsequently, networks of cells containing biocytin were identified by immunohistochemistry. All passive cells (n = 27; MP = -70.4 ± 0.8 mV) were coupled to a network of other cells. The network of biocytin positive cells consisted on average of 40 ± 7 cells (*Fig. 26A, E*). On the other hand, biocytin spread from weakly fluorescent cells (n = 16; MP = -71.6 ± 1.0 mV) with complex currents was also observed. On average, these significantly smaller networks consisted of 13 ± 3 cells (*Fig. 26B, E*).

Similarly, gap junction coupling in GFAP positive cells 4 and 7 days after mild ischemia was also assessed. Interestingly, complex cells found 7 days after MCAo/reperfusion showed a significant increase in size of coupling networks compared to control. In all recorded complex cells (n = 17; MP = -75.3 ± 1.3 mV), tracer spread from single injected astrocyte to a total of 58 ± 14 surrounding cells (*Fig. 26C, E*). On the contrary, passive cells found at this time point (n = 11) were coupled to only 17 ± 5 cells, significantly lower than control passive cells.

### 4.5.4 AMPA/KA glutamate receptor expression

KA was used to test for functional expression of AMPA/KA glutamate receptors in GFAP positive cells. Series of de- and hyperpolarizing voltage jumps ranging from -130 to +90 mV from a HP of -70 mV were applied repeatedly every 6 s. In all weakly fluorescent cells in control animals, KA (500 µM) triggered current response of 1057.6 ± 91.4 pA measured

at -70 mV (n = 27; *Fig. 27A*). KA evoked a complex response, which was composed of three different components (*Fig. 27A, C*). The difference between I/V curves obtained at various time points reflected current components which changed over time. Within few seconds after application, the resting $K^+$ conductance decreased and the reversal potential of this blocked conductance was at -70 mV. Subsequently, a conductance increase developed which had a reversal potential of 0 mV indicating that a cationic current was activated. This conductance increase returned to baseline within about 4 min after washout of KA. In 10 out of 30 cells, an outward rectifying current developed with a delay of 3 to 4 min after washout of KA. The reversal potential of this current was at -70 mV. This $K^+$ conductance increase was transient and returned to baseline after about 5 min. The resting $K^+$ conductance, which was reduced in amplitude at the beginning of the response, remained reduced in 20 out of 30 cells, even after 20 min recording time. In conclusion, KA triggered in all cells, 1) a transient cationic current; 2) a rapid and sometimes long-lasting blockade of the resting $K^+$ conductance; and in some cells, 3) a transient increase of an outwardly directed $K^+$ current with a significant delay. Whereas subsequent bath application of KA after a 5-10 min washout elicited a second current response in the same cell with about half the amplitude of the first one, this complex response to KA was completely blocked by 50 µM CNQX, the AMPA/KA glutamate subtype receptor blocker (n = 5; *Fig. 27A*). On the other hand, current response in brightly fluorescent cells consisted of only one component, namely a conductance increase with a reversal potential close to 0 mV (*Fig. 27B, C*). Only 52% of brightly fluorescent cells responded to KA with significantly smaller amplitude of 248.8 ± 64.9 pA measured at -70 mV (n = 23).

Over 1, 4, 7, 18, 28, 70 days after 30 min MCAo/reperfusion, 3 – 4 animals were sacrificed at each time point to test for KA-induced current response. All complex cells showed KA-induced complex current response which consisted of three components, similar to the complex response found in weakly fluorescent cells in control animals. The amplitude, however, was significantly smaller after stroke with a mean ± SEM value reaching only 748.5 ± 73.1 pA at -70 mV (n = 50; *Fig. 27C*).

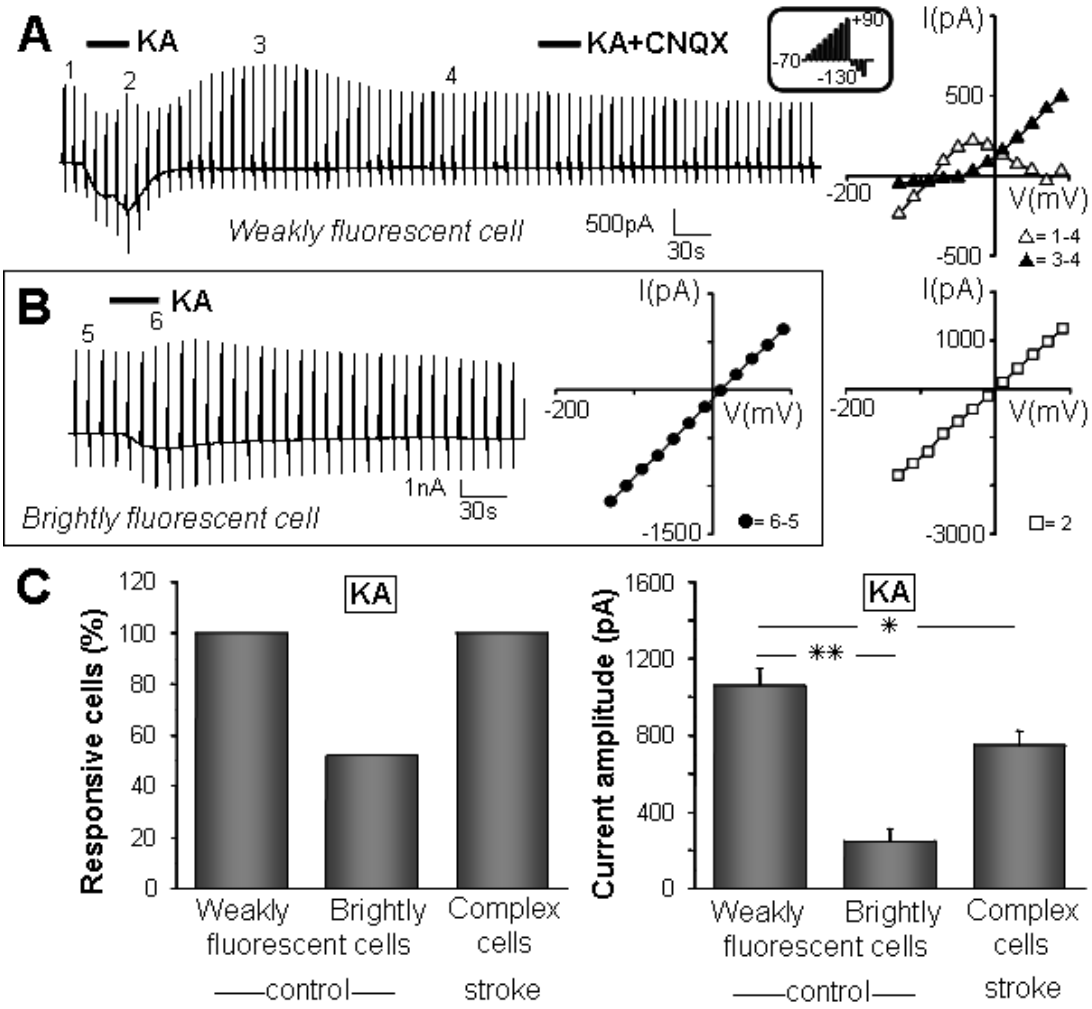


**Fig. 27. Effect of stroke on AMPA/KA receptor expression in striatal astrocytes. (A)** Membrane current was recorded in a weakly fluorescent GFAP positive cell in response to series of de- and hyperpolarizing voltage steps as shown in inset repeated every 6 s. Bath application of kainate (KA; 0.5 mM for 30 s) triggered a complex current response. In the presence of 50 μM CNQX, KA did not trigger any response (KA+CNQX). I/V curves were generated by subtracting currents as indicated by symbols and numbers. **(B)** Similar approach as in **A** in a brightly fluorescent GFAP positive cell. Note that KA-induced response contains only single component. **(C)** Bar charts showing proportion of cells responsive to KA (*left*) and mean ± SEM amplitudes of KA-induced inward current measured at -70 mV (*right*) for weakly, brightly fluorescent cells in control striatum and complex cells found after stroke. To minimize indirect effects by neuronal activity, recordings were carried out in the presence of 0.5 μM TTX and 0.1 mM $CdCl_2$. *, $p<0.05$; **, $p<0.01$.

### 4.5.5 Glutamate transporter expression

The expression of glutamate transporters was tested using D-aspartate (D-Asp), a substrate for glutamate transporters but not a ligand for the receptors. D-Asp triggered a small current response of 85.1 ± 9.6 pA measured at -70 mV in only 29% of weakly fluorescent cells (n = 31). In 85% of the brightly fluorescent cells, however, D-Asp induced

current response of 158.9 ± 21.3 pA at -70 mV (n = 27; *Fig. 28A, B*). The I/V curve of the D-Asp-induced current in brightly fluorescent cells showed an extrapolated reversal potential at high positive potentials. The response however did not reverse even at potentials as positive as 100 mV. At all time points after 30-min MCAo/reperfusion, 51% of complex cells responded to D-Asp with an amplitude of 70.0 ± 16.3 pA at -70 mV (n = 43; *Fig. 28B*), similar to what was observed in control weakly fluorescent cells. Thus, in the control striatum, the majority of weakly fluorescent cells showed receptor current while brightly fluorescent cells had transporter current. In response to stroke, brightly fluorescent cells dominated the lesion site with complex membrane properties similar to control weakly fluorescent cells and preferentially expressed glutamate receptors over transporters.

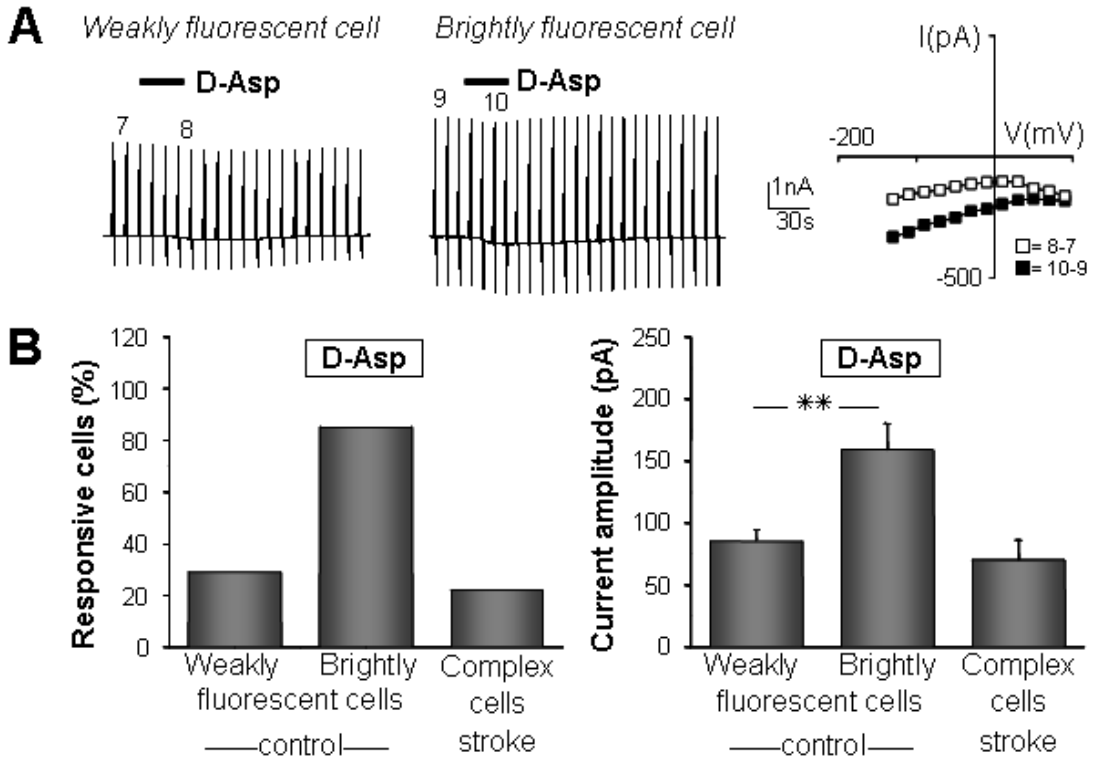


**Fig. 28. Effect of stroke on glutamate transporter expression in striatal astrocytes. (A)** Membrane current was recorded in a weakly (*left*) and brightly (*middle*) fluorescent GFAP positive cell in response to series of de- and hyperpolarizing voltage steps repeated every 6 s as shown in inset of *Fig. 27*. Bath application of D-aspartate (D-Asp; 0.5 mM for 30 s) triggered current responses. I/V curves (*right*) were generated by subtracting currents as indicated by symbols and numbers. **(B)** Bar charts showing proportion of cells responsive to D-Asp (*left*) and mean ± SEM amplitudes of D-Asp-induced inward currents measured at -70 mV (*right*) for weakly and brightly fluorescent cells in control striatum as well as complex cells found after stroke. To exclude an indirect contribution from neuronal glutamate receptors, recordings were carried out in the presence of 0.5 μM TTX, 0.1 mM $CdCl_2$ and 50 μM CNQX. *, $p<0.05$; **, $p<0.01$.

# 5 Discussion

## *5.1 Invading microglia sense GABAergic activities in the developing brain*

### 5.1.1 $GABA_A$ receptor expression on macroglia and neurons in postnatal brain

Prior to synapse formation, the neurotransmitter GABA is released by a vesicular mechanism from growth cones of developing axons. It occurs spontaneously and is enhanced by increased neuronal activities (Gao and van den Pol, 2000). At this stage of development, it acts as a trophic factor which modulates developmental processes like neuronal growth, migration, proliferation and differentiation. It also participates in the formation of synapse and construction of brain networks (Ben-Ari et al., 2007). The notion that neuronal precursor cells and immature neurons express functional $GABA_A$ receptors before synapse formation is well established (Owens and Kriegstein, 2002). Thus, it is conceivable that GABA is released in the developing corpus callosum. Using a receptor specific agonist, muscimol, it was observed in the present study that astrocytes, oligodendrocytes and glial precursor cells in the corpus callosum of postnatal brain slices as well as cortical neurons near this region show current response mediated by functional $GABA_A$ receptors expression. Associated reversal potentials near 0 mV indicated the opening of $Cl^-$ channels. These observations are supported by several previous studies. Specific $GABA_A$ receptor-mediated current response was detected in cultured astrocytes (Bormann and Kettenmann, 1988) and oligodendrocytes (Von Blankenfeld et al., 1991). Berger et al. (1992) characterized $GABA_A$ receptors in glial precursors and promyelinating oligodendrocytes in mouse corpus callosum brain slices during first two postnatal weeks. The expression of astrocytic $GABA_A$ receptors in grey matter is well documented (Steinhauser et al., 1994). In addition, complex glial cells in rat hippocampus respond towards $GABA_A$ but not $GABA_B$ receptor agonist (Bekar et al., 1999). Functions of glial $GABA_A$ receptors have been proposed as a way to sense neuronal activities (von Blankenfeld and Kettenmann, 1991), regulate extracellular pH (Kaila et al., 1991) and $K^+$ homeostasis (Barres et al., 1990). Thus, in the developing mouse corpus callosum, macroglia and neurons can sense GABAergic innervations via $GABA_A$ receptors.

### 5.1.2 Elevation of extracellular potassium upon membrane depolarization

The classical inhibitory neurotransmitter GABA has a depolarizing action in the developing brain due to high $[Cl^-]_i$ in immature neurons and glial cells (Ben-Ari et al., 2007). Membrane depolarization is accompanied by the efflux of $K^+$ and $Cl^-$. Thus an increase in $[K^+]_0$ upon $GABA_A$ receptor stimulation is often observed (Hoppe and Kettenmann, 1989; Muller et al., 1989). Depolarization of glial precursor cells even activates $Ca^{2+}$ channels (Kirchhoff and Kettenmann, 1992). In the present study, a transient $Ca^{2+}$ response upon specific $GABA_A$ receptor stimulation was detected in astrocytes presumably as a result of membrane depolarization. Thus, it is likely that elevation of $[K^+]_0$ detected in postnatal brain slices is due to $K^+$ efflux from glial cells and immature neurons. $[K^+]_0$ elevation was twice as large within than on the surface of corpus callosum postnatal brain slices, reaching up to 5 mM of increase. This can be explained by the presence of more cells, presumed source of $K^+$, within the brain slices as reflected by faster $K^+$ accumulation. The rate of removal, on the other hand, increased proportionally despite less efficient washout below surface implying the presence of an additional removal mechanism which became more effective with higher $K^+$ release. Uptake of $K^+$ released during neuronal activity by astrocytes in the process of $K^+$ spatial buffering is a likely explanation (Butt and Kalsi, 2006). $K^+$ release was not specific to the corpus callosum and could also be detected within cortical region. In fact, neurons with cell bodies in neighboring cortical region showed larger current response towards muscimol compared to glial cells. Furthermore, muscimol-induced $[K^+]_0$ elevation appeared to be age-dependent in that it was significantly smaller in adult brain slices. As neurons mature, $GABA_A$ receptors become inhibitory resulting in membrane hyperpolarization. This E-I switch of GABA action in neurons begins around postnatal days 5 - 8 (Kuner and Augustine, 2000; Marandi et al., 2002). As it was reported that GABA facilitates this switch (Ganguly et al., 2001), it is likely that during this short window of time which coincides with the occurrence of invading microglia, extracellular GABA level thus depolarization-induced $K^+$ efflux is favored.

### 5.1.3 Current response of microglia towards elevated extracellular potassium

Cultured microglia and ramified microglia *in situ* express metabotropic $GABA_B$ receptor triggering outward $K^+$ current and $Ca^{2+}$ response modulating cytokine release (Kuhn et al.,

2004). In the developing brain, however, the action of GABA is primarily through depolarizing $GABA_A$ receptors (Ben-Ari et al., 2007). Using a model where invading microglia could be identified *in situ* at the corpus callosum of postnatal brain slices, possible contribution of microglia to GABAergic innervations was studies. AMG have similar membrane properties as observed in cultured microglia despite different morphology. Whereas AMG were about 10 µm in diameter, round, and highly motile with filopodia-like processes extending in all directions; cultured microglia attached to glass coverslips were relatively flat with mobile edges. Similar to previously described studies, membrane profiles recorded in this study under voltage-clamp configuration showed that both AMG and cultured microglia express prominent inwardly but no outwardly rectifying $K^+$ channels (Kettenmann et al., 1990; Brockhaus et al., 1993). In both preparations, $K_{ir}$ current displayed time-dependent inactivation. At a HP of -70 mV, comparable MP and $R_m$ were detected between these preparations. It was previously reported that extracellular $Ba^{2+}$ at a range of 1-100 µM inhibited microglial $K_{ir}$ current but had no effect on $K_{dr}$ current (Franchini et al., 2004). In AMG, muscimol always triggered an increase in conductance of a current which showed inward rectification, reversed at -70 mV and was sensitive to 100 µM $BaCl_2$, suggesting that it was mediated by intrinsic $K_{ir}$ channels.

Although considerable variations in neurotransmitter receptor expression exist between different microglial preparations (Pocock and Kettenmann, 2007), the complete lack of $GABA_A$ receptor-induced current response on cultured microglia suggested that the current response in AMG could be indirect. Furthermore, muscimol-induced response in AMG often occurred later than those detected in neighboring cells and those elicited by ATP in the same cells. The progressive loss of muscimol-induced current response in isolated AMG at increasing distance away from brain slice surface strongly suggested the significance of being in close contact with neighboring cells. The elicited current response by placing brain slices on otherwise non-responsive cultured microglia further confirmed that muscimol-induced inward current observed in AMG was secondary.

The increase in $[K^+]_0$ upon $GABA_A$ receptor stimulation and the detected opening of $K_{ir}$ channels on AMG strongly implied that this secondary response was mediated by extracellular $K^+$. $K_{ir}$ channel activity *in vitro* is strongly dependent on $[K^+]_0$. An increase in $[K^+]_0$ increased cord conductance of the channel and shifted reversal potential to more

positive direction (Kettenmann et al., 1990). In the present study, moderate elevation in $[K^+]_0$ by 2.5, 5, and 7.5 mM from 5 mM dose-dependently increased $K^+$ conductance in AMG. More pronounced effect was observed in cultured microglia. $K^+$-induced current response lasted longer in AMG than in cultured microglia likely due to more efficient wash out from coverslips. Similar amplitudes and kinetics were observed when comparing current responses induced by muscimol and 5 mM KCl. $K^+$-induced response also occurred sooner than muscimol indicating a more direct effect of $K^+$.

Considerably smaller $[K^+]_0$ elevation observed upon consecutive muscimol stimulations could presumably be due to $GABA_A$ receptor desensitization often observed in neurons (Hutcheon et al., 2000). It was also observed that after the first current response towards muscimol, subsequent application of KCl but not muscimol elicited a second response in AMG. Thus, it is apparent that there is a threshold of $[K^+]_0$ increase above which is detectable by AMG. Furthermore, higher muscimol-induced increase in $[K^+]_0$ in postnatal than adult brain is an explanation for the absence of current response in adult microglia. The ramified cells typically had very small $K_{ir}$ current, as previously reported by Boucsein (2000), which translates to lower sensitivity towards changes in $[K^+]_0$.

It is clearly evident that an increase of $[K^+]_0$ due to membrane depolarization upon $GABA_A$ receptor activities opens $K_{ir}$ channels on microglia in the developing brain; but is too small to be detectable in the developed brain by ramified microglia which are also less responsive.

### 5.1.4 Cytokine release upon GABAergic innervations

The majority of studies on microglial chemokine release and receptor expression focus on neurodegenerative and inflammatory conditions where microglial response is rapidly induced (Hanisch, 2002). Due to low and undetectable levels of constitutive release, the roles of chemokines under physiological conditions are often neglected. Recently, emerging data suggest potential functions of chemokines in modulating brain activities in addition to their classical roles in inflammatory responses. Evidence for their involvement in normal brain functions including development have been demonstrated (Rostene et al., 2007). In the present study, unstimulated microglial cytokine release into culture medium over 24 hr could be detected using ELISA. Among various cytokines tested, induction of

MIP-1α release by elevated $[K^+]_0$ suggests specific actions of this chemokine. MIP-1 belongs to the CC chemokine subfamily. Its four members are MIP-1α, MIP-1β, MIP-1δ, and MIP-1γ (Menten et al., 2002). Although constitutively expressed in low amounts, astrocytes and fetal microglia promptly synthesize and release MIP-1 proteins *in vitro* upon stimulation (McManus et al., 1998; Miyamoto and Kim, 1999). MIP-1α binds to G-protein coupled receptors CCR1 and CCR5 leading to downstream processes important for many inflammatory conditions (Murdoch and Finn, 2000; Maurer and von Stebut, 2004). The role of MIP-1α and CCR1 in postnatal development of the cerebellum has been implicated (Cowell and Silverstein, 2003). In this brain region, immunoreactivity of CCR1 was observed in neurons, Bergmann glia, astrocytes and resting microglia which peaked between P7 and P21. MIP-1α expression in white matter microglia was detectable between P7 and P14, which coincides with the period of neuronal and glial maturation (Cowell and Silverstein, 2003). Interestingly, MIP-1α positive cells were often found near processes and cell bodies of CCR1-immunoreactive cells. As differential expression and release of chemokines and their receptors across developmental stages exists, it is essential to relate *in vitro* effect of elevated $[K^+]_0$ to the developing brain. Here, $K^+$-induced significant increase of basal MIP-1α release was also measured from postnatal acute brain slices over as short as 1.5 hr. Although no direct evidence confirmed source of MIP-1α release from brain slices, *in vitro* experiments suggest that microglia could contribute to the release. While muscimol had no effect on cultured microglia, similar effects of muscimol and elevated $[K^+]_0$ could be demonstrated *in situ*. It is postulated that microglial MIP-1α release *in situ* could be indirectly modulated upon $GABA_A$ receptor stimulation via elevated $[K^+]_0$.

During immediate early phase of acute neurodegeneration, release of TNF-$\alpha$ and IL-1 was detected as early as 1 hr after insult (Allan and Rothwell, 2001). It was also observed that the release of TNF-$\alpha$ and IL-6 from microglia in response to bacterial antigens requires only short-term stimulation (Hanisch et al., 2001). In the present developmental model, however, 15-min short stimulation could not induce MIP-1α release *in situ* indicating that prolonged presence of stimulus, namely GABAergic activities, may be required to take its effect. It is likely that vesicular release of GABA from axonal growth cones during development occurs in pulses upon action potentials (Gao and van den Pol, 2000). It could

be possible that MIP-1α release is only required when GABAergic activities in the brain remains consistently strong.

It was reported that MIP-1α regulates proliferation of a subpopulation of hematopoietic stem cells *in vivo* and *in vitro* and regulate hematopoiesis depending on the stages of development (Owen-Lynch et al., 1998; Broxmeyer and Kim, 1999). While impaired hematopoiesis was observed in CCR1 -/- mice, normal growth and development was not affected in these animals implying compensation of other MIP-1$\alpha$ receptor subtypes (Gao et al., 1997). Chemokines such as MCP-1 and MIP-1$\alpha$ also promote microglial migration and cytoskeleton reorganization *in vitro* (Cross and Woodroofe, 1999; Maciejewski-Lenoir et al., 1999). Effects of MIP-1α on properties of glial cells have also been discovered. MIP-1α and MCP-1 treatment could promote astrocyte migration *in vitro* possibly via novel astrocytic receptors (Heesen et al., 1996). Moreover, subnanomolar concentration of MIP-1α could induce chemotactic response in astrocytes *in vitro* (Tanabe et al., 1997). In view of these *in vitro* reports, observations *in situ* of the present study support the potential of MIP-1$\alpha$ released upon $GABA_A$ receptor stimulation in interacting with astrocytes and precursor cells in the developing corpus callosum.

### 5.1.5 Microglial properties upon GABAergic innervations

Microglial proliferation and migration are two important and well-documented processes of invading microglia (Cuadros and Navascues, 2001). There have been reports demonstrating that microglia in the developing quail retina go through alternating stages of migration and mitosis (Marin-Teva et al., 1999). The process of proliferation peaks between postnatal day 5 and 10 in the developing brain (Perry and Gordon, 1991; Ling and Wong, 1993). It was observed that AMG in many brain regions including the corpus callosum make use of their processes in dispersing themselves (Brockhaus et al., 1996; Cuadros et al., 1997). As naturally occurring cellular processes could regulate microglial proliferation and migration (Cuadros and Navascues, 2001), the potential of GABAergic innervations in the developing brain in promoting these events was tested in the present study. Whereas increased $[K^+]_0$ upon $GABA_A$ receptor stimulation elicited current response in AMG and cultured microglia, an effect on microglial proliferation *in vitro* was not observed. Chemotaxis was also unaffected by the presence of increasing $K^+$ gradient. Despite reports

indicating the roles of $K^+$ channels in microglial proliferation, volume changes and migration (Eder, 2005), $K^+$-mediated current changes in microglia observed in this study was not associated with cell proliferation and migration. However, it cannot be ruled out that cultured microglia behave differently than AMG *in situ*. As mentioned, microglia, even the resting ramified ones, continuously monitor their surroundings with moving processes (Davalos et al., 2005; Nimmerjahn et al., 2005). It was first observed by Brockhaus et al. (1996) that invading microglia in postnatal corpus callosum used velum-like processes to actively screen and phagocytoze dead or damaged cells in their surroundings. In the present study, movement of these processes was systematically quantified and compared. It was observed that muscimol significantly enhanced relative arm movement of AMG but displacement of the cells away from its original position was not affected. With increased sensitivity to their surroundings, AMG may be able to better perform their characteristic tasks including removal of cellular debris in the developing brain where GABAergic activity is strong. To establish this claim, further studies of *in situ* phagocytosis upon muscimol stimulation is warranted. Additionally, apart from neighboring astrocytes, $Ca^{2+}$ response was also observed in AMG upon muscimol stimulation. The decreased number of responding AMG at a distance above surface and lack of response in cultured microglia suggest that, similar to current response observed, $[Ca^{2+}]_i$ increase was also an indirect effect which was strongest at the surface of the brain slice. Unlike current response, however, $Ca^{2+}$ response in single AMG at 300 µm above surface of brain slice was still detectable, although much less frequently. Microglia *in vitro* respond to neuropeptides like kinins with mobilization of intracellular $Ca^{2+}$ and migration (Noda et al., 2006). $Ca^{2+}$ response towards a series of neurotransmitters including GABA via $GABA_B$ receptors have also been observed (Kuhn et al., 2004; Pocock and Kettenmann, 2007). Here, the lack of functional $GABA_A$ receptor on AMG demonstrated by electrophysiological studies indicates that direct receptor mediated effect is unlikely. Extracellular $K^+$, the substance mediating microglial current response and cytokine release, had only little effect on arm movement and no effect on $Ca^{2+}$ response implying alternative mechanisms which are yet unknown. Nevertheless, it is evident that in the presence of $GABA_A$ receptor agonist, enhanced arm movement and $Ca^{2+}$ response in AMG could be observed in postnatal brain slice. However, the mechanisms involved should be further investigated.

### 5.1.6 Approaches to study microglial properties

Microglia comprise of a largely heterogeneous population which varies across species, brain regions, developmental stages as well as preparations (Hanisch and Kettenmann, 2007). Among these, the invading microglia in early and postnatal development display distinctive characteristics not observed in other stages. Using acute brain slices obtained from postnatal mouse brain, AMG accumulation on the surface of the corpus callosum made physiological studies of this unique population possible (Brockhaus et al., 1993; Brockhaus et al., 1996; Haas et al., 1996; Farber et al., 2005). These *in situ* studies have the advantage that the environment of the developing corpus callosum is preserved to some extent. However, the presence of activities of neighboring cells may also obscure or mask response from AMG. One of the objectives of the present study is to address this problem by devising methods to understand microglial response in relations to their surroundings. By lifting up AMG via patch pipettes according to previously described methods (Walz et al., 1993; Haas et al., 1996), whole cell voltage-clamp or $Ca^{2+}$ imaging experiments could be performed at various distances above surface of brain slices. The contact between AMG and the tip of patch pipettes was usually tight enough to withstand slow mechanical manipulations of height within continuous bath perfusion and downward force generated by the weight of the large cell. A resting period of 5 min at the destination was necessary for the cells to recover from stress. ATP-induced current and $Ca^{2+}$ response detected in all of these isolated AMG before the end recordings confirmed cell viability and good patch quality. Although not tested in this study, by including $Ca^{2+}$ sensitive dyes in the pipette solution with appropriate salt concentrations, it is possible to perform $Ca^{2+}$ imaging and patch-clamp experiments simultaneously.

An apparent constraint of using cultured microglia is that culture manipulations disturb or even activate naive microglia (Walz and Bekar, 2001). Contents of culture medium may also alter their response (Eder et al., 1995a). Besides, in the absence of intact brain tissue, some indirect microglial response may not be detectable, like in the present study. This problem can be overcome by placing freshly prepared acute brain slices on coverslips of cultured cells. Similar to the AMG liftup approach, properties of cultured microglia can be assessed within minutes. However, long-term effect of reintroducing brain slice

environment beyond few hours cannot be performed due to limited time within which fresh brain slices can be kept.

Most studies assessing microglial motility use time-lapse microscopy to measure distance travelled by cells on coverslips over hours of stimulation (Ifuku et al., 2007). This is useful when general or directional migration of cells is of interest. In the present study, however, AMG on the surface of brain slices did not migrate considerably within minutes of stimulation. Instead, their processes were responsive in this time frame. AMG have distinct morphology different from cultured microglia where many of their functions rely on their moving arms. Their phagocytotic activities for example, do not require significant displacement of cells from its original location (Brockhaus et al., 1996). In many cases, it takes only minutes for an AMG to respond to and phagocytoze cell debris. These properties cannot be observed *in vitro*. Although there has been reports characterizing this type of movement in cultures (Nolte et al., 1996; Rezaie et al., 2002b), no previous study has quantified arm movements of AMG. By measuring changes of intensity around the perimeter of these round cells, relative movement of arms could be estimated. In order to detect only moving arms, a sampling rate of 2 s was chosen so that arms which remained stationary over 2 s were excluded in the calculation by obtaining the difference between consecutive images. This also successfully removed stationary background. After using a filter to enhance edges, background became darker and moving arms brighter. With CytoD pretreatment, arms of AMG retracted considerably which was reflected in the quantification. This method, however, is only reliable in cases where the AMG did not move significantly from its original position or out of focus thus only the first 5 min of stimulation was analyzed and compared to the first 5 min of control period. It should also be noted that extension of arms without movement along the perimeter which is also of interest with regards to phagocytosis could not be detected using this method. An attempt to measure this would be to increase the size of the sampling circle to detect moving objects at various distances from the center of the cell. This would also require a very stable image recording.

## *5.2 Unique physiological properties in striatal astrocytes in response to stroke*

### 5.2.1 Subpopulations of astrocytes with distinct properties in the striatum

Distinctions between astrocytic populations in terms of “complex” and “passive” membrane properties were previously established *in situ* (Steinhauser et al., 1994) and were subsequently supported by further studies (Seifert and Steinhauser, 1995; Zhou and Kimelberg, 2001). The generation of GFAP-EGFP transgenic mice allowed observations and electrophysiological recordings of a population of astroglial cells in many brain regions including the cortex, cerebellum, striatum, corpus callosum and hippocampus (Nolte et al., 2001). In the present study, two types of GFAP-EGFP positive astrocytes in roughly equal proportion were identified in adult mouse striatum. Based on GFAP-EGFP expression, they could be divided into brightly and weakly fluorescent cells. Brightly fluorescent cells had larger soma surrounded by fine, ramified processes. They always lacked voltage-gated channels resulting in passive membrane current profiles. The majority of these cells displayed glutamate transporter activities as similarly described previously (Zhou and Kimelberg, 2001). Weakly fluorescent cells in the striatum, on the other hand, had smaller soma and clearly distinguishable processes most of which were only visible by dye filling via patch pipettes. They expressed delayed rectifying $K^+$ outward thus were complex cells and showed large AMPA/KA receptor response which was also similarly demonstrated by Zhou and Kimelberg (2001). These distinct characteristics also parallel previous reports in the hippocampus (Matthias et al., 2003) and brain stem (Grass et al., 2004) using the same transgenic model. However, unlike the hippocampus, glutamate receptor/transporter responses were not exclusive to one cell type in the striatum implying the possibility of co-expression of glutamate receptors and transporters in a small proportion of cells. That is, in the striatum, KA and D-Asp also triggered small and infrequent responses in brightly and weakly fluorescent cells, respectively. While KA triggered only classical cationic conductance of glutamate receptor response in brightly fluorescent cells, the corresponding current response in weakly fluorescent cells was composed of complex current components involving a cationic conductance. Furthermore, 20-min biocytin dye-filling into patched cells revealed that brightly fluorescent passive cells were highly coupled via gap

junctions. This high coupling rate among passive cells which resembled the classical protoplasmic astrocytes supported their proposed role in spatial buffering of extracellular glutamate and $K^+$ released by neurons (Anderson and Swanson, 2000). However, in contrast to the hippocampus where weakly fluorescent cells were uncoupled (Wallraff et al., 2004), those in the striatum were found to be coupled albeit to a significantly smaller extent than brightly fluorescent ones. Further studies are warranted to investigate the functional significance of the presence of gap junction coupling in complex cells of the striatum.

Thus, in the healthy striatum, it is shown in the present *in situ* study that like in other brain regions, two populations of astrocytes exist with distinctive ion channel expression and differential response towards glutamate. They also differ in terms of their mode of communication via gap junction coupling which implies different mechanisms of transporting and distributing substances among cells.

### 5.2.2 Ischemia-induced changes in astrocytic properties

In the striatum, GFAP-EGFP positive cells over days after 30-min MCAo/reperfusion displayed a collection of unique properties not exclusively present in any one cell type in control animals. Most obviously, GFAP-EGFP expression increased within the ischemic lesion area as compared to the contralateral hemisphere similar to previous observations upon cortical stab wounds (Nolte et al., 2001). In the injured striatum, clear distinction between brightly and weakly fluorescent cells could not be made, however cells with complex membrane current became progressively dominant over days after MCAo/reperfusion. In fact, up-regulation of outwardly rectifying $K^+$ currents which appeared to play a role in proliferation of reactive astrocytes have been demonstrated *in situ* and *in vitro* (MacFarlane and Sontheimer, 1997; Bordey and Sontheimer, 1998; Anderova et al., 2004). Furthermore, the increased proportion of complex cells was accompanied by increased expression of glutamate receptor on astroglia in the striatum. It was reported in the cerebellum that over-expression of AMPA receptors lead to elongated glial processes (Ishiuchi et al., 2001) whereas a down-regulation resulted in retraction in Bergmann glia (Iino et al., 2001). In line with these reports, it was indeed observed in the present study that weakly fluorescent cells in control tissue and cells after stroke have more extended

processes than brightly fluorescent cells correlating with expression of AMPA/KA receptors. These together may enhance the ability of astrocytes in detecting areas of high extracellular glutamate concentration and respond accordingly. Another fascinating observation is that these complex cells were found to be highly coupled; even more than passive cells in control striatum. On the other hand, passive cells showed decreased gap junction coupling compared to those in control striatum. This could be explained by the observation that they were rarely found in the ischemic striatum. Beneficial effects of astrocytic gap junction coupling have been demonstrated by increased ischemic infarct size in connexin 43 (Cx43) deficient mice (Siushansian et al., 2001) and enhanced neuronal death in Cx43 +/- mice (Nakase et al., 2003a; 2003b). A recent report demonstrated that decreased Cx43 protein expression resulted in impaired gap junction coupling only in the injured hemisphere upon photothrombotic lesion (Haupt et al., 2007). In other studies, astrocytic gap junction coupling appeared to promote brain damage by providing a pathway for propagation of toxic signals throughout the brain (Lin et al., 1998; Frantseva et al., 2002). Since astrocytes do not undergo cell death in the present MCAo/reperfusion model (Katchanov et al., 2001; Kronenberg et al., 2005), it is postulated that the observed increase in coupling network may be neuroprotective. In fact, neuronal death which began 18 hr and peaked after 72 hr after MCAo (Katchanov et al., 2001) preceded enhanced astrocytic coupling which was detected only after at least 4 days. This could imply different time frames of action where brain damage precedes repair mechanisms. It is also interesting that the expression of glutamate transporter in these astrocytes after stroke was not up-regulated. Glutamate transporters are normally considered as a means through which extracellular glutamate can be removed during glutamatergic synaptic activities and from the injured sites (Anderson and Swanson, 2000). In this case, the lack of increased glutamate transporter expression together with a higher coupling rate among astrocytes suggest the possibility that, neuroprotective substances outside of the lesion area could reach the site of injury via network of astrocytes without having to sacrifice for the spreading of glutamate into healthier surrounding brain regions. In order to establish this claim, details of the composition and regulations of the coupling network among complex reactive astrocytes in the striatum in response to stroke should be further defined.

## *5.3 Proposed roles of invading microglia and striatal astrocytes*

According to the present observations, invading microglia, although lacking functional $GABA_A$ receptors, could sense $GABA_A$ receptor activities in neighboring macroglia and neurons via intrinsic $K_{ir}$ channels (*Fig. 29*). This was accompanied by induced release of the chemokine MIP-1α from microglia *in vitro* and from postnatal brain slices which may potentially attract astrocytes and neural stem cells towards the developing white matter. In addition, $GABA_A$ receptor activities also stimulated arm movement and intracellular $Ca^{2+}$ response in invading microglia *in situ* which may have functional significance in microglial properties like phagocytosis. Together, these may contribute to the development of postnatal white matter where trophic actions of GABA are important.

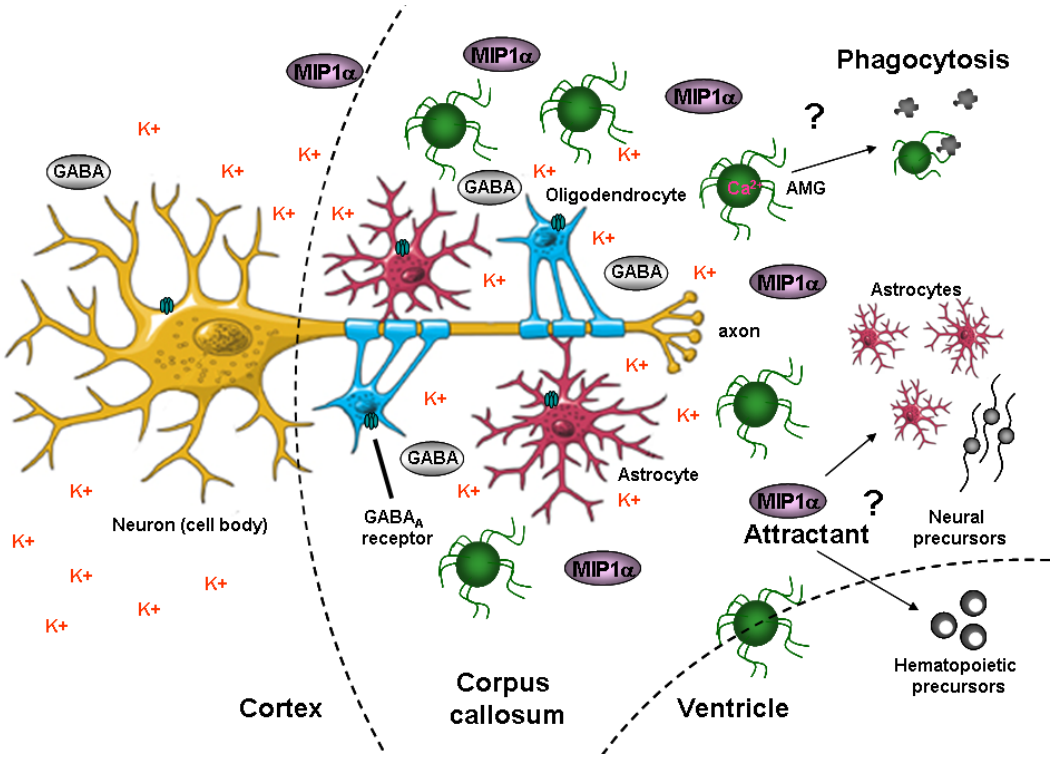


**Fig. 29. Invading microglia sense GABAergic activities in the developing brain.** A proposed series of events occurring at the postnatal corpus callosum is illustrated. GABAergic innervations stimulate $GABA_A$ receptors on macroglia and cortical neurons. This is followed by membrane depolarization and thus $K^+$ efflux from these cells. The resulting increase in $[K^+]_0$ opens $K_{ir}$ channels on ameboid microglia (AMG) which have invaded the brain from sites including the ventricles. This in turn enhanced chemokine MIP-1α release which may attract neural or hematopoietic precursors and astrocytes. Through mechanisms yet to be elucidated, enhanced arm movement and elicited $Ca^{2+}$ response in AMG have potential functional significance in phagocytotic activities. *Images of cells are modified from http://www.helpforheadaches.com/articles/nihsheets/life-neuron.htm.*

On the other hand, properties of astrocytes in response to mild focal ischemia were characterized. Similar to other brain regions, two distinct subtypes of GFAP-EGFP positive astrocytes could be observed in a healthy striatum (*Fig. 30*). In response to MCAo/reperfusion, a unique population of astrocytes unlike any observed in healthy mice dominated the stroke lesion over days. These cells had increased GFAP-EGFP fluorescence, voltage-gated membrane currents and glutamate receptor expression. Furthermore, they also generated large gap junction network which may confer long-term protection of the brain.

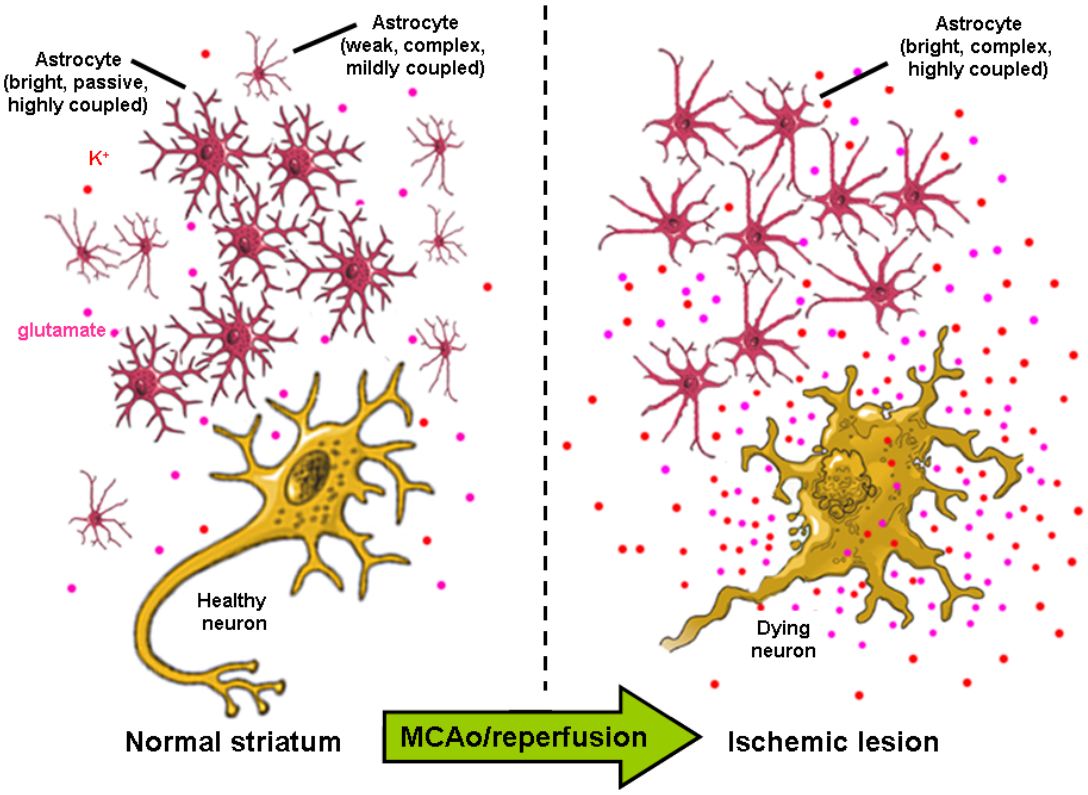


**Fig. 30. Unique physiological properties in striatal astrocytes in response to stroke.** A proposed series of events occurring in the striatum after stroke is illustrated. Two types of GFAP-EGFP positive astrocytes with distinctive morphology and current pattern could be identified in normal striatum where healthy neurons are found. They show different response towards glutamate in that the complex cells which are mildly coupled mostly express AMPA/KA receptors while the majority of the passive cells form large gap junction networks and express transporters. In response to MCAo/reperfusion, the lesion is dominated by complex astrocytes with up-regulated GFAP-EGFP fluorescence and hypertrophic processes. These cells sense glutamate from the extracellular space via AMPA/KA receptors and become highly coupled. This process persisted over days after MCAo and may confer long-term protection of the brain. *Images of cells are modified from http://www.helpforheadaches.com/articles/nihsheets/life-neuron.htm.*

# 6 Summary

Emerging findings demonstrate that in the central nervous system, glial cells interact with neuronal networks and thereby modulate brain activities. In particular, microglia and astrocytes respond rapidly towards the environment with morphological and physiological changes. In two separate projects, the functions of invading microglia in the developing brain (*Project 1*) and properties of astrocytes in response to mild focal ischemia (*Project 2*) were investigated:

**Project 1:** Microglia invade the brain during early stages of development and migrate along fiber tracts to their final destinations where they become resident. However, specific signals through which they communicate with the developing brain are yet largely unknown. The present study utilized ameboid microglia at the corpus callosum of postnatal mouse acute brain slices as a model for invading microglia. Their response towards $GABA_A$ receptor activities, which is essential for trophic actions of GABA in brain development, was studied. Whole cell patch-clamp experiments revealed that muscimol, a specific agonist for $GABA_A$ receptor, triggered a transient increase in $K^+$ conductance in ameboid microglia. Such response was progressively lost in single cells lifted up from slice surface and was observed in cultured microglia only in close vicinity to brain slices suggesting that it was indirect. Muscimol also stimulated $GABA_A$ receptors on macroglia and neurons in postnatal brain leading to an elevation of extracellular $K^+$ concentration ($[K^+]_0$). In addition, an experimental increase of $[K^+]_0$ mimicked muscimol-induced current response in microglia. These results indicated that invading microglia in early postnatal development sense GABAergic activities indirectly via sensing changes in $[K^+]_0$. This in turn stimulated the release of a chemokine, macrophage inflammatory protein-1 alpha, from microglia *in vitro* and from postnatal brain slices; while the release of a number of other cytokines, microglial chemotaxis and proliferation were not affected. Moreover, in adult brain slices, muscimol only led to a small increase in $[K^+]_0$ which failed to elicit current response in ramified microglia suggesting functional significance specific for the developing brain. Concurrently, motility and intracellular $Ca^{2+}$ level of ameboid microglia were also enhanced upon $GABA_A$ receptor stimulation.

**Project 2:** There is at present no consensus about the beneficial or detrimental roles of astrocytes in brain injuries. Using adult transgenic mice expressing enhanced green fluorescent protein under the glial fibrillary acidic protein (GFAP) promoter, astrocytes in the striatum were characterized before and after mild focal ischemia. In healthy striatum, two types of GFAP positive astrocytes with distinctive properties could be identified; 1) brightly fluorescent cells were characterized by bushy processes, passive membrane properties, glutamate transporter activity, and formed large gap junction coupling network; 2) weakly fluorescent cells generally had thin and clearly distinguishable processes, voltage-gated currents, complex current responses to kainate, and low coupling rate. While the brightly fluorescent cells have properties typical for classical astrocytes, the weakly fluorescent ones resemble a glial cell subtype recently described in the hippocampus. To investigate properties of these cell populations upon brain injury, short middle cerebral artery occlusion (MCAo) followed by reperfusion which leads to delayed neuronal cell death and astrogliosis in the striatum was used as a model for mild focal ischemia. In response to MCAo/reperfusion, brightly fluorescent cells became dominant over days within the ischemic lesion and the majority of these cells expressed voltage-gated channels and showed complex responses to kainate. Interestingly, they had high coupling rate which even exceeded that of control brightly fluorescent cells. Conversely, a minority of cells found after ischemia had passive membrane properties and decreased coupling rate.

Taken together, findings from these projects demonstrated properties of glial cells in the developing and injured brains suggesting possible functional significance. Invading microglia, although they did not express functional $GABA_A$ receptor subtype, could sense GABAergic activities in neighboring cells of the developing brain via $[K^+]_0$ increase. This modulated microglial properties which may contribute to white matter development. Striatal astrocytes, on the other hand, underwent distinct pathophysiological changes after ischemic insults and constituted a novel physiological phenotype which formed large syncytium. The delayed and long-lasting effects suggested possible neuroprotective functions of these reactive astrocytes.

# 7 Zusammenfassung

Jüngere Forschungsergebnisse zeigen, dass Gliazellen eine wichtige Rolle im Zentralnervensystem spielen, die darin besteht, dass sie mit neuronalen Netzwerken interagieren und somit Hirntätigkeiten modulieren. Besonders Mikroglia und Astrozyten reagieren unmittelbar mit aktiver Änderung ihrer Zellmorphologie und – physiologie auf Reize ihrer Umgebung. Somit wurde in zwei getrennten Projekten die Funktionen einwandernder Mikroglia im sich entwickelnden Gehirn (*Projekt 1*) sowie die Eigenschaften von Astrozyten als Reaktion auf Fokale Ischämie (*Projekt 2*) untersucht:

**Projekt 1:** Mikroglia dringen während früher Entwicklungsstadien in das Gehirn ein und wandern entlang von Fasertrakten zu ihrem Zielort, an dem sie in die ruhende Form übergehen. Dennoch sind die Signale, durch die sie mit dem sich entwickelnden Gehirn kommunizieren, noch immer weitgehend unbekannt. Die hier vorgelegte Studie nutzte amöboide Mikroglia aus dem Corpus callosum akuter Hirnschnitte aus postnatalen Mäusen als ein Modell für einwandernde Mikroglia. Es wurde deren Reaktion auf $GABA_A$ Rezeptoraktivität, welche essentiell für die trophische Wirkung von GABA während der Hirnentwicklung ist, untersucht. Whole cell patch clamp Experimente erbrachten den Beweis, dass Muscimol, ein spezifischer $GABA_A$ Rezeptor-Agonist, eine transiente Erhöhung der Kaliumleitfähigkeit in amöboiden Mikrogliazellen erzeugt. Diese Reaktion verschwandt sukzessive als einzelne Mikroglia über die Schnittoberfläche angehoben wurden. Ebenso war die Reaktion in Kultur nur in unmittelbarer Nähe zu einem Hirnschnitt zu beobachten, was auf einen indirekten Effekt schließen lässt. Muscimol aktivierte im postnatalen Gehirn $GABA_A$ Rezeptoren auf benachbarten Makroglia sowie auf Neuronen, was zu einer Erhöhung der extrazellulären Kaliumkonzentration ($[K^+]_O$) führte. Zusätzlich konnte eine experimentelle $[K^+]_O$ Erhöhung den Effekt von Muscimol imitieren. Diese Ergebnisse zeigten, dass eindringende Mikroglia während der frühen postnatalen Entwicklung GABAerge Aktivität indirekt durch Änderungen der $[K^+]_O$ detektieren. Dies wiederum stimulierte die Freisetzung eines Chemokins namens macrophage inflammatory protein-1 alpha sowohl aus postnatalen Hirnschnitten als auch aus Mikrogliazellen in Kultur; die Freisetzung anderer Zytokine, die mikrogliale Chemotaxis sowie Proliferation wurden nicht beeinflusst. Des weiteren führte Muscimol in Hirnschnitten von adulten

Mäusen nur zu einem geringen Anstieg der $[K^+]_O$, welcher nicht in der Lage war, eine Stromantwort in ramifizierten Mikroglia hervorzurufen. Dies legt eine funktionelle Signifikanz spezifisch für das sich entwickelnde Gehirn nahe. Gleichzeitig führte die $GABA_A$ Rezeptor Stimulation zu einer Erhöhung der Motilität und der intrazellulären Kalziumkonzentrationen amöboider Mikroglia.

**Projekt 2:** Derzeit besteht keine Einigkeit bezüglich der förderlichen oder schädlichen Rolle von Astrozyten bei Hirnverletzungen. Unter Zuhilfenahme adulter transgener Mäuse, die das enhanced green fluorescence protein (EGFP) unter dem Promotor von glial fibrillary acidic protein (GFAP) exprimieren, wurden Populationen von Astrozyten im Striatum vor und nach Fokaler Ischämie untersucht. In akuten Schnitten, die aus gesunden Hirnen gewonnen wurden, konnten zwei Typen von GFAP-positiven Astrozyten im Striatum ausgemacht werden. 1) Hell fluoreszierende Zellen, charakterisiert durch buschige Fortsätze, passive Membraneigenschaften, Glutamattransporter-Aktivität und Kopplung durch Gap Junction Netzwerke. 2) Schwach fluoreszierende Zellen mit dünnen und klar zu identifizierenden Fortsätzen, spannungsaktivierten Strömen, einer komplexen Stromantwort auf Kainat und einer geringen Kopplungsrate. Während die hell fluoreszierenden Zellen Charakteristika klassischer Astrozyten zeigten, hatten die schwach fluoreszierenden Zellen Ähnlichkeit mit einem kürzlich im Hippocampus beschriebenen astrozytären Subtyp. Um die Eigenschaften dieser Zellpopulationen in Reaktion auf Hirnverletzungen zu untersuchen, wurden kurze Okklusionen der mittleren zerebralen Arterie (MCAo), gefolgt von Reperfusion, durchgeführt. Dies führte zu verzögerten neuronalen Zelltod und Astrogliose im Striatum und diente als Modell für Fokale Ischämie. Als Antwort auf MCAo/Reperfusion zeigte sich, dass stark fluoreszierende Zellen im Laufe mehrerer Tage dominant im Bereich der ischämischen Läsion wurden. Die Mehrheit dieser Zellen exprimierte spannungsaktivierte Kanäle und zeigte komplexe Antworten auf Kainat. Interessanterweise zeigten diese Zellen eine höhere Kopplungsrate als Kontrollzellen mit starker Fluoreszenz. Eine Minderheit der Zellen hingegen zeigte passive Membraneigenschaften und wies im Vergleich zu passiven Kontrollzellen eine verminderte Kopplungsrate auf.

Zusammengefasst zeigen die Ergebnisse aus dieser Studie Eigenschaften von Gliazellen im sich entwickelnden und verletzten adulten Gehirn, die eine funktionelle Signifikanz

nahelegen. Einwandernde Mikroglia können GABAerge Aktivitäten in benachbarten Zellen des sich entwickelnden Gehirns teilweise detektieren obwohl sie keine funktionellen $GABA_A$ Rezeptoren exprimieren. Dies findet durch eine Erhöhung der $[K^+]_O$ statt, welche die mikroglialen Eigenschaften moduliert, was möglicherweise zur Entwicklung der weißen Substanz beiträgt. Andererseits unterlagen striatale Astrozyten verschiedenen pathophysiologischen Änderungen nach einer Ischämie und stellten einen neuen physiologischen Phänotyp dar, der ein großes Synzytium bildete. Der verzögerte und lang anhaltende Effekt legt eine mögliche neuroprotektive Funktion reaktiver Astrozyten nahe.

# 8 References

Albright AV et al. (1999) Microglia express CCR5, CXCR4, and CCR3, but of these, CCR5 is the principal coreceptor for human immunodeficiency virus type 1 dementia isolates. J Virol 73:205-213.

Allan SM, Rothwell NJ (2001) Cytokines and acute neurodegeneration. Nat Rev Neurosci 2:734-744.

Aloisi F (2001) Immune function of microglia. Glia 36:165-179.

Ambrosini E, Aloisi F (2004) Chemokines and glial cells: a complex network in the central nervous system. Neurochem Res 29:1017-1038.

Anderova M et al. (2004) Voltage-dependent potassium currents in hypertrophied rat astrocytes after a cortical stab wound. Glia 48:311-326.

Anderson CM, Swanson RA (2000) Astrocyte glutamate transport: review of properties, regulation, and physiological functions. Glia 32:1-14.

Bajetto A et al. (2002) Characterization of chemokines and their receptors in the central nervous system: physiopathological implications. J Neurochem 82:1311-1329.

Balslev Y et al. (1996) Synaptogenesis in the neocortical anlage and early developing neocortex of rat embryos. Acta Anat (Basel) 156:2-10.

Barbin G et al. (1993) Involvement of GABAA receptors in the outgrowth of cultured hippocampal neurons. Neurosci Lett 152:150-154.

Barres BA et al. (1990) Ion channels in vertebrate glia. Annu Rev Neurosci 13:441-474.

Bekar LK et al. (1999) GABAA receptor agonists modulate K+ currents in adult hippocampal glial cells in situ. Glia 26:129-138.

Ben-Ari Y et al. (2007) GABA: a pioneer transmitter that excites immature neurons and generates primitive oscillations. Physiol Rev 87:1215-1284.

Ben-Ari Y et al. (1997) GABAA, NMDA and AMPA receptors: a developmentally regulated 'menage a trois'. Trends Neurosci 20:523-529.

Berger T et al. (1992) GABA- and glutamate-activated currents in glial cells of the mouse corpus callosum slice. J Neurosci Res 31:21-27.

Bergles DE et al. (2000) Glutamatergic synapses on oligodendrocyte precursor cells in the hippocampus. Nature 405:187-191.

Biber K et al. (2001) Ischemia-induced neuronal expression of the microglia attracting chemokine Secondary Lymphoid-tissue Chemokine (SLC). Glia 34:121-133.

Blanc EM et al. (1998) Astrocytic gap junctional communication decreases neuronal vulnerability to oxidative stress-induced disruption of Ca2+ homeostasis and cell death. J Neurochem 70:958-970.

Boddeke EW et al. (1999) Cultured rat microglia express functional beta-chemokine receptors. J Neuroimmunol 98:176-184.

Bordey A, Sontheimer H (1998) Properties of human glial cells associated with epileptic seizure foci. Epilepsy Res 32:286-303.

Bordey A et al. (2000) Reactive astrocytes show enhanced inwardly rectifying K+ currents in situ. Neuroreport 11:3151-3155.

Bordey A et al. (2001) Electrophysiological characteristics of reactive astrocytes in experimental cortical dysplasia. J Neurophysiol 85:1719-1731.

Bormann J, Kettenmann H (1988) Patch-clamp study of gamma-aminobutyric acid receptor Cl- channels in cultured astrocytes. Proc Natl Acad Sci U S A 85:9336-9340.

Boucsein C et al. (2000) Electrophysiological properties of microglial cells in normal and pathologic rat brain slices. Eur J Neurosci 12:2049-2058.

Bowman CL, Kimelberg HK (1984) Excitatory amino acids directly depolarize rat brain astrocytes in primary culture. Nature 311:656-659.

Brockhaus J et al. (1996) Phagocytozing ameboid microglial cells studied in a mouse corpus callosum slice preparation. Glia 16:81-90.

Brockhaus J et al. (1993) Membrane properties of ameboid microglial cells in the corpus callosum slice from early postnatal mice. J Neurosci 13:4412-4421.

Broxmeyer HE, Kim CH (1999) Regulation of hematopoiesis in a sea of chemokine family members with a plethora of redundant activities. Exp Hematol 27:1113-1123.

Butt AM, Kalsi A (2006) Inwardly rectifying potassium channels (Kir) in central nervous system glia: a special role for Kir4.1 in glial functions. J Cell Mol Med 10:33-44.

Callewaere C et al. (2006) The chemokine SDF-1/CXCL12 modulates the firing pattern of vasopressin neurons and counteracts induced vasopressin release through CXCR4. Proc Natl Acad Sci U S A 103:8221-8226.

Cartier L et al. (2005) Chemokine receptors in the central nervous system: role in brain inflammation and neurodegenerative diseases. Brain Res Brain Res Rev 48:16-42.

Chamak B et al. (1994) Brain macrophages stimulate neurite growth and regeneration by secreting thrombospondin. J Neurosci Res 38:221-233.

Chamak B et al. (1995) Immunohistochemical detection of thrombospondin in microglia in the developing rat brain. Neuroscience 69:177-187.

Contreras JE et al. (2004) Role of connexin-based gap junction channels and hemichannels in ischemia-induced cell death in nervous tissue. Brain Res Brain Res Rev 47:290-303.

Cowell RM, Silverstein FS (2003) Developmental changes in the expression of chemokine receptor CCR1 in the rat cerebellum. J Comp Neurol 457:7-23.

Cross AK, Woodroofe MN (1999) Chemokines induce migration and changes in actin polymerization in adult rat brain microglia and a human fetal microglial cell line in vitro. J Neurosci Res 55:17-23.

Cuadros MA, Navascues J (1998) The origin and differentiation of microglial cells during development. Prog Neurobiol 56:173-189.

Cuadros MA, Navascues J (2001) Early origin and colonization of the developing central nervous system by microglial precursors. Prog Brain Res 132:51-59.

Cuadros MA et al. (1994) Development of microglia in the quail optic tectum. J Comp Neurol 348:207-224.

Cuadros MA et al. (1997) Microglia development in the quail cerebellum. J Comp Neurol 389:390-401.

D'Ambrosio R et al. (1998) Functional specialization and topographic segregation of hippocampal astrocytes. J Neurosci 18:4425-4438.

Davalos D et al. (2005) ATP mediates rapid microglial response to local brain injury in vivo. Nat Neurosci 8:752-758.

DeCoursey TE et al. (1996) Ion channel expression in PMA-differentiated human THP-1 macrophages. J Membr Biol 152:141-157.

Del-Rio H (1932) In: Cytology and Cellular Pathology of the Nervous System (Penfield W, ed), pp 481-534. New York: Hoeber.

Dobbertin A et al. (1997) Neurons promote macrophage proliferation by producing transforming growth factor-beta2. J Neurosci 17:5305-5315.

Eder C (2005) Regulation of microglial behavior by ion channel activity. J Neurosci Res 81:314-321.

Eder C et al. (1997) Distinct soluble astrocytic factors induce expression of outward K+ currents and ramification of brain macrophages. Neurosci Lett 226:147-150.

Eder C et al. (1995a) Properties of voltage-gated currents of microglia developed using macrophage colony-stimulating factor. Pflugers Arch 430:526-533.

Eder C et al. (1995b) Properties of voltage-gated potassium currents of microglia differentiated with granulocyte/macrophage colony-stimulating factor. J Membr Biol 147:137-146.

Elkabes S et al. (1996) Brain microglia/macrophages express neurotrophins that selectively regulate microglial proliferation and function. J Neurosci 16:2508-2521.

Endres M et al. (1998) Attenuation of delayed neuronal death after mild focal ischemia in mice by inhibition of the caspase family. J Cereb Blood Flow Metab 18:238-247.

Farber K, Kettenmann H (2005) Physiology of microglial cells. Brain Res Brain Res Rev 48:133-143.

Farber K, Kettenmann H (2006) Purinergic signaling and microglia. Pflugers Arch 452:615-621.

Farber K et al. (2005) Dopamine and noradrenaline control distinct functions in rodent microglial cells. Mol Cell Neurosci 29:128-138.

Farber K et al. (2008) The ectonucleotidase cd39/ENTPDase1 modulates purinergic-mediated microglial migration. Glia 56:331-341.

Ferrer I et al. (1990) Naturally occurring cell death in the cerebral cortex of the rat and removal of dead cells by transitory phagocytes. Neuroscience 39:451-458.

Franchini L et al. (2004) Inwardly rectifying K+ channels influence Ca2+ entry due to nucleotide receptor activation in microglia. Cell Calcium 35:449-459.

Frantseva MV et al. (2002) Ischemia-induced brain damage depends on specific gap-junctional coupling. J Cereb Blood Flow Metab 22:453-462.

Fujita H et al. (1998) Adrenergic agonists suppress the proliferation of microglia through beta 2-adrenergic receptor. Neurosci Lett 242:37-40.

Gaiarsa JL et al. (1995) Postnatal development of pre- and postsynaptic GABAB-mediated inhibitions in the CA3 hippocampal region of the rat. J Neurophysiol 73:246-255.

Ganguly K et al. (2001) GABA itself promotes the developmental switch of neuronal GABAergic responses from excitation to inhibition. Cell 105:521-532.

Gao JL et al. (1997) Impaired host defense, hematopoiesis, granulomatous inflammation and type 1-type 2 cytokine balance in mice lacking CC chemokine receptor 1. J Exp Med 185:1959-1968.

Gao XB, van den Pol AN (2000) GABA release from mouse axonal growth cones. J Physiol 523 Pt 3:629-637.

Ge WP et al. (2006) Long-term potentiation of neuron-glia synapses mediated by Ca2+-permeable AMPA receptors. Science 312:1533-1537.

Giaume C, McCarthy KD (1996) Control of gap-junctional communication in astrocytic networks. Trends Neurosci 19:319-325.

Gilbert P et al. (1984) gamma-Aminobutyric acid directly depolarizes cultured oligodendrocytes. J Neurosci 4:561-569.

Giovannelli A et al. (1998) CXC chemokines interleukin-8 (IL-8) and growth-related gene product alpha (GROalpha) modulate Purkinje neuron activity in mouse cerebellum. J Neuroimmunol 92:122-132.

Grass D et al. (2004) Diversity of functional astroglial properties in the respiratory network. J Neurosci 24:1358-1365.

Gulledge AT, Stuart GJ (2003) Excitatory actions of GABA in the cortex. Neuron 37:299-309.

Haas S et al. (1996) ATP-induced membrane currents in ameboid microglia acutely isolated from mouse brain slices. Neuroscience 75:257-261.

Hagino Y et al. (2004) Heterogeneity and potentiation of AMPA type of glutamate receptors in rat cultured microglia. Glia 47:68-77.

Hamill OP et al. (1981) Improved patch-clamp techniques for high-resolution current recording from cells and cell-free membrane patches. Pflugers Arch 391:85-100.

Hanisch UK (2002) Microglia as a source and target of cytokines. Glia 40:140-155.

Hanisch UK, Kettenmann H (2007) Microglia: active sensor and versatile effector cells in the normal and pathologic brain. Nat Neurosci 10:1387-1394.

Hanisch UK et al. (2001) The protein tyrosine kinase inhibitor AG126 prevents the massive microglial cytokine induction by pneumococcal cell walls. Eur J Immunol 31:2104-2115.

Haupt C et al. (2007) Temporal profile of connexin 43 expression after photothrombotic lesion in rat brain. Neuroscience 144:562-570.

Haydon PG (2001) GLIA: listening and talking to the synapse. Nat Rev Neurosci 2:185-193.

Haynes SE et al. (2006) The P2Y12 receptor regulates microglial activation by extracellular nucleotides. Nat Neurosci 9:1512-1519.

Heesen M et al. (1996) Mouse astrocytes respond to the chemokines MCP-1 and KC, but reverse transcriptase-polymerase chain reaction does not detect mRNA for the KC or new MCP-1 receptor. J Neurosci Res 45:382-391.

Heinemann U, Arens, J. (1992) Production and calibration of ion-sensitive microelectrodes. In: Practical Electrophysiological Methods (Kettenmann H, Grantyn R., ed), pp 206-212. New York: Wiley-Liss.

Hide I et al. (2000) Extracellular ATP triggers tumor necrosis factor-alpha release from rat microglia. J Neurochem 75:965-972.

Hinterkeuser S et al. (2000) Astrocytes in the hippocampus of patients with temporal lobe epilepsy display changes in potassium conductances. Eur J Neurosci 12:2087-2096.

Hirasawa T et al. (2005) Visualization of microglia in living tissues using Iba1-EGFP transgenic mice. J Neurosci Res 81:357-362.

Honda S et al. (2001) Extracellular ATP or ADP induce chemotaxis of cultured microglia through Gi/o-coupled P2Y receptors. J Neurosci 21:1975-1982.

Hoppe D, Kettenmann H (1989) GABA triggers a Cl- efflux from cultured mouse oligodendrocytes. Neurosci Lett 97:334-339.

Horio Y (2001) Potassium channels of glial cells: distribution and function. Jpn J Pharmacol 87:1-6.

Hutcheon B et al. (2000) Developmental change in GABAA receptor desensitization kinetics and its role in synapse function in rat cortical neurons. J Physiol 522 Pt 1:3-17.

Ifuku M et al. (2007) Bradykinin-induced microglial migration mediated by B1-bradykinin receptors depends on Ca2+ influx via reverse-mode activity of the Na+/Ca2+ exchanger. J Neurosci 27:13065-13073.

Iino M et al. (2001) Glia-synapse interaction through Ca2+-permeable AMPA receptors in Bergmann glia. Science 292:926-929.

Imamoto K, Leblond CP (1978) Radioautographic investigation of gliogenesis in the corpus callosum of young rats. II. Origin of microglial cells. J Comp Neurol 180:139-163.

Isaac JT et al. (1997) Silent synapses during development of thalamocortical inputs. Neuron 18:269-280.

Ishiuchi S et al. (2001) Extension of glial processes by activation of Ca2+-permeable AMPA receptor channels. Neuroreport 12:745-748.

Kaila K (1994) Ionic basis of GABAA receptor channel function in the nervous system. Prog Neurobiol 42:489-537.

Kaila K et al. (1991) Fall in intracellular pH mediated by GABAA receptors in cultured rat astrocytes. Neurosci Lett 126:9-12.

Kann O et al. (2003) Metabotropic receptor-mediated Ca2+ signaling elevates mitochondrial Ca2+ and stimulates oxidative metabolism in hippocampal slice cultures. J Neurophysiol 90:613-621.

Katchanov J et al. (2003) Selective neuronal vulnerability following mild focal brain ischemia in the mouse. Brain Pathol 13:452-464.

Katchanov J et al. (2001) Mild cerebral ischemia induces loss of cyclin-dependent kinase inhibitors and activation of cell cycle machinery before delayed neuronal cell death. J Neurosci 21:5045-5053.

Kaur C, Ling EA (1991) Study of the transformation of amoeboid microglial cells into microglia labelled with the isolectin Griffonia simplicifolia in postnatal rats. Acta Anat (Basel) 142:118-125.

Kettenmann H et al. (1990) Cultured microglial cells have a distinct pattern of membrane channels different from peritoneal macrophages. J Neurosci Res 26:278-287.

Kirchhoff F, Kettenmann H (1992) GABA Triggers a [Ca2+]i Increase in Murine Precursor Cells of the Oligodendrocyte Lineage. Eur J Neurosci 4:1049-1058.

Koizumi S et al. (2007) UDP acting at P2Y6 receptors is a mediator of microglial phagocytosis. Nature 446:1091-1095.

Kotecha SA, Schlichter LC (1999) A Kv1.5 to Kv1.3 switch in endogenous hippocampal microglia and a role in proliferation. J Neurosci 19:10680-10693.

Kronenberg G et al. (2005) Nestin-expressing cells divide and adopt a complex electrophysiologic phenotype after transient brain ischemia. J Cereb Blood Flow Metab 25:1613-1624.

Kubo Y et al. (1993) Primary structure and functional expression of a mouse inward rectifier potassium channel. Nature 362:127-133.

Kuhn SA et al. (2004) Microglia express GABA(B) receptors to modulate interleukin release. Mol Cell Neurosci 25:312-322.

Kullmann DM et al. (1996) LTP of AMPA and NMDA receptor-mediated signals: evidence for presynaptic expression and extrasynaptic glutamate spill-over. Neuron 17:461-474.

Kuner T, Augustine GJ (2000) A genetically encoded ratiometric indicator for chloride: capturing chloride transients in cultured hippocampal neurons. Neuron 27:447-459.

Ladeby R et al. (2005) Microglial cell population dynamics in the injured adult central nervous system. Brain Res Brain Res Rev 48:196-206.

Laing KJ, Secombes CJ (2004) Chemokines. Dev Comp Immunol 28:443-460.

Lawson LJ et al. (1992) Turnover of resident microglia in the normal adult mouse brain. Neuroscience 48:405-415.

Lazarini F et al. (2000) Differential signalling of the chemokine receptor CXCR4 by stromal cell-derived factor 1 and the HIV glycoprotein in rat neurons and astrocytes. Eur J Neurosci 12:117-125.

Lin JH et al. (1998) Gap-junction-mediated propagation and amplification of cell injury. Nat Neurosci 1:494-500.

Ling EA (1979) Transformation of monocytes into amoeboid microglia in the corpus callosum of postnatal rats, as shown by labelling monocytes by carbon particles. J Anat 128:847-858.

Ling EA, Tan CK (1974) Amoeboid microglial cells in the corpus callosum of neonatal rats. Arch Histol Jpn 36:265-280.

Ling EA, Wong WC (1993) The origin and nature of ramified and amoeboid microglia: a historical review and current concepts. Glia 7:9-18.

Ma Q et al. (1998) Impaired B-lymphopoiesis, myelopoiesis, and derailed cerebellar neuron migration in CXCR4- and SDF-1-deficient mice. Proc Natl Acad Sci U S A 95:9448-9453.

MacFarlane SN, Sontheimer H (1997) Electrophysiological changes that accompany reactive gliosis in vitro. J Neurosci 17:7316-7329.

Maciejewski-Lenoir D et al. (1999) Characterization of fractalkine in rat brain cells: migratory and activation signals for CX3CR-1-expressing microglia. J Immunol 163:1628-1635.

Mallat M, Chamak B (1994) Brain macrophages: neurotoxic or neurotrophic effector cells? J Leukoc Biol 56:416-422.

Marandi N et al. (2002) Two-photon chloride imaging in neurons of brain slices. Pflugers Arch 445:357-365.

Maric D et al. (2001) GABA expression dominates neuronal lineage progression in the embryonic rat neocortex and facilitates neurite outgrowth via GABA(A) autoreceptor/Cl-channels. J Neurosci 21:2343-2360.

Marin-Teva JL et al. (1999) Proliferation of actively migrating ameboid microglia in the developing quail retina. Anat Embryol (Berl) 200:289-300.

Martina M et al. (2001) Cell-type-specific GABA responses and chloride homeostasis in the cortex and amygdala. J Neurophysiol 86:2887-2895.

Matthias K et al. (2003) Segregated expression of AMPA-type glutamate receptors and glutamate transporters defines distinct astrocyte populations in the mouse hippocampus. J Neurosci 23:1750-1758.

Maurer M, von Stebut E (2004) Macrophage inflammatory protein-1. Int J Biochem Cell Biol 36:1882-1886.

McManus CM et al. (1998) Cytokine induction of MIP-1 alpha and MIP-1 beta in human fetal microglia. J Immunol 160:1449-1455.

Menten P et al. (2002) Macrophage inflammatory protein-1. Cytokine Growth Factor Rev 13:455-481.

Milligan CE et al. (1991) Differential immunochemical markers reveal the normal distribution of brain macrophages and microglia in the developing rat brain. J Comp Neurol 314:125-135.

Mitani A, Tanaka K (2003) Functional changes of glial glutamate transporter GLT-1 during ischemia: an in vivo study in the hippocampal CA1 of normal mice and mutant mice lacking GLT-1. J Neurosci 23:7176-7182.

Miyamoto Y, Kim SU (1999) Cytokine-induced production of macrophage inflammatory protein-1alpha (MIP-1alpha) in cultured human astrocytes. J Neurosci Res 55:245-251.

Montana V et al. (2006) Vesicular transmitter release from astrocytes. Glia 54:700-715.

Muller T et al. (1994) Developmental regulation of voltage-gated K+ channel and GABAA receptor expression in Bergmann glial cells. J Neurosci 14:2503-2514.

Muller W et al. (1989) gamma-Aminobutyric acid-induced ion movements in the guinea pig hippocampal slice. Brain Res 484:184-191.

Murdoch C, Finn A (2000) Chemokine receptors and their role in inflammation and infectious diseases. Blood 95:3032-3043.

Nakase T et al. (2003a) Astrocytic gap junctions composed of connexin 43 reduce apoptotic neuronal damage in cerebral ischemia. Stroke 34:1987-1993.

Nakase T et al. (2003b) Neuroprotective role of astrocytic gap junctions in ischemic stroke. Cell Commun Adhes 10:413-417.

Navascues J et al. (2000) Entry, dispersion and differentiation of microglia in the developing central nervous system. An Acad Bras Cienc 72:91-102.

Nimmerjahn A et al. (2005) Resting microglial cells are highly dynamic surveillants of brain parenchyma in vivo. Science 308:1314-1318.

Noda M et al. (2006) Anti-inflammatory effects of kinins via microglia in the central nervous system. Biol Chem 387:167-171.

Noda M et al. (2000) AMPA-kainate subtypes of glutamate receptor in rat cerebral microglia. J Neurosci 20:251-258.

Nolte C et al. (1996) Complement 5a controls motility of murine microglial cells in vitro via activation of an inhibitory G-protein and the rearrangement of the actin cytoskeleton. Neuroscience 73:1091-1107.

Nolte C et al. (2001) GFAP promoter-controlled EGFP-expressing transgenic mice: a tool to visualize astrocytes and astrogliosis in living brain tissue. Glia 33:72-86.

Norenberg W et al. (1992) Inflammatory stimuli induce a new K+ outward current in cultured rat microglia. Neurosci Lett 147:171-174.

Norenberg W et al. (1994) Voltage-dependent potassium channels in activated rat microglia. J Physiol 475:15-32.

Ottersen OP et al. (1996) Ischemic disruption of glutamate homeostasis in brain: quantitative immunocytochemical analyses. J Chem Neuroanat 12:1-14.

Owen-Lynch PJ et al. (1998) The growth inhibitory role and potential clinical value of macrophage inflammatory protein 1 alpha in myeloid leukaemias. Leuk Lymphoma 30:41-53.

Owens DF, Kriegstein AR (2002) Is there more to GABA than synaptic inhibition? Nat Rev Neurosci 3:715-727.

Pannasch U et al. (2006) The potassium channels Kv1.5 and Kv1.3 modulate distinct functions of microglia. Mol Cell Neurosci 33:401-411.

Patneau DK, Mayer ML (1990) Structure-activity relationships for amino acid transmitter candidates acting at N-methyl-D-aspartate and quisqualate receptors. J Neurosci 10:2385-2399.

Pearson HE et al. (1993) Microglial invasion and activation in response to naturally occurring neuronal degeneration in the ganglion cell layer of the postnatal cat retina. Brain Res Dev Brain Res 76:249-255.

Perez Velazquez JL et al. (2003) Gap junctions and neuronal injury: protectants or executioners? Neuroscientist 9:5-9.

Perillan PR et al. (1999) K(+) inward rectifier currents in reactive astrocytes from adult rat brain. Glia 27:213-225.

Perillan PR et al. (2000) Inward rectifier K(+) channel Kir2.3 (IRK3) in reactive astrocytes from adult rat brain. Glia 31:181-192.

Perry VH, Gordon S (1991) Macrophages and the nervous system. Int Rev Cytol 125:203-244.

Perry VH et al. (1985) Immunohistochemical localization of macrophages and microglia in the adult and developing mouse brain. Neuroscience 15:313-326.

Phillis JW et al. (1996) Changes in extracellular amino acid neurotransmitters and purines during and following ischemias of different durations in the rat cerebral cortex. Neurochem Int 29:115-120.

Phillis JW et al. (2000) Transporter reversal as a mechanism of glutamate release from the ischemic rat cerebral cortex: studies with DL-threo-beta-benzyloxyaspartate. Brain Res 868:105-112.

Pin JP, Duvoisin R (1995) The metabotropic glutamate receptors: structure and functions. Neuropharmacology 34:1-26.

Pocock JM, Kettenmann H (2007) Neurotransmitter receptors on microglia. Trends Neurosci 30:527-535.

Prinz M et al. (1999) Microglial activation by components of gram-positive and -negative bacteria: distinct and common routes to the induction of ion channels and cytokines. J Neuropathol Exp Neurol 58:1078-1089.

Provis JM et al. (1996) Microglia in human retina: a heterogeneous population with distinct ontogenies. Perspect Dev Neurobiol 3:213-222.

Pujol F et al. (2005) The chemokine SDF-1 differentially regulates axonal elongation and branching in hippocampal neurons. J Cell Sci 118:1071-1080.

Rappert A et al. (2002) Secondary lymphoid tissue chemokine (CCL21) activates CXCR3 to trigger a Cl- current and chemotaxis in murine microglia. J Immunol 168:3221-3226.

Rezaie P et al. (2002a) Expression of beta-chemokines and chemokine receptors in human fetal astrocyte and microglial co-cultures: potential role of chemokines in the developing CNS. Glia 37:64-75.

Rezaie P et al. (2002b) Motility and ramification of human fetal microglia in culture: an investigation using time-lapse video microscopy and image analysis. Exp Cell Res 274:68-82.

Ringheim GE (1995) Mitogenic effects of interleukin-5 on microglia. Neurosci Lett 201:131-134.

Robinson S et al. (1998) The chemokine growth-regulated oncogene-alpha promotes spinal cord oligodendrocyte precursor proliferation. J Neurosci 18:10457-10463.

Rossi DJ et al. (2000) Glutamate release in severe brain ischaemia is mainly by reversed uptake. Nature 403:316-321.

Rossi DJ et al. (2007) Astrocyte metabolism and signaling during brain ischemia. Nat Neurosci 10:1377-1386.

Rostene W et al. (2007) Chemokines: a new class of neuromodulator? Nat Rev Neurosci 8:895-903.

Schilling T et al. (2000) Upregulation of Kv1.3 K(+) channels in microglia deactivated by TGF-beta. Am J Physiol Cell Physiol 279:C1123-1134.

Schipke CG et al. (2002) Astrocyte Ca2+ waves trigger responses in microglial cells in brain slices. FASEB J 16:255-257.

Schlichter LC et al. (1996) Properties of K+ and Cl- channels and their involvement in proliferation of rat microglial cells. Glia 17:225-236.

Seifert G, Steinhauser C (1995) Glial cells in the mouse hippocampus express AMPA receptors with an intermediate Ca2+ permeability. Eur J Neurosci 7:1872-1881.

Silver IA et al. (1997) Ion homeostasis in brain cells: differences in intracellular ion responses to energy limitation between cultured neurons and glial cells. Neuroscience 78:589-601.

Siushansian R et al. (2001) Connexin43 null mutation increases infarct size after stroke. J Comp Neurol 440:387-394.

Skrzydelski D et al. (2007) The chemokine stromal cell-derived factor-1/CXCL12 activates the nigrostriatal dopamine system. J Neurochem 102:1175-1183.

Standen NB, Stanfield PR (1979) Potassium depletion and sodium block of potassium currents under hyperpolarization in frog sartorius muscle. J Physiol 294:497-520.

Steinhauser C et al. (1994) Properties of GABA and glutamate responses in identified glial cells of the mouse hippocampal slice. Hippocampus 4:19-35.

Steinhauser C et al. (1992) Heterogeneity in the Membrane Current Pattern of Identified Glial Cells in the Hippocampal Slice. Eur J Neurosci 4:472-484.

Streit WJ et al. (1988) Functional plasticity of microglia: a review. Glia 1:301-307.

Streit WJ et al. (1999) Reactive microgliosis. Prog Neurobiol 57:563-581.

Sugita Y et al. (1997) Pigment epithelium-derived factor (PEDF) has direct effects on the metabolism and proliferation of microglia and indirect effects on astrocytes. J Neurosci Res 49:710-718.

Suzuki T et al. (2004) Production and release of neuroprotective tumor necrosis factor by P2X7 receptor-activated microglia. J Neurosci 24:1-7.

Suzumura A et al. (1994) Interleukin-4 induces proliferation and activation of microglia but suppresses their induction of class II major histocompatibility complex antigen expression. J Neuroimmunol 53:209-218.

Tanabe S et al. (1997) Murine astrocytes express a functional chemokine receptor. J Neurosci 17:6522-6528.

Tanaka J et al. (1999) Morphological differentiation of microglial cells in culture: involvement of insoluble factors derived from astrocytes. Neurosci Res 34:207-215.

Taylor DL et al. (2003) Activation of microglial group III metabotropic glutamate receptors protects neurons against microglial neurotoxicity. J Neurosci 23:2150-2160.

Taylor DL et al. (2005) Stimulation of microglial metabotropic glutamate receptor mGlu2 triggers tumor necrosis factor alpha-induced neurotoxicity in concert with microglial-derived Fas ligand. J Neurosci 25:2952-2964.

Thery C et al. (1991) Cytotoxic Effect of Brain Macrophages on Developing. Eur J Neurosci 3:1155-1164.

Tran PB et al. (2004) Chemokine receptors are expressed widely by embryonic and adult neural progenitor cells. J Neurosci Res 76:20-34.

Verkhratsky A, Steinhauser C (2000) Ion channels in glial cells. Brain Res Brain Res Rev 32:380-412.

von Blankenfeld G, Kettenmann H (1991) Glutamate and GABA receptors in vertebrate glial cells. Mol Neurobiol 5:31-43.

Von Blankenfeld G et al. (1991) Expression and Developmental Regulation of a GABAA Receptor in Cultured Murine Cells of the Oligodendrocyte Lineage. Eur J Neurosci 3:310-316.

Wallraff A et al. (2004) Distinct types of astroglial cells in the hippocampus differ in gap junction coupling. Glia 48:36-43.

Walz W, Bekar LK (2001) Ion channels in cultured microglia. Microsc Res Tech 54:26-33.

Xu J et al. (1993) Variation with age in the labelling of amoeboid microglial cells in rats following intraperitoneal or intravenous injection of a fluorescent dye. J Anat 182 ( Pt 1):55-63.

Zhou M, Kimelberg HK (2001) Freshly isolated hippocampal CA1 astrocytes comprise two populations differing in glutamate transporter and AMPA receptor expression. J Neurosci 21:7901-7908.

# Curriculum Vitae

Mein Lebenslauf wird aus datenschutzrechtlichen Gründen in der elektronischen Version meiner Arbeit nicht veröffentlicht.

# Publications

Wang L*, **Cheung G***, Kronenberg G, Gertz K, Ji S, Kempermann G, Endres M, Kettenmann H. Mild brain ischemia induces unique physiological properties in striatal astrocytes. Glia, (2008, in press)

**Cheung G**, Kann O, Färber K, Kettenmann H. $GABA_A$ receptor activity in postnatal mouse brain enhances macrophage inflammatory protein 1 alpha release and microglial motility. (2008, in preparation)

Klempin F, Kronenberg G, **Cheung G**, Kettenmann H, Kempermann G. Investigation into the properties of doublecortin-expressing cells in the adult mouse piriform cortex as compared to the dentate gyrus. (2008, in preparation)

Färber K, **Cheung G**, Mitchell D, Wallis R, Kettenmann H. Complement C1q is a proinflammatory stimulus, and mannose-binding lectin is an anti-inflammatory stimulus, for microglia activation. J Neurosci Res (2008, submitted)

Ifuku M, Färber K, Okuno Y, Yamakawa Y, Miyamoto T, Nolte C, Merrino VF, Kita S, Iwamoto T, Komuro I, Wang B, **Cheung G**, Ishikawa E, Ooboshi H, Bader M, Wada K, Kettenmann H, Noda M. Bradykinin-induced microglial migration mediated by B1-bradykinin receptors depends on Ca2+ influx via reverse-mode activity of the Na+/Ca2+ exchanger. Journal of Neuroscience. 27: 13065-13073, 2007

Babu H, **Cheung G**, Kettenmann H, Palmer TD, Kempermann G. Enriched monolayer precursor cell cultures from micro-dissected adult mouse dentate gyrus yield functional granule cell-like neurons. PLoS ONE. 2:e388, 2007

* Authors contributed equally

## Meetings and Presentations

**Cheung G**, Kann O, Färber K, Kettenmann H. Ameboid microglia in developing brain indirectly respond to GABA- and glutamatergic activities by sensing the resulting increase in extracellular potassium *(FENS Forum 2008-submitted abstract, Geneva, Switzerland)*.

**Cheung G**, Kann O, Färber K, Kettenmann H. Ameboid microglia in developing brain indirectly respond to GABA- and glutamatergic activities by sensing the resulting increase in extracellular potassium *(Berlin Neuroscience Forum 2008-submitted abstract, Bad Liebenwalde, Germany)*.

**Cheung G**, Kann O, Färber K, Kettenmann H. Ameboid microglia in developing brain sense $GABA_A$ and glutamate receptor activities by intrinsic potassium channels *(Berlin Brain Days 2007-poster, Berlin, Germany)*.

**Cheung G**, Wang LP, Kronenberg G, Gertz K, Ji Shengbo, Kempermann G, Endres M, Kettenmann H. Unique physiological properties in striatal astrocytes induced by mild stroke *(SFN 2007-poster, San Diego, USA)*.

**Cheung G**, Färber K, Kann O, Kettenmann H. Microglia respond indirectly to GABAergic stimulation in early postnatal corpus callosum (*Euroglia 2007-poster, London, UK*).

**Cheung G**, Färber K, Kann O, Kettenmann H. Microglia respond indirectly to GABAergic stimulation in early postnatal corpus callosum (*Berlin Brain Days 2006-poster, Berlin, Germany*).

**Cheung G**, Färber K, Kann O, Kettenmann H. Microglia respond indirectly to GABAergic stimulation in early postnatal corpus callosum (*MDC PhD Retreat 2006-poster, Berlin, Germany*).

**Cheung G**, Färber K, Kettenmann H. Response of microglia to GABAergic stimulation in early postnatal corpus callosum. (*Berlin Neuroscience Forum 2006-poster, Bad Liebenwalde, Germany*).

**Cheung G**, Färber K, Kettenmann H. Response of microglia to GABAergic stimulation. (*Berlin Brain Days 2005-poster, Berlin, Germany*).

**Cheung G**, Färber K, Kettenmann H. Response of microglial cells to $GABA_A$ receptor stimulation. (*MDC PhD Retreat 2005-poster, Berlin, Germany*).

# Erklärung

„Ich, Giselle Cheung, erkläre, dass ich die vorgelegte Dissertationsschrift mit dem Thema: *Properties and functions of glial cells in the developing and injured brains* selbst verfasst und keine anderen als die angegebenen Quellen und Hilfsmittel benutzt, ohne die (unzulässige) Hilfe Dritter verfasst und auch in Teilen keine Kopien anderer Arbeiten dargestellt habe."

Berlin, den

_____

Giselle Cheung